Serie Correlación Geológica, 29 (1): 21-80
Tucumán, 2013 - ISSN 1514-4186 - ISSN en línea 1666-9479

The Gondwana-South America Iapetus margin evolution as recorded by Lower Paleozoic units of western Precordillera, Argentina: The Bonilla Complex, Uspallata

Daniel A. GREGORI[1*], Juan C. MARTINEZ[2], and Leonardo BENEDINI[1]

Abstract: *THE GONDWANA SOUTH AMERICA IAPETUS MARGIN EVOLUTION AS RECORDED BY LOWER PALEOZOIC UNITS OF WESTERN PRECORDILLERA, ARGENTINA.*
The Cambro-Ordovician belt of western Precordillera, that includes slightly metamorphosed sandstones and pelites with interbedded basalts and ultramafic bodies, were considered part of the allochthonous Cuyania Terrane, accreted to Gondwana South America during Ordovician times. The Bonilla Complex, which represents the southern tip of the Precordillera, is constituted of metasedimentary rocks of internal and external platform environments. Paleocurrents inferred from sedimentary structures indicate provenance from the northeast and southeast (actual coordinates). The limestones of this complex, located in the eastern part of the outcrops, suggest evolution toward a carbonate-dominated Late Neoproterozoic to Cambrian passive margin. Mafic volcanic rocks were emplaced coevally with sedimentation, whereas ultramafic rocks were later tectonically emplaced. Chemical evidence suggests that the protolith of the metasedimentary rocks was derived from an older exhumed felsic basement belonging to an upper continental crust. The most prominent population of detrital zircons (~500-600 Ma) from the Bonilla Complex support the hypothesis that these rocks are equivalent to those of the Sierras Pampeanas and the northern Patagonia. The most proximal source of the Pampean zircons found in the Bonilla Complex is the Sierras Pampeanas, located immediately to the east (present coordinates). The Bonilla Complex was deposited in an open marine basin considerably earlier (~50 Ma) than the supposed detachment of the Cuyania Terrane from the Ouachita embayment in the Laurentia margin. It is therefore not necessary to invoke the presence of an allochthonous terrane between the Bonilla Complex and the Gondwana margin to explain the 1 Ga zircon populations. Silurian to Devonian deformation was characterized by metamorphism and imbrication within an accretionary prism, the consequence of eastward subduction in the western margin of Gondwana. Therefore, the Bonilla Complex, as well as equivalent units in western Precordillera, was originally deposited as sediments on a continental shelf at the southwestern margin of Gondwana, covering a basement that was already part of the Gondwana continent by Neoproterozoic-Cambrian times.

Resumen: *LA EVOLUCIÓN DEL MARGEN DEL OCEANO IAPETUS EN EL CONTINENTE GONDWANA-SUDAMERICA REGISTRADO EN UNIDADES DEL PALEOZOICO INFERIOR DE LA PRECORDILLERA DE ARGENTINA.*
La faja de rocas Cambro-Ordovícicas de la Precordillera occidental, que incluye areniscas ligeramente metamorfizadas y pelitas con basaltos interestratificados y cuerpos ultramáficos, fue considerado como parte del Terreno alóctono Cuyania, que se habría acrecionado a la parte Sudamericana del continente de Gondwana durante tiempos ordovícicos. El Complejo Bonilla, que representa el extremo sur de este cinturón, está constituido por rocas metasedimentarias depositadas en plataformas marinas internas y externas. Los datos de paleocorrientes deducidos a partir de estructuras sedimentarias indican procedencias del noreste y sureste, considerando coordenadas actuales. Las calizas de este complejo, situadas en la parte oriental de los afloramientos, sugieren una evolución hacia una plataforma marina dominantemente carbonática de margen pasivo durante el Neoproterozoico tardío al Cámbrico. Las rocas subvolcánicas máficas fueron emplazadas coetáneamente con la sedimentación, mientras que rocas ultramáficas fueron emplazadas tectónicamente más tarde. Los datos químicos sugieren que los protolitos de las rocas metasedimentarias se derivaron de un antiguo basamento félsico exhumado perteneciente a una corteza continental superior. La población más prominente de circones detríticos (~ 500-600 Ma) del Complejo Bonilla

[1)] INGEOSUR, Cátedra de Geología Argentina, Universidad Nacional del Sur and CONICET, San Juan 670, 8000 Bahía Blanca, Argentina.
[2)] INGEOSUR, Cátedra de Petrología, Universidad Nacional del Sur and CONICET, San Juan 670, 8000 Bahía Blanca, Argentina.

apoyan la hipótesis de que estas rocas son equivalentes a las de las Sierras Pampeanas y de la Patagonia Norte. La fuente más próxima de los circones de edad Pampeana que se encuentran en el Complejo Bonilla son las Sierras Pampeanas, situadas inmediatamente al este (coordenadas actuales). El Complejo Bonilla fue depositado en una cuenca marina abierta, considerablemente antes (~ 50 Ma) que la supuesta separación del Terreno Cuyania de la bahía Ouachita en el margen de Laurencia. Por lo tanto, no es necesario invocar la presencia de un Terreno alóctono entre el Complejo Bonilla y el margen de Gondwana para explicar las poblaciones de circones de 1 Ga. La deformación Silúrica-Devónica se caracterizó por metamorfismo y deformación dentro de un prisma de acreción, consecuente con procesos de subducción dirigidos hacia el este (siempre coordenadas actuales) en la margen occidental de Gondwana. Por lo tanto, el Complejo Bonilla, así como otras unidades equivalentes en Precordillera occidental, fueron originalmente depositadas como sedimentos sobre una plataforma marina en el margen suroeste de Gondwana, cubriendo un basamento que ya era parte del continente de Gondwana en el Neoproterozoico-Cámbrico.

Keywords: Bonilla Complex, passive margin, western Gondwana, Gondwana provenance, Argentina.

Palabras clave: Complejo Bonilla, margen pasivo, Gondwana occidental, procedencia gondwánica, Argentina.

Introduction

The Grenville orogeny (1.1–0.9 Ga) was produced by collisional events during the amalgamation of Rodinia (Murphy et al., 2010). The disconnection of Laurentia from western Gondwana at ca. 570 Ma (Cawood et al., 2001) is documented by the generation of rift structures and related magmatism formed along the Laurentian margin of Iapetus.

The Neoproterozoic Brasiliano-Pan African cycle (850 - 500 Ma) describes the assembly of western Gondwana from the breakup of the Rodinia supercontinent to the closure of all oceanic basins, over a series of subduction and collisional events, up to its final agglutination. According to Unrug (1992, 1994) the paleomagnetic data, and age of suturing belts, permits distinction between eastern and western Gondwana with different Neoproterozoic histories. The former comprised the Kalahari-Grunehogna craton of Africa and East Antarctica, Madagascar, India, Antarctica, and Australia. Western Gondwana included the Archean-Paleoproterozoic East Sahara-Nile, West African, Amazonian, and Río de la Plata cratons.

West of the Río de la Plata Craton, in the central part of Argentina, four geological regions appear which are predominantly composed of low to high-degree metamorphic and sedimentary rocks of the Neoproterozoic to Paleozoic age (Fig. 1).

The easternmost area, known as Sierras Pampeanas, includes low and high-degree metamorphic rocks, as well as limestones and marbles. Radiometric dating by Varela and Dalla Salda (1992), Ramos et al. (1996), Varela et al. (1996), Pankhurst and Rapela (1998), and Söllner et al. (2000) identify ages between 500 and 600 Ma. The limestones and marbles form extensive outcrops in the Sierras Pampeanas de Córdoba, San Luis, San Juan, Catamarca, Tucuman and Salta Provinces in an area 1000 km long in the north-south direction (24° to 33° 15´S) and 360 km wide in the east-west direction (64° 18´to 68° 06´W). The calcareous rocks are interbedded in the Ediacaran-Cambrian metasedimentary rocks, assigned to the Puncoviscana and equivalent formations (Aceñolaza and Toselli, 1981). The age is strongly documented by means of detrital zircons and fossil remains. Outcrops of rocks ~1Ga were recognized in the Sierra de Pie de Palo and Sierra de Umango in the Western Sierras Pampeanas (Varela and Dalla Salda, 1992; Varela et al., 1996, 2011).

Westwards of the Sierras Pampeanas is the Precordillera mountain range and its southern extension, the San Rafael Block. The range extend between 28º to 36º 30´ S, and is mainly characterized by Lower Paleozoic marine limestones. Grenvillian ages have been reported

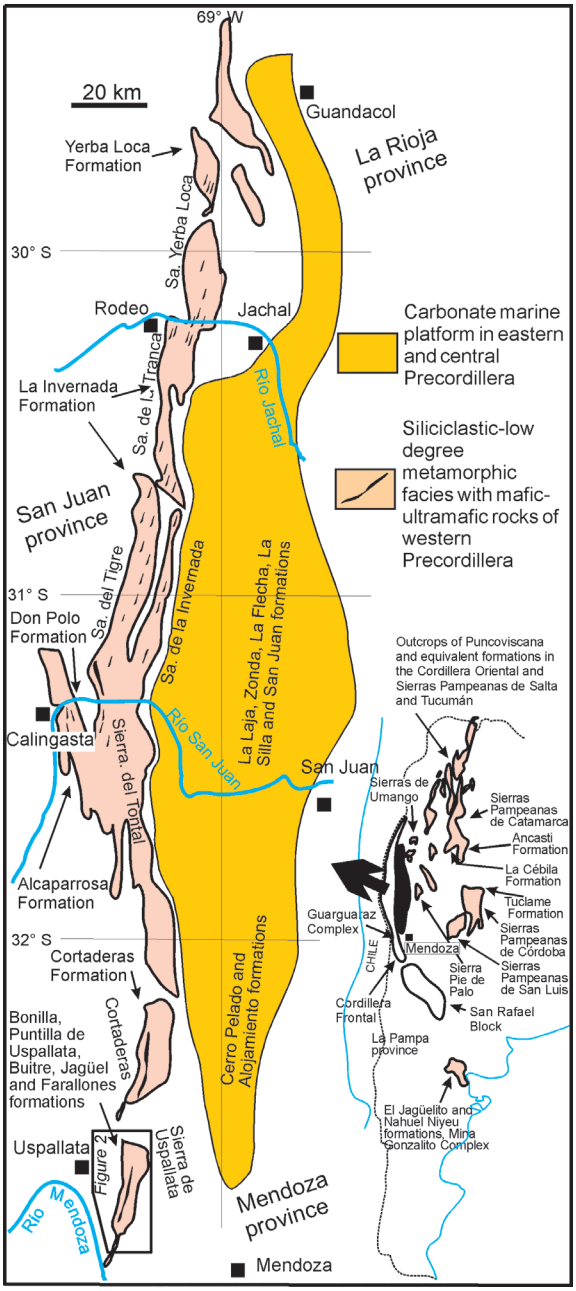

Figure 1. Simplified map of Precordillera displaying the distribution of the Neoproterozoic-Ordovician carbonate marine platforms and the siliciclastic low-degree metamorphic facies. Location of the studied area (Fig. 2) is also shown. Cordillera Frontal, Sierras Pampeanas, northern Patagonia and localization of Puncoviscana Formation are indicated apart.

Figura 1. Mapa simplificado de Precordillera mostrando la distribución de las plataformas marinas carbonáticas del Neoproterozoico-Ordovícico y la facies metamórficas de bajo grado siliciclásticas. También se muestra la ubicación de la zona estudiada (Fig. 2). La localización de la Cordillera Frontal, Sierras Pampeanas, norte de Patagonia y de la Formación Puncoviscana figuran aparte.

for detrital zircons in Devonian sandstone of the Precordillera (Loske, 1992). Scarce Tertiary volcanic rocks (Leveratto, 1968) carry basement xenoliths that were dated by Abbruzzi et al. (1993) and Kay et al. (1996) at 1188 ± 122 Ma. confirm the existence of rock of such age below the Precordillera. In the San Rafael Block, basement rocks were dated by Astini et al. (1996), Cingolani and Varela (1999) and Sato et al. (1998, 1999, 2000), giving ages between 1212 ± 47 Ma and 1188 ± 47 Ma.

The Cordillera Frontal is located immediately to the west and includes low and high-degree metamorphic rocks of an Ediacaran-Lower Paleozoic age (López and Gregori, 2004). U-Pb dating of the zircon of the low and high-degree metamorphic rocks shows an age of 1069 ± 36 Ma. (Ramos and Basei, 1997). However, Lopez (2005) found several genera of acritarchs *(Siphonophycus, Bavlinella, Leiosphaeridia)* which are typical of Vendian times, considering that the sedimentation of these rocks is Neoproterozoic to Lower Cambrian.

The Grenvillian-aged rocks (~ 1 Ga) were related to Laurentian-derived exotic terranes docked to the western margin of Gondwana during the Early Paleozoic Famatinian orogeny.

Lastly, Ramos (1995) and Ramos et al. (1996, 1998) grouped the Precordillera Terrane and areas of the Sierras Pampeanas with the ~ 1 Ga basement ages in the Cuyania Terrane (Fig. 1). This includes the Cambrian marine limestones with the Laurentian-affinities faunas of Precordillera, San Rafael Block and rocks of western Sierras Pampeanas with ages ~ 1 Ga. The accretion of the Cuyania terrane to the western Gondwana margin apparently occurred during the Middle Ordovician time (Astini et al., 1995). According to Astini et al. (1995), Cuyania originated as a conjugate margin of the Ouachita embayment, south of the Appalachian platform, during Early Cambrian times. The changing of faunal assemblages in the carbonate platform depicts the subsequent travel toward the Gondwana protomargin. The age of the collision with this margin is indicated by the ages of peak of regional metamorphism (460 Ma) in the basement rocks of the Sierra de Pie de Palo.

There are considerable debates about the existence of the Laurentian-derived exotic terranes docked to the margin of western Gondwana.

Finney (2007) showed, by means of stratigraphic, paleobiogeographical records and U-Pb geochronology of detrital zircons from the Cambrian and Ordovician sandstones of Precordillera, that evidence points to a parautochthonous origin of the Cuyania terrane.

According to Finney (2007), the Middle-Upper Ordovician siliciclastic successions of Cuyania do not represent a peripheral foreland basin, but instead were deposited in strike-slip related basins in a transform fault zone. The Middle Ordovician K-bentonites of Precordillera do not indicate that Cuyania was approaching the Famatinian magmatic arc from the west (actual coordinates), but instead that it was located to the southeast. According to Fanning et al., (2004) the Ordovician K-bentonites of Precordillera show an age of 469.5 ± 3.2 Ma and 470.1 ± 3.3 Ma, strongly concordant with the 462 ± 2 Ma U-Pb age of Huff et al., (1997). According to Fanning et al., (2004) is highly probable that the Famatinian arc volcanoes provided the ash for the K-bentonite horizons, suggesting proximity to the Precordillera terrane during the deposition of the Lower Cambrian to Middle Ordovician platform carbonates. According these authors these data could also be compatible with a parautochthonous model for docking of the Precordillera terrane, by movement along the Pacific margin of Gondwana, rather than across the Iapetus Ocean.

The paleomagnetic data of Cambrian strata of Cuyania is consistent not only with the location of the Ouachita embayment of Laurentia, but also with the southern margin of West Gondwana.

According to Finney (2007), the potential basement rocks of Cuyania of Early

Mesoproterozoic to Early Cambrian age are characteristic of Gondwana, rather than Laurentia. The Pb isotopic ratios of Grenvillian-aged basement rocks are not only similar to those of the Grenvillian basement in Laurentia but also to those in other areas of Western Gondwana, like the Namaqua-Natal Metamorphic province of South Africa, the Meredith Complex on the Falkland Plateau, the Nubian Shield granitoids and the basement of Western Antarctica (Wareham et al., 1998).

In the parautochthonous model of Finney (2007), Cuyania migrated along a transform fault from a position on the southern margin of West Gondwana (present coordinates) in the Middle Ordovician to its modern position outboard of the Famatina magmatic belt in Devonian time.

Despite these advances in the understanding of the basement rocks and the stratigraphy of the Cambrian-Ordovician carbonate platform of eastern and central Precordillera, there are few studies of the provenance, age and deformation of the low-degree metamorphic rocks of the same age of western Precordillera.

The age of these units in the southwestern part of Precordillera are still not constrained by robust methods, and field relationships between different units are unclear, hindering a better establishment of the relative stratigraphy.

Their relationships with the low to high-degree metamorphic rocks of the Cordillera Frontal (Guarguaraz Complex) have not been described, despite their continuity along fault zones. The metamorphic rocks of both regions, western Precordillera and Cordillera Frontal, share many petrologic and geochemical characteristics, and also belts of mafic and ultramafic rocks are indicative of a common geological evolution. López and Gregori (2004) proposed a Gondwana provenance for the protolith of the Guarguaraz Complex, which were deposited in an accretionary wedge in the western margin of Gondwana.

The U/Pb zircon age of a gneiss from the Cordón del Portillo, which are of the southern outcrops of the Guarguaraz Complex, yield ages of 1069 ± 36 Ma and 1081± 45 Ma, which allowed Ramos and Basei (1997) to propose two possibilities: that the rocks are sliced parts of the Cuyania Terrane or represent the Chilenia basement. Basei et al. (1998) also proposed a Laurentian source for the protolith of the metamorphic rocks from the Cordón del Plata and Cordón del Portillo in the Cordillera Frontal, based on Sm/Nd model ages in gneisses (1427 to 1734 Ma). Willner et al. (2008) indicated that the age spectrum of the detrital zircons from the Guarguaraz Complex and the assumed Lower Paleozoic depositional age of its metasediments suggest that the detritus were derived from the Cuyania Terrane, already accreted to Gondwana. These sediments were subducted within a suture zone located west of the Cuyania Terrane. According to Willner et al. (2008), later accretion of a microplate (Chilenia Terrane) resulted in high P-T conditions of metamorphism in a collisional accretionary prism (Massonne and Calderon, 2008).

López de Azarevich et al. (2009) indicated that the Guarguaraz Complex, located further south in the Cordillera Frontal with an age of 655 ± 76 Ma, represents a remnant of an oceanic basin that developed west of the Grenville-aged Cuyania terrane during the Neoproterozoic.

Abre et al., (2012) used a combination of petrographical and geochemical analysis, as well as, Sm-Nd, Pb-Pb isotope and U-Pb detrital zircon dating to study fourteen Ordovician to Silurian units of Precordillera. They results indicated that there were no important changes in the provenance, dominated by upper crustal components within these units.

The detrital zircon dating constrain the source rock ages mainly to the Mesoproterozoic, considered as belonging to the Sunsás cycle, although contributions from older

(Transamazonian) and younger ages (Pampean and Famatinian cycles) are also found.

It is the intention of this paper to address some of these statements.

We present here a review of the main geological attributes of the Bonilla Complex of western Precordillera, including facies arrangement, geochemistry, limits, previous geochronology, and geotectonic models. We provide new field information, geochemistry of the metasedimentary and igneous rocks and geochronological data on detrital zircon.

Comparison with geochemical and geochronological data of the rocks of the Cordillera Frontal, the Sierras Pampeanas and northern Patagonia was used to build an evolutionary model of the Gondwana margin during the Neoproterozoic and Lower Paleozoic times.

Geological setting of the Cambro-Ordovician rocks in Precordillera

In eastern and central Precordillera, the Cambro-Ordovician marine sedimentary rocks are widely represented by an internal calcareous platform (Fig. 1). The distribution is not continuous, and has been modified during the Tertiary orogenies. Units included in this facies are La Laja, Zonda, La Flecha, La Silla and San Juan formations among others. They are not metamorphosed and their age is widely documented by the fossil remains they carry (summary in Keller, 1999). In southern Precordillera, these units are represented by the Cerro Pelado and Alojamiento formations. They are unconformably covered by the marine Ordovician-Devonian rocks of the Villavicencio Formation.

The Cambro-Ordovician rocks in western Precordillera extend between the La Rioja Province to the Uspallata locality in the Mendoza Province, more than 400 km in a north-south direction. These rocks, due to the presence of ultramafic bodies, were earlier considered by Haller and Ramos (1993) as being part of an ophiolite located in a suture zone between the Chilenia and Precordillera terranes. The Cambro-Ordovician rocks include slightly metamorphosed sandstones and pelites with interbedded basalts, and ultramafic bodies that possibly represent talus facies (Bordonaro, 1992). The northwestern part of Precordillera is represented by the Yerba Loca, La Invernada, Don Polo, and Alcaparrosa formations. The first unit carries Caradoc to Ashgill graptolite (Ortega et al., 1991, Brussa et al.,1999). The Alcaparrosa Formation include sandstones, siltites, pelites and subvolcanic bodies, lava flows and dikes of mafic rocks interpreted as ophiolites by Borrello (1969) and Schauer et al. (1987). Its age is Middle to Upper Ordovician (Amos et al., 1971; Aparicio and Cuerda, 1976). The Don Polo Formation share lithological and deformational similarities with the Alcaparrosa Formation, and are considered coeval (Turco Greco and Zardini, 1984). Alonso et al. (2008) describes extensional structures developed in a passive margin represented by the above cited units. The presence of slump folds coeval with the extensional deformation, support the interpretation that gravitational collapse related to submarine sliding was the cause for extensional deformation during Middle to Upper Ordovician times.

In the southwestern area of Precordillera, the slightly metamorphosed rocks are represented by Bonilla, Puntilla de Uspallata, Buitre, Jagüel, Farallones and Cortaderas formations. Nearly all carry mafic and ultramafic bodies and dikes and are constituted by metasandstones, pelites, phyllites, limestones, marls and sometimes marbles. The Ordovician to Devonian is represented by the Villavicencio and Puntilla de Uspallata formations and Cienaga del Medio Group, (Cortés et al., 1997) which are formed by graywakes, sandstones, pelites and interbedded basalts deposited in marine basins, possibly open to the west.

In the Villavicencio Formation, which was divided in three members (Cortés et al.,

1997) graptolites were found in the Empozada Member by Cuerda et al. (1988), indicating Dapingian to Hirnantian ages (472 to 444 Ma). Palynomorphs and flora fossil remains were found in the Canota Member, indicative of a Lower Devonian age (Late Pragian to Early Emsian, ~407 Ma, Rubinstein and Steemans, 2007).

The Lower Devonian (416 Ma, Cortés, 1992) Cienaga del Medio Group is composed of massive green graywackes with a turbiditic arrangement displaying a distinctive hectometric deformation similar to other Devonian units in the Precordillera, with no evidences of metamorphism. The Puntilla de Uspallata and Villavicencio formations cropping out 5 km west, and 3 km east of the Bonilla Complex outcrops display the same style of deformation and lithological characteristics as the Devonian Cienaga del Medio Group.

The Carboniferous sediments, that are overthrusted on or laying uncomfortably over the metasedimentary rocks, represents a wide marine basins that can be continued far west, to Cordillera Frontal, and possibly to Chile. Permian and Triassic times are characterized by intrusive, volcanic and pyroclastic rocks (Fig. 1). East vergence folding and overthrusting occurred during Gondwanan and Andean Orogenies.

Geology of the Bonilla Complex

East of the Uspallata village appears a 30 km N-S long and 8 km wide belt of slightly metamorphosed rocks assigned by Keidel (1939) to "Conjunto de Farallones, Conjunto de Bonilla, Manto de Buitre, and Manto de Jagüelito" (Figs. 1 and 2). Later, the former three were assigned to formations (Borrello, 1969b; Varela, 1973) and included in the Bonilla Group by Folguera et al. (2004). The Manto de Buitre was considered Devonian (386 ± 20 and 369 ± 20 Ma) by Cortes et al. (1997) and Folguera et al. (2004), due to K-Ar radiometric dating of an alkaline mafic body emplaced in this unit at Quebrada de los Burros (Fig. 3).

According to the above cited authors, all units consist of quartz schists, phyllites, greenschists, marbles, limestones, dolomites, meta-gabbros, and serpentinites. Nearly all units are partially cut by mafic dikes and sills interbedded in the sequences. Due to the heterogeneous composition of this succession that includes sedimentary, metasedimentary and mafic and ultramafic rocks, we propose naming this unit the Bonilla Complex.

The maps (Figs. 2, 3, 4 and 5) and detailed profiles allow five lithofacies of the Bonilla Complex to be recognized as follows:

I) Facies of sandstones, calcareous sandstones, pelites, marls, limestones and small mafic bodies.

II) Facies of graphitic phyllites, slates, phyllites with intercalations of feldspar-rich quartzites and marls (Fig. 7a).

III) Facies of laminated and crystalline limestones and marls.

IV) Facies of mafic bodies.

V) Facies of ultramafic bodies.

Sandstones, calcareous sandstones, pelites, marls, limestones and small mafic bodies

These rocks outcrop in the western part of the belt, between Quebrada del Guanaco Muerto and Quebrada Angosta (Figs. 2, 3, 4, 5 and 6a, b) forming the western slope of the Cordón Jarillal, as well as the summit and the western slope of the Cordon de Bonilla.

This facies is equivalent, in part, to the older Farallones Formation. The metasedimentary pile is located above the Carboniferous marine Santa Elena Formation due to a back-thrust that marks the western extension of the Bonilla Complex. Since this facies is slightly folded and shows a nearly constant dip of around 25 degrees to the east, forming a homoclinal structure, we have been able to establish its thickness, which reaches 1,000 m.

As depicted in Figure 7b, sandy levels, which are not greatly abundant, pass transitionally to calcareous sandstone bars. These structures appear countless times in the sequence. Individual thicknesses range from 1 to 2 m. Sandstones are mainly composed (75%) of rounded to subangular grains of quartz, detrital micas, and variable quantities of calcite.

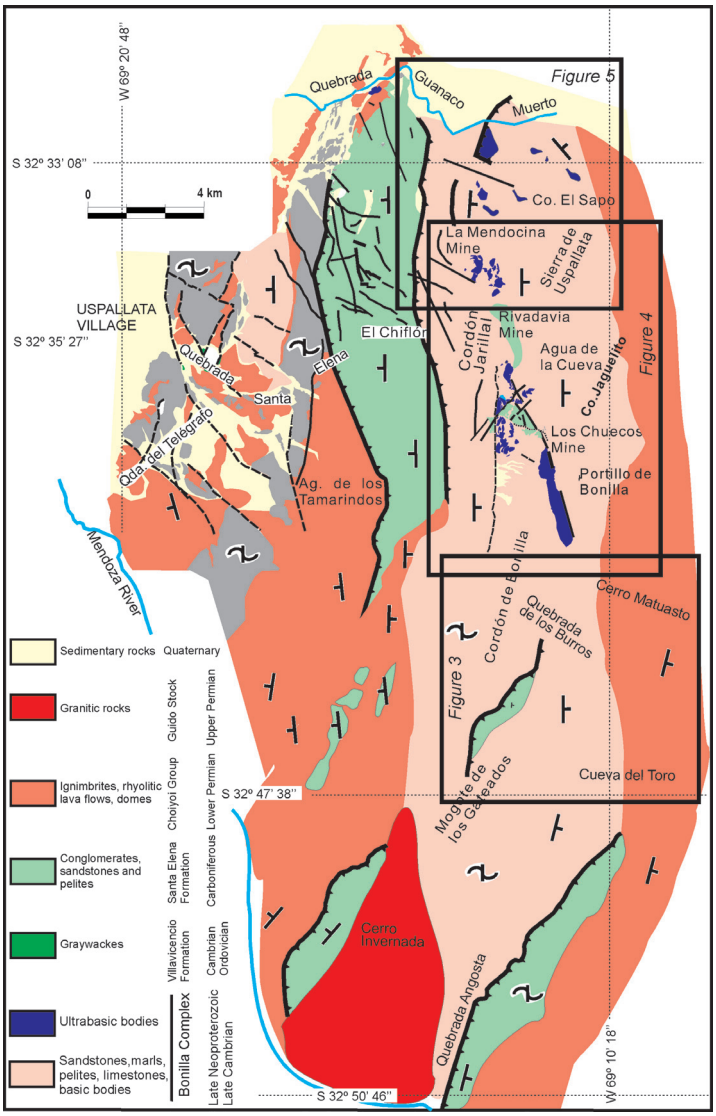

Figure 2. Geological sketch of the Uspallata area showing the distribution of the geological units. Location of the detailed maps of the Bonilla Complex is indicated.

Figura 2. Bosquejo geológico de la zona de Uspallata que muestra la distribución de las unidades geológicas. Se indica la ubicación de los mapas detallados del Complejo Bonilla.

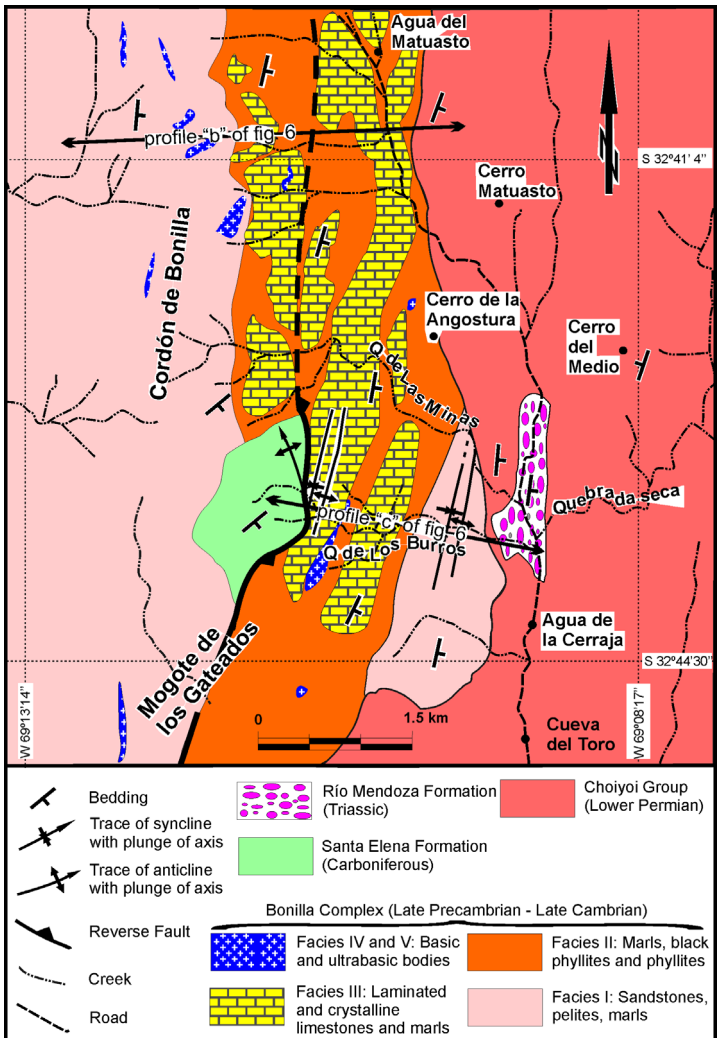

Figure 3. Geological map of the Bonilla Complex between Agua del Matuasto and Cueva del Toro.
Figura 3. Mapa geológico del Complejo Bonilla entre Agua del Matuasto y Cueva del Toro.

The groundmass is composed of pale color fine grained micas and chlorite, located between quartz grains or forming small ribbons along the stratification (Fig. 7g).

The limestones are small levels that do not exceed 2 m thick. Above and below they show transition to marls, becoming abundant in the lower and upper parts of the sequence. These levels show a fine grained texture, composed of rounded grains (5 μm) of calcite, displaying an incipient lamination. Scattered grains of quartz can be recognized. Small levels of quartzites are also present. The pelites are rare, and the limestones are more abundant toward the top of these facies. The volcanic rocks are of basic composition, forming small sills. Their contacts with the metasedimentary rocks are mostly sharp, but irregular. Pillow or lava flows were not observed. Dimensions of mafic sills are highly variable but most are 5 to 10 m thick and less than 50 m long. They are scattered throughout the sequence. This

facies passes transitionally to facies II, located immediately east of the road between Mina Rivadavia and Portillo de Bonilla (Fig. 2).

The lithological characteristics and sedimentary structures show that facies I can be considered to represent the shallow portion of a marine platform, possibly near the coast, strongly affected by the action of tides and waves. The measurement of festoon structures in sandstones, as well as the architecture of the calcareous sandstone bars, indicates a flow from the east, considering actual coordinates.

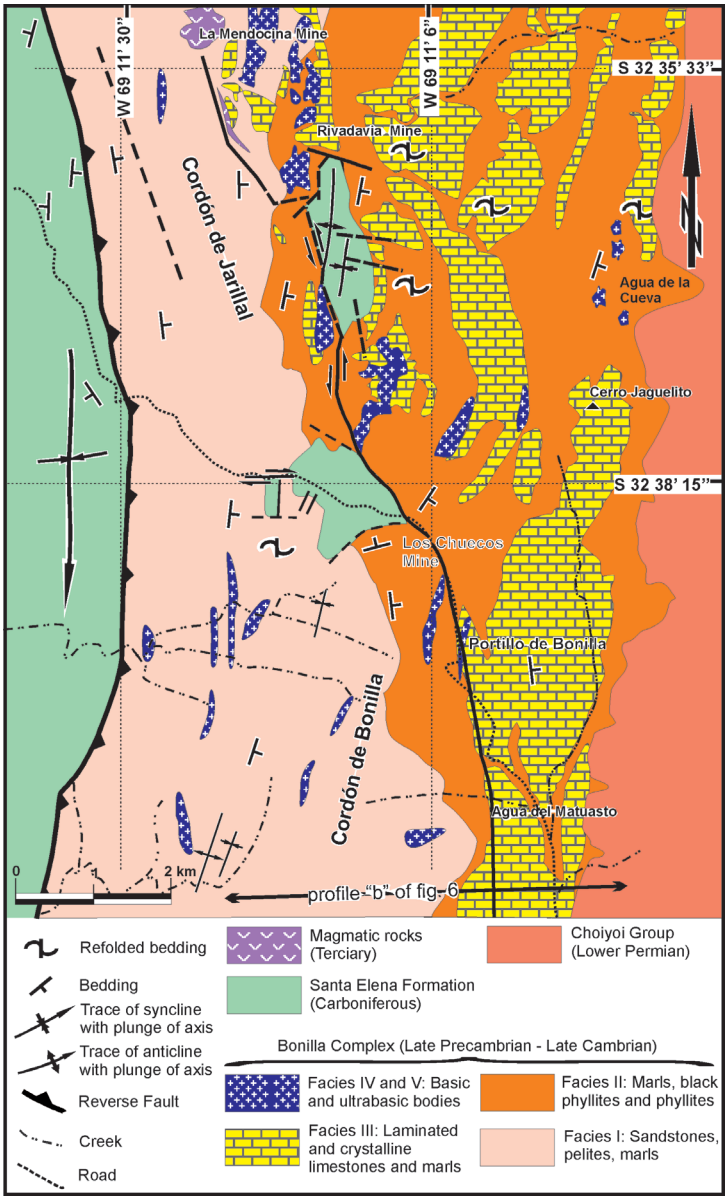

Figure 4. Geological map of the Bonilla Complex between Agua del Matuasto and Mendocina Mine.
Figura 4. Mapa geológico del Complejo Bonilla entre Agua del Matuasto y mina Mendocina.

MARLS, BLACK PHYLLITES AND PHYLLITES. This facies forms two domains, one located in the central part of the belt and the other in the eastern border, both more than 1 km wide in a W-E direction (Figs. 3, 4, 5, 6b, 6c and 7a). The central domain is transitional to facies I in the eastern slope of Cordón Jarillal, whereas the eastern one is unconformably covered by Permian volcanic rocks of the Choiyoi Group. The central domain extends from the Quebrada Guanaco Muerto to the Mogote de los Gateados, (Fig. 3) in the western slope of the Cordón de Bonilla. The eastern domain extends between Cerro El Sapo and Cerro Jagüelito, disappearing southwards.

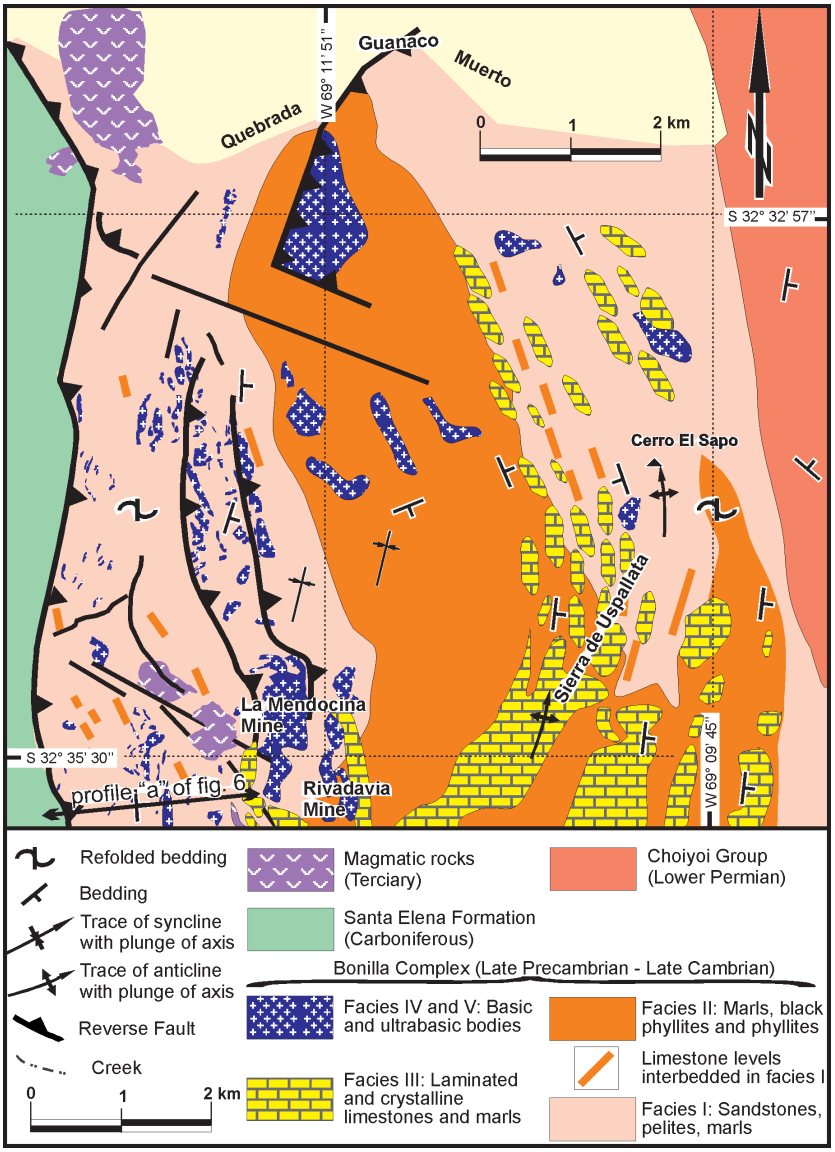

Figure 5. Geological map of the Bonilla Complex between Mendocina Mine and Quebrada Guanaco Muerto.
Figura 5. Mapa geológico del Complejo Bonilla entre mina Mendocina y Quebrada Guanaco Muerto.

The type area, located east of Cordon del Jarillal, shows a thickness near to 1,000 m. This thickness is tentative because in this area several ultramafic bodies were tectonically emplaced, producing deformation in the host rocks.

The most abundant rocks are laminated marls. They are east-dipping and show scarce deformation, except in the vicinity of the ultramafic bodies where local deformation is important. Texturally, they show a micrometric lamination, mostly composed of bands of small mica flakes, elongated within the stratification. Abundant, but isolated spots, 500 x 250 µm of calcite appear irregularly scattered between the micas. Some of them are aligned with the stratification and form short ribbons.

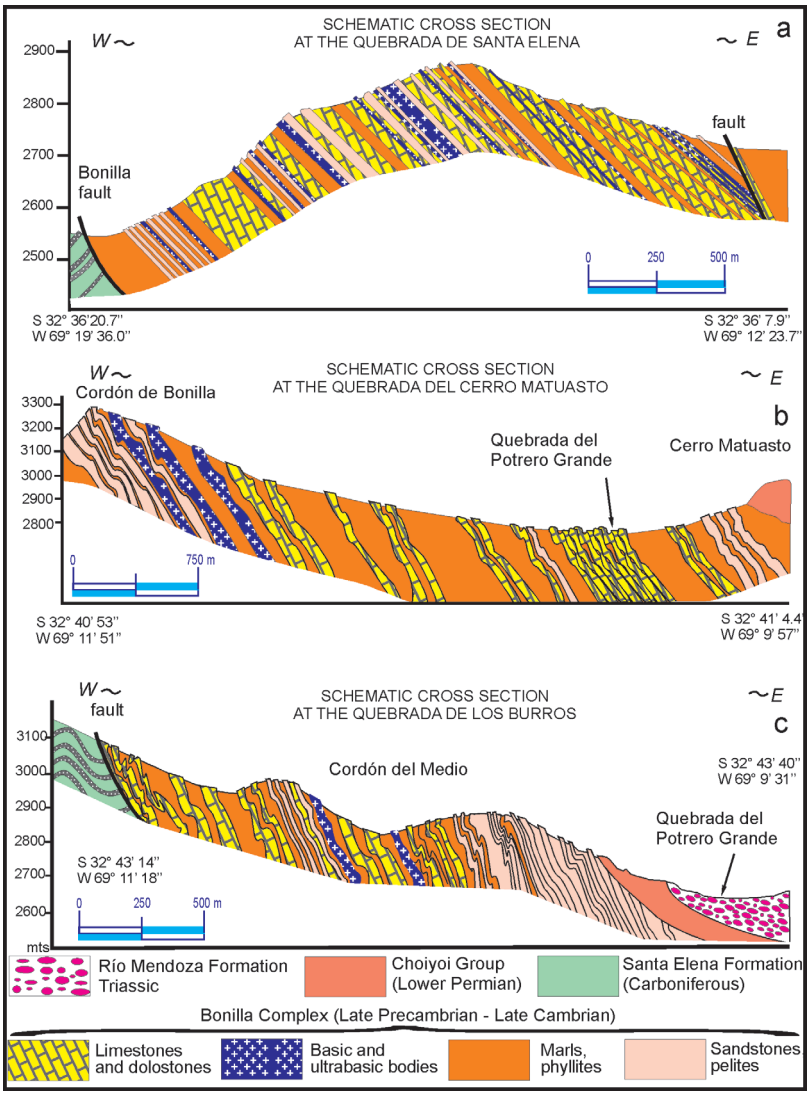

Figure 6. Geological schematic cross-sections at a) Quebrada de Santa Elena, b) Quebrada del Cerro Matuasto and c) Quebrada de los Burros.

Figura 6. Cortes transversales esquemáticos en a) Quebrada de Santa Elena, b) Quebrada del Cerro Matuasto y c) Quebrada de los Burros.

The phyllites are generally gray in color and are interbedded within the marls, also showing a millimetric lamination. These rocks, as indicated above, show an alternated laminated stratification, 1 to 2 mm thick. Bands are of quartz, mica and carbonate. The first appears as small, round grains, showing sometimes ondulose extinction. The average size is 120 μm, but larger, subhedral crystals, possibly related to incipient recrystallization, can be observed. Micas appear in ribbons, 1 mm thick, with flakes growing parallel to the stratification. Sericite is common, but small, scarce, detrital muscovite occasionally occurs. Chlorite was also observed. Micas show bending, kink bands and are refolded.

The black phyllites and slates are mainly located near the contact with facies I, but occasionally appear in the Cerro Jagüelito area. They show a micrometric lamination, composed mainly of a fine grained dark material, possibly organic matter, and small quantities of quartz and calcite. All mineral are aligned along the stratification.

Sporadically, in the central domain of facies II, levels of limestones are recognized, which become more common eastwards, being transitional to facies III.

According to the abundance of fine grained sediments, absence of high-energy sedimentary structures and their homogeneous lithology, we considered this facies as representing the middle to lower part of an offshore platform, away from the action of waves and tides.

LAMINATED AND CRYSTALLINE LIMESTONES AND MARLS. This facies outcrops in the eastern part of the belt, forming the southern tip of the curved Sierra de Uspallata (Fig. 5). It appears in the Cerro El Sapo area, along the Sierra de Uspallata until the Rivadavia Mine. Eastwards is transitional to the eastern domain of facies II. Southwards, there are small spots north of Los Chuecos Mine, but near Cerro Jagüelito and Portillo de Bonilla larger outcrops appear. South of Quebrada de los Burros there are few outcrops of these rocks. The thickness of this facies can be estimated as near to 500 m in the area of Cerro El Sapo, increasing to 1 km east of the Rivadavia Mine.

A demonstrative section of this facies can be observed immediately east of the Rivadavia Mine. There, the sequence starts with interbedding between marls of facies II and limestones of facies III. Small levels of compact, pale orange limestones (Fig. 7c) occur between the eroded light gray marls, which further east are replaced by abundant laminated limestones. In this area, the limestones are between 1 and 30 cm thick. They are west-vergent folded and refolded in a centimetric to metric scale. The folding is strongly asymmetrical, with high-angle limbs dipping to the west and gently to the east. In many cases recumbent folds are recognized in the western part of the outcrops. Small-scale back-thrusts displacing the limestones and emplacing little fragments of mafic rocks in the sequence can be observed along the profile. Reduced slices of marls and phyllites were occasionally recognized, passing quickly to laminated limestones. Limestones are fine-grained, mostly composed of sub-rounded grains of calcite and a few of dolomite (Fig. 7e). Crystalline limestones are rare and reduced to small levels associated to movement between strata.

MAFIC BODIES. Mafic bodies are dikes, sills and layers of different sizes interbedded and emplaced in the metasedimentary sequence. Dikes are common in the Quebrada Guanaco Muerto area. They are subvertical, up to 7 m thick and sharply cut some sections of facies I. In the Mendocina Mine area they form layers that follow the stratification of the metasedimentary rocks. Sizes vary between 10 cm to 20 m thick, and 5 to 100 m long. Near the Mendocina Mine occurs a 40 m thick, 150 m long body interbedded in the metasedimentary sequence of facies I. This body shows a porphyritic texture in contact with the metasediments, coarsening to the centre of the body to an inequigranular texture. The borders of these bodies show

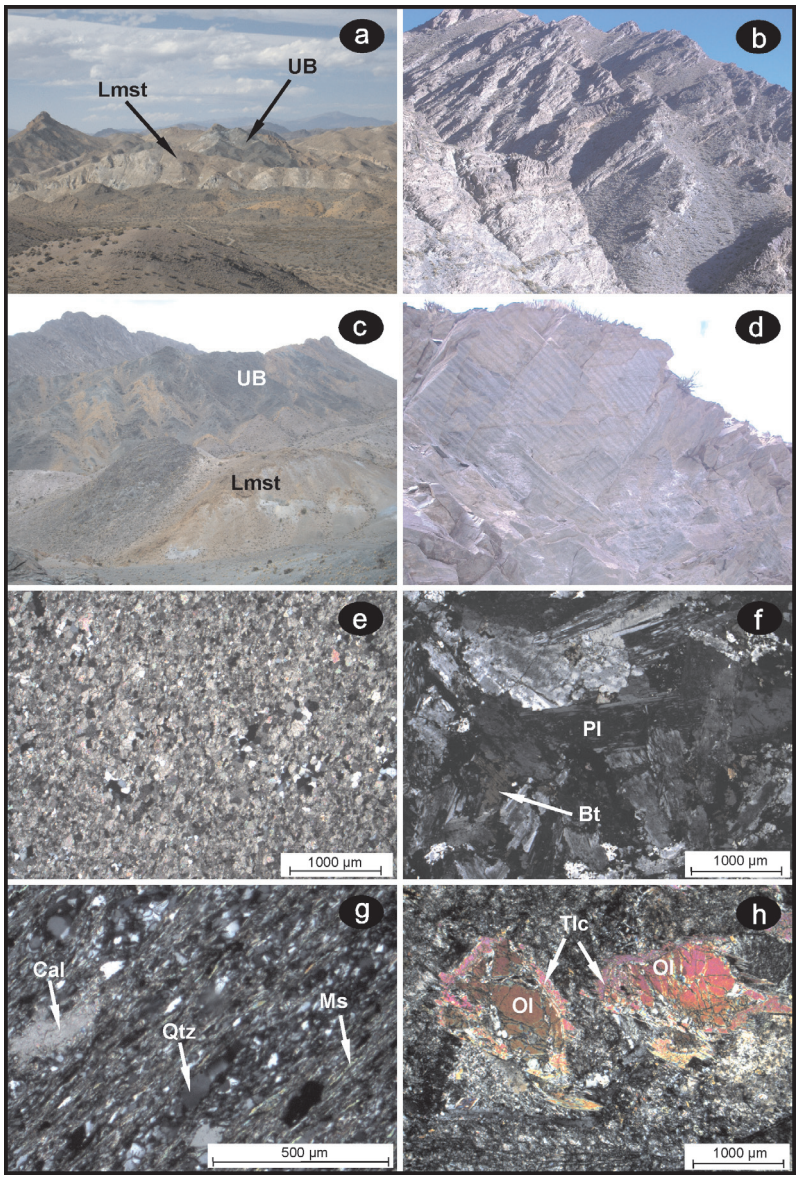

Figure 7. a) Typical outcrops of the Bonilla Complex rocks, 2 km south of the Mendocina Mine, looking north. Tertiary magmatic rocks form the peak in the left part of the picture. In the central part, there are outcrops of the Bonilla Complex, facies II and limestones (Lmst) of facies III. Behind which is the ultramafic body (UB) of Rivadavia Mine, b) Profile "a" of figure 6. Most levels are calcareous sandstones, but few basic bodies appear in this sequence. Sample B1 was taken from the middle part, in a quartz–mica rich sandstone, c) ultramafic bodies disrupted and emplaced in facies II, near Rivadavia Mine. Orange limestones (Lmst), due to the serpentinization of the ultramafic bodies are common, d) Ripple-marks in the sandstone levels from where sample X4 was selected, e) Fine-grained, laminated limestone from facies III, located 2km east of Rivadavia Mine, f) Coarse-grained gabbro from Quebrada de los Burros. Large- plagioclase (Pl) crystals and biotite (Bt) are common, g) Microphotograph of sample B6, fine-grained sandstone - siltstone, mostly composed by quartz (Qtz), micas (Ms), calcite (Cal), chlorite and few plagioclase. h) Relict olivine (Ol), surrounded talc (Tlc) and serpentine minerals, chlorite and epidote groundmass, from the Rivadavia ultrabasic body.

Figura 7. a) Afloramientos típicos de las rocas del Complejo Bonilla, 2 km al sur de la mina Mendocina, mirando al norte. Rocas magmáticos terciarias forman el pico en la parte izquierda de la imagen. En la parte central aparecen afloramientos de la facies II y calizas (Lmst) de la facies III del Complejo Bonilla. Atrás de los mismo se ubica el cuerpo ultramáfico (UB) de mina de Rivadavia, b) perfil "a" de la figura 6. La mayoría de los niveles son areniscas calcáreas, pero también alguno cuerpos básicos aparecen en esta secuencia. La muestra B1 fue tomada en la parte media, en una arenisca rica en cuarzo y mica, c) cuerpos ultramáficos disturbado ubicado en la facies II, cerca de la mina Rivadavia. Las calizas naranjas (Lmst), debidas a la serpentinización de los cuerpos ultramáficos son comunes, d) ondulitas en los niveles de arenisca donde fue tomada la muestra 4 X, e) caliza de grano fino, laminada de la facies III, ubicada a 2 km al este de la mina Rivadavia, f) gabro de grano grueso de la Quebrada de los Burros. Los cristales de plagioclasa (Pl) y biotita (Bt) son comunes, g) Microfotografía de la muestra B6, una limoarenisca de grano fino, compuesta principalmente por cuarzo (Qtz), micas (Ms), calcita (Cal), clorita y pocos plagioclasa. h) Olivino relíctico (Ol), rodeado por talco, (Tlc) y minerales del grupo de la serpentina, masa de clorita y epidota, del cuerpo ultramáfico de mina Rivadavia.

a cleavage that mimics those of the metasedimentary host rock. Layers of mafic bodies are relatively common in the facies I, west of the Mendocina Mine area.

Sills are rare and appear in the eastern part of the Quebrada Guanaco Muerto area, westward of Agua de la Cueva and in the Quebrada de los Burros (Fig. 7f). These bodies are rudely elliptical, with a long axis exceeding 150 m and minor axis of about 40 m. Most are emplaced in facies II and a few in facies I. They show sharp contact with the host rocks, cutting the stratification of the metasedimentary sequences, and seem to represent the pipes that fed the largest subvolcanic bodies, although such association was never recognized in the field. They have an intergranular texture composed by plagioclase laths (70%), biotite (10%), pyroxene (5%), apatite, illmenite and opaque minerals. Large plagioclases (1 mm long) enclose interstitial crystals of pyroxene, biotite and other minerals. There is not evidence of deformation, but alteration of plagioclases to calcite and sericite is common.

Ultramafic bodies. These rocks appears as isolated major, or as strings of minor, bodies tectonically emplaced in facies II and to a lesser extent in facies I. Those emplaced in facies II are located northwards of the Rivadavia and Mendocina Mines. An ultramafic body located 3 km NW of the Cerro El Sapo is 100 m thick, 1.3 km long and 800 m wide and is overthrusted top-to-the-west on the phyllites of facies II. Another isolated body (85 m x 250 m x 350 m) is located 1 km NE of Cerro El Sapo, but its contact with the rocks of facies II is unclear.

A string of N-S elongated bodies can be observed between Quebrada Guanaco Muerto and Quebrada de Santa Elena, over 6 km. Between the Mendocina Mine and Quebrada Guanaco Muerto appear four ultramafic bodies, the most important being one that is 1.5 km long and 400 m wide. In the Quebrada Guanaco Muerto a small, oval body shows intense foliated borders and mineral lineation indicative of top-to-the-west movement. From the Mendocina Mine to the south the string is formed by smaller bodies that follow a N340° strike and are emplaced along a strike-slip fault that intersect the Cordón de Bonilla (Fig. 4). Further south the ultramafic bodies disappear.

Another string of ultramafic bodies are located 500 m eastwards of those described above. Here bodies are more elongated (200 m long, 80 m wide) and look more affected by later deformation. The body at Rivadavia Mine is the largest in this area, with a width of 400 m. The eastern border of this string is marked by a top-to-the west overthrust of the phyllites of facies II on the ultramafic bodies. Small ultramafic bodies, possibly belonging to this string, can be observed a few kilometers west of Cerro Jagüelito. These rocks show a compact, finely grained dark texture. Due to hydrothermal alteration, the bodies are mainly composed of serpentine minerals forming a mesh of flakes with different orientations. Chlorite and talc are also abundant. Relicts of olivine and pyroxenes were recognized but are

scarce, and it is not possible to classify the rocks under the microscope (Fig. 7h). The original mineralogy can only be indirectly inferred by means of chemical analyses.

Geochemistry of the Bonilla Complex

Geochemical investigation has been carried out by analyzing 17 samples for major and trace elements of metasedimentary rocks, 13 samples of mafic rocks and 10 of ultramafic rocks. The results are listed in tables 1, 2 and 3 respectively. The analyses were conducted using INAA and ICP-MS at ACTLABS (Canada). International geostandards were used for calibration.

GEOCHEMISTRY OF THE METASEDIMENTARY ROCKS. Rocks were classified in the field and microscopically as metasandstones, metapelites and crystalline limestones plot in the Al_2O_3+Fe_2O_3-SiO_2-MgO+CaO diagram (Fig. 8a) of Pettijohn et al. (1987) in the sandstones, lutite-pelite and limestone fields, respectively. The log SiO_2/Al_2O_3-log Na_2O/K_2O diagram of Pettijohn et al. (1987) shows graywacke and lithic arenite compositions (Fig. 8b).

Diagrams and chemical analyses indicate that these lithologies show a relatively restricted range in major and trace element chemistry. Silica varies between 67 and 76 wt%, alumina between 9 and 13 wt%, and Na_2O between 0 and 6 wt%.

PROVENANCE. The relative abundance of Al_2O_3, CaO, Na_2O and K_2O, as shown on the molar-proportion diagrams (Nesbitt and Young, 1996), are consistent with typical continental alteration trends influenced by the weathering of plagioclase-alkaline feldspar to form illite-sericite (Fig. 8c).

Samples were plot on a Th/Sc vs. Cr/Th diagram (Totten et al., 2000). This plot contrasts the different proportions of continental and mafic sources. As shown in Fig. 8d, samples of the Bonilla Complex plot near the average of the upper continental crust, which is indeed near the average of granitic rocks, discarding a two-component mixing model between felsic and mafic end members. Samples are nearly coincident with those of the Guarguaraz Complex and the metasedimentary rocks of the Cordón del Portillo.

No evidence of amphiboles or pyroxenes in the original sediments can be recognized through these diagrams. Altogether, additionally, the low concentrations of MgO, Fe_2O_3 and TiO_2 suggest no contribution from mafic source rocks. Metasedimentary rocks of the Cordón del Portillo (Vujovich and Gregori, 2002) and the Guarguaraz Complex (López and Gregori, 2004) follow that trend.

The La/Sc vs. Th/Sc diagram (Totten et al., 2000) indicates that the rocks of the Bonilla Complex plot around the field of NASC (North American Shale Composite, Haskin and Haskin, 1966), are equivalent to those of the Guarguaraz Complex and the metasedimentary facies of the Portillo area (Fig. 8d).

MAJOR ELEMENT ANALYSES . Roser and Korsch (1986) have developed a bivariant tectonic discriminator for sandstones and mudstones using SiO_2/Al_2O_3 vs. K_2O/Na_2O. The fields are based on ancient sandstone-mudstone pairs, cross-checked against modern sediments from known tectonic settings, from which they differentiated sediments derived from volcanic island arcs, the active continental margin and passive margin. The Roser and Korsch (1986) tectonic diagram indicates that the samples from the Bonilla Complex are passive margin-derived, which imply that metasedimentary protoliths were derived from stable continental areas and were deposited in intra-cratonic basins or passive continental margins (Fig. 9a). Similar results were obtained for the Guarguaraz Complex by López and Gregori (2004).

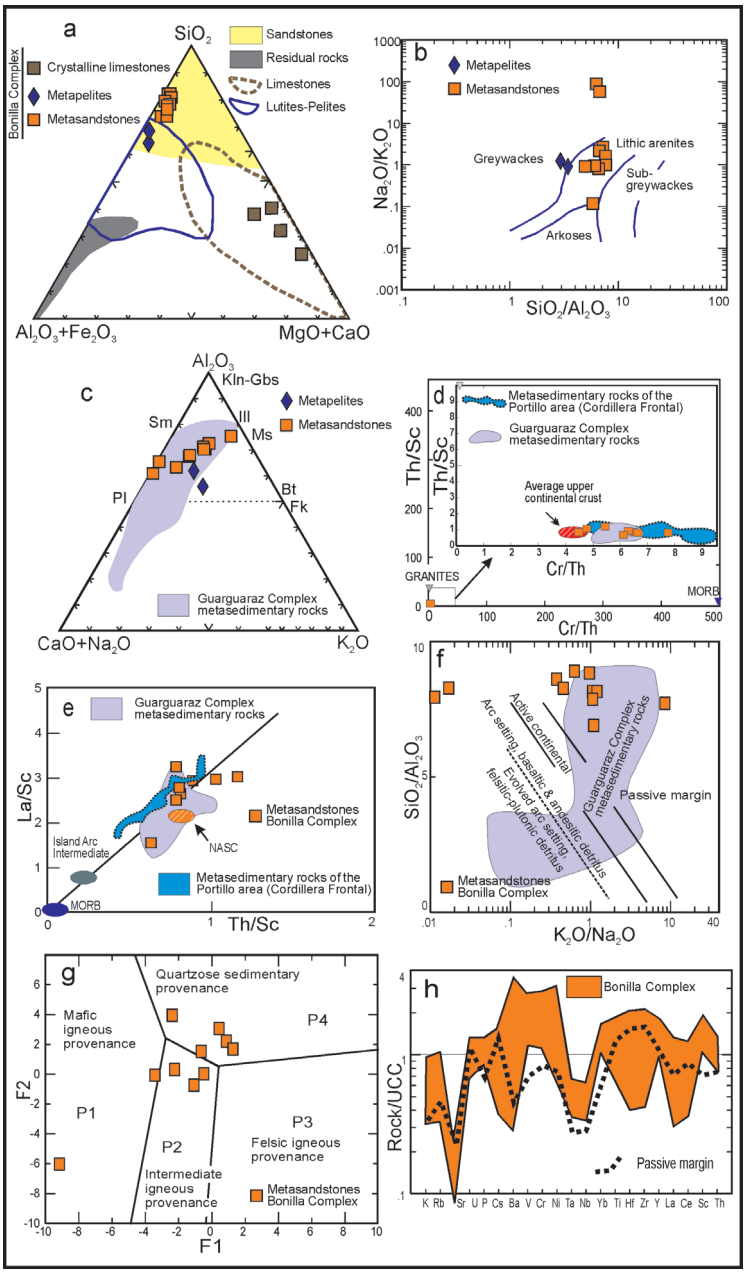

Figure 8. Chemical classification of the metasedimentary rocks according to major element analyses, plot in: a) Al_2O_3+Fe_2O_3-SiO_2-MgO+CaO diagram (Pettijohn et al. 1987), b) Na_2O- Fe_2O_{3t}+SiO_2-K_2O diagram (Blatt et al. 1980), c) CaO+Na_2O-Al_2O_3-K_2O triangle (modified from Nesbitt and Young, 1996), d) Cr/Th vs. Th/Sc diagram (Totten et al. 2000), showing the field for Upper Continental Crust (average), e) Th/Sc vs. La/Sc diagram (Totten et al. 2000), showing the field for NASC (Haskin and Haskin, 1966), f) Depositional setting of the metasedimentary rocks from the SiO_2/Al_2O_3 vs. K_2O/Na_2O discrimination diagram (Roser and Korsch, 1986), g) Provenance of the protoliths on a Roser and Korsch (1988) discrimination diagram, using Al_2O_3, TiO_2, Fe_2O_{3t}, MgO, CaO, Na_2O and K_2O, and h) Trace element plot normalized to upper continental crust (Taylor and McLennan, 1985) of the Bonilla Complex metasedimentary rocks and average greywackes from passive margin settings.

Figura 8. Clasificación química de las rocas metasedimentarias de acuerdo con los análisis de elementos principales, graficados en a) diagrama Al_2O_3 + Fe_2O_3-SiO_2-MgO + CaO (Pettijohn et al. 1987), b) diagrama Na_2O - Fe_2O_3t + SiO_2-K_2O (Blatt et al 1980), c) triángulo CaO + Na_2O-Al_2O_3-K_2O (modificado de Nesbitt y Young, 1996), d) diagrama Cr/Th vs Th/Sc (Totten et al 2000), que muestra el campo de la corteza continental superior (promedio), e) diagrama Th/Sc vs La/Sc (Totten et al., 2000) que muestra el campo de NASC (Haskin y Haskin, 1966), f) condiciones de depositación de las rocas metasedimentarias a partir del diagrama de discriminación de SiO2/Al2O3 vs K_2O/Na_2O (Roser y Korsch, 1986), g) procedencia de los protolitos en un diagrama de discriminación de Roser y Korsch (1988), utilizando valores de Al_2O_3, TiO_2, Fe_2O_3t, MgO, CaO, Na_2O y K_2O y h) diagrama de oligoelementos normalizada a la corteza continental superior (Taylor y McLennan1985) de las rocas metasedimentarias del Complejo Bonilla y de grauvacas promedio de márgenes pasivos.

The discriminant functions of Roser and Korsch (1988), using Al_2O_3, TiO_2, Fe_2O_3t, MgO, CaO, Na_2O and K_2O contents as the variables, were designed to discriminate between four sedimentary provenance types: mafic (P1, ocean island arc source), intermediate (P2, mature island arc), felsic (P3), and recycled (P4, granitic-gneissic or sedimentary source areas).

The majority of the metasedimentary rocks of the Bonilla Complex, as well as the Cordón del Portillo metasedimentary rocks, plot within the P4 (recycled) and P2 fields (Fig. 8g), supporting the interpretation that they are derived from a craton interior or a recycled orogenic terrane.

NORMALIZED MULTI-ELEMENTS PLOTS. Trace-element plots are useful for tectonic setting discrimination, although some diagrams are influenced by sorting, heavy mineral content and the proportion of mafic input.

Floyd et al. (1991) proposed the use of the full range of elements for tectonic setting discrimination, in order to avoid the spreading of rock series across geologically unrelated tectonic fields. Upper continental crust-normalized multi-element plots of Taylor and McLennan (1985) were used by Floyd et al. (1991) to compare the compositions of graywackes and sandstones from different tectonic environments: passive margin, oceanic island arc and continental arc and active margin. The elements are arranged (from left to right) in order of decreasing oceanic residence times, and comprise a mobile group (K-Ni) and a relatively stable group (Ta-Th). Diagrams of the Bonilla Complex were compared with average graywackes from the above cited settings. A notable concordance can be observed (Fig. 8h) with graywackes deposited in passive margin environments.

RARE EARTH ELEMENT ANALYSES. Rare earth elements are considered to be immobile under weathering, diagenesis and up to moderate levels of metamorphism and, for clastic sediments, its concentrations is equivalent to those of the source rocks.

In the REE spiderdiagram (Fig. 9a), rocks of the metasedimentary assemblage show similar patterns to PAAS rocks (Post-Archean Average Australian Sedimentary, McLennan, 1989) and NASC (North American Shale Composite, Haskin and Haskin, 1966). They are between 80-200 times LREE enriched, with a nearly flat HREE pattern 10-30 times enriched, and with small negative Eu anomalies. They are nearly coincident with the metasedimentary rocks of the Guarguaraz Complex and the Portillo area (Vujovich and Gregori, 2002).

The geochemical signature of REE suggests that the rocks of the Bonilla Complex are composed of sediments derived from an old upper continental crust and/or young differentiated arc material. According to McLennan et al. (1990), these provenance components are found in several basin types, but rarely in a fore-arc setting.

GEOCHEMISTRY OF THE MAFIC ROCKS

MAJOR ELEMENT ANALYSES. Metabasites from the Bonilla Complex have SiO_2: 41- 51 wt%,

Al_2O_3: 12-18 wt%, and MgO: 3-9 wt%, classifying as them picrobasalts, basalts, basaltic andesites and basanites in the TAS diagram (Fig. 9b) of Le Maitre et al. (1989), showing a more restricted composition when compared with samples of the Guarguaraz Complex.

The TAS vs SiO_2 diagram (not shown) indicates an alkaline composition, overlapping in part with the composition of the Guarguaraz Complex and Metales belt metabasites (Gregori and Bjerg, 1997). A tholeiitic behavior can be recognized in the AFM diagram of Irvine and Baragar (1971), which follows a similar but more restricted trend to the samples of the Metales belt metabasites (Fig. 9c).

In the Ni-MgO diagram, samples of the Bonilla Complex lie on the field of the Guarguaraz Complex (Fig. 9d) and also over the dikes of the Troodos complex and the E-MORB basalts of the Lau basin. In a FeOt/MgO-TiO_2 diagram (Fig. 9d), the mafic rock assemblages exhibit few correlation with the Reykejanes Ridge basalts (Tarney et al., 1979) and other rocks used for comparison, possibly due to alteration.

TRACE ELEMENTS. Trace element concentrations were normalized to EMORB (not shown), according to Sun and McDonough (1989). Most samples have a very similar pattern for elements ranging from Sr to Yb, displaying EMORB signatures. All samples show Pb anomalies of 8-20 times over EMORB, indicating crustal (sediment) contamination.

Rb, Nb and K are scattered, possibly due to mobility in an aqueous phase (Pearce, 1983). The LILE have the following maximum concentrations: Ba (703 ppm), Sr (920 ppm), Rb (68 ppm). Values for HFSE are: Ta (4.9 ppm), Nb (63 ppm), Hf (8 ppm) and Th (6 ppm). Cs shows a higher concentration than EMORB. In the Th/Yb vs. Ta/Yb diagram (Pearce, 1983), which differentiates between subduction-related basalts and oceanic basalts, samples display compositions ranging between MORB and EMORB (Fig. 9e) with mixed signatures of a depleted and enriched mantle source, excluding arc signatures.

RARE EARTH ELEMENTS. Compared with chondrite composition, most samples are 10 to 100 times LREE enriched with small positive Eu anomalies, due to plagioclase fractionation (Fig. 9f).They can be classified as EMORB. Samples of the Bonilla Complex have a similar composition to the Precordilleran Ordovician basalts (Kay et al., 1984), the Guarguaraz Complex and the Metales Belt. (Gregori and Bjerg, 1997; López and Gregori, 2004).

GEOCHEMISTRY OF THE ULTRAMAFIC ROCKS

MAJOR ELEMENTS. Ultramafic rocks have SiO_2: 38-41 wt%. They plot near the FeOt component of the CaO-FeOt-Al_2O_3 system, indicative of the absence of remobilization in these rocks. Also they plot away from the ultramafic rocks of the Guarguaraz Complex, which are strongly affected by deformation and alteration due to the presence of intrusive acidic bodies (Fig. 9g). In the Px-Pl-Ol diagram (Yoder and Tilley, 1962) they classify as Pl-bearing ultramafic rocks (Fig. 9h), although they cannot be recognized in thin section. These samples cannot be compared with the samples of the Guarguaraz Complex, which are richer in plagioclase.

RARE EARTH ELEMENTS. In a chondrite-normalized REE plot (Fig. 10a), samples with the highest REE concentration show 100 times enrichment over chondrite in LREE. These rocks display a pattern more characteristic of a plagioclase-rich gabbro. The second group shows nearly flat patterns, slightly enriched over chondrite. Some have a small negative Eu anomaly and other some irregularities in Tb, Dy and Ho concentrations, possibly due to hydrothermal alteration.

Detrital zircon U-Pb geochronology of the Bonilla Complex

Two detrital zircon samples from the Bonilla Group were analyzed for geochronology at the Arizona LaserChron Center, Department of Geosciences, University of Arizona using the procedures described by Gehrels et al. (2008). Both belong to facies I. Sample B1 is located at 32°35´56´´ S-69°13´47´´ W in the Quebrada Santa Elena and corresponds to a quartz–mica metasandstone (Fig. 6, profile a). A total of 98 zircons from sample B1 were analyzed. A concordia diagram is shown in Figure 10b. A large part of the zircons (Table 4) were formed during an age interval of 0.7–0.5 Ga. (Fig. 10c). Other, less pronounced, age accumulations can be found at 1.5–1.0 Ga and around 2 Ga. There are single ages at 2.4 Ga and 2.8 Ga.

Sample X4 is a sandstone of the lower part of the sequence located west of Portillo de Bonilla at 32° 39´13´´ S-69°13´14´´ W and also correspond to a quartz–mica metasandstone of facies I. Results were plot in the concordia diagram of Figure 10d. Zircons from sample X4 provided 96 analyses, which define six dominant ages of 592 Ma, 656 Ma, 713 Ma, 1135 Ma, 1242 Ma and 1950 Ma. Two grains give ages of ca. 2.6 and 2.8 Ga (Fig. 10e). This apparently "oldest" sample, in which zircons with ages between 1,135 and 1,245 Ma forms an important population, may be considerably younger than 592 Ma. Instead, in sample B1 younger zircons (Cambrian) are more abundant, coincident with the diminution of the 1,012-1,220 Ma population, possibly representing a younger portion of the sedimentary pile.

Therefore the maximum age of deposition is 592 Ma, (Fig. 10c), indicating Ediacaran times (International Commission on Stratigraphy, 2009). Microfossils recognized in the Cortaderas and Bonilla areas yielding ages between the uppermost Precambrian and the Devonian, but Middle to Upper Ordovician ages (Fig. 11c) were considered more appropriate by Davis et al. (1999).

Rapela et al. (1998a) reported U-Pb SHRIMP detrital zircon ages from a high-grade metapelitic migmatite in the Rio del Suquía area of the Sierras de Córdoba, with ages of 600–650 and 800–1000 Ma and two grains older than 1400 Ma.

In the Sierras Pampeanas of San Luis, Sims et al. (1998) reported U-Pb SHRIMP analyses of detrital zircon grains from four high-grade metasedimentary rocks, which show clusters of ages ranging between ~500–700 and 900–1100 Ma, and more isolated results between 1.45 and 2.5 Ga.

Schwartz and Gromet (2004) analyzed a sand/silt layer within pelitic gneisses located near La Puerta, and a quartz-rich layer in the Tuclame Formation of the Sierras de Córdoba. Of the 19 grains analyzed, 5 yielded ages between 550 and 750 Ma, 2 around 850 Ma, 11 yielded ages between 950 and 1050 Ma, and 1 grain shows an age of approximately 1900 Ma.

The La Cébila Formation, located in southwestern part of Sierra de Ambato, Catamarca Province (Fig. 10f), and constituted by quartz-feldspathic metasedimentary rocks was sampled Rapela et al. (2007). The age pattern is dominated by Neoproterozoic zircons with a peak at 640 Ma, and a subpopulation at~530 Ma. Minor peaks occur at 790 Ma, 1.77 and 2.1 Ga with minor contributions of Mesoproterozoic and Archean ages.

The Ancasti Formation (Willner et al., 1983) of the Sierras Pampeanas de Catamarca is composed of banded schists. Rapela et al. (2007) reported ages of detrital zircons of this unit. They have a bimodal age distribution, dominated by Mesoproterozoic (1100–960 Ma) and Neoproterozoic (680–570 Ma) components, with the youngest grains indicating a Neoproterozoic depositional age (≤570 Ma). There are minor components represented by Late Paleoproterozoic concordant grains (~1.85 Ga), with absence of concordant zircons in the 2.02–2.26 Ga interval (Fig. 10g).

In northern Patagonia, the El Jagüelito and Nahuel Niyeu formations have Cambrian trace fossil content typical of the Sierras Pampeanas of northern and central Argentina (González et al., 2002). Zircon ages from the El Jagüelito Formation (Fig. 10h) have their main provenance at 535–540 Ma, suggesting Early Cambrian deposition (Pankhurst et al., 2006). Such a pattern of age distribution is nearly coincident with sample B1 of the Bonilla Complex.

The detrital zircons of the metamorphic rocks known as Guarguaraz Complex, in the Cordillera Frontal (Willner et al., 2008), yield ages of 555, 581, 935, 1092, 1228, 1361, 1794, 1893, 2505 and 2788 Ma (Fig. 11a). This sample shows coincidences with sample X4 of the Bonilla Complex which also displays ages of 592, 1135 Ma, 1242, 1950, 2600 and 2800 Ma.

The Puncoviscana Formation of northwestern Argentina (Fig. 11b) shows important contributions at 523, 534, 551, 583, 612, 623, 650, 979, 1000, and minor at 2370, 2513 and 2590 Ma. (Adams et al., 2011).

The bimodal pattern of the Bonilla Complex, with peaks at 1.5–1.0 Ga and 0.5-0.7 Ga, is coincident with the pattern of the Puncoviscana Formation and also with the metasedimentary rocks of the Sierras Pampeanas of Catamarca, Córdoba and the Sierra de San Luis (Sims et al., 1998; Pankhurst et al., 2000; Schwartz and Gromet, 2004; Escayola et al., 2007, Steenken et al., 2006; Adams et al., 2011), indicating that the source area for the whole Pampean belt and the Bonilla Complex was dominated by Meso- and Neoproterozoic components. The presence of ~1.8 Ga Late Paleoproterozoic zircons in the B1 sample and ~1.9 Ga zircons in the X4 sample has been also observed in the Sierras de Córdoba (Schwartz and Gromet, 2004) and in the Sierra de Ancasti (Rapela et al., 2007).

According to Pankhurst et al. (2006), the low-degree metamorphic rocks of the northeastern North Patagonian Massif appear to have been originally deposited as sediments on a continental shelf at the southern margin of Gondwana, underlain by basement rocks that were already part of the Gondwana continent by Cambrian times.

All units show important contributions around 500 Ma and 1.0 Ga, with peaks at 2.2, 2.3 and 2.65 Ga. Comparison of samples B1 and X4 of the Bonilla Complex, with zircon patterns of the Cambrian low-grade metasediments of NE Patagonia (Pankhurst et al., 2006) is straightforward.

The contributions at ~720, ~713 Ma recognized in both samples are consistent with the A-type magmatism (774 ± 6 Ma) detected by Baldo et al. (2005) in Sierra de Pie de Palo, and with the N and EMORB rocks (Gregori and Bjerg, 1997) of the Guarguaraz Complex, which yielded an age of 655 ± 76 Ma. (López de Azarevich et al. 2009). This magmatism represents evidence of crustal rifting during the break-up of Rodinia.

Discussion

PROVENANCE AND CORRELATION. Petrographic and geochemical studies reveal that the protoliths of the Bonilla Complex were dominantly quartzitic and feldspathic in nature. Architectural sedimentary arrangements indicate that these rocks were deposited in internal and external platform environments, whereas measurements of cross-stratification and festoons show paleocurrents from the northeast and southeast (actual coordinates).

The geochemical signature of the protolith, which is typical of felsic to intermediate upper continental crustal rocks, suggests the presence of an older exhumed basement eastwards (actual coordinates) of western Precordillera. Candidates are the actual Sierras

Pampeanas of Córdoba, San Luis and San Juan.

Extensional setting for the deposition of the Bonilla Complex is also recorded by the geochemical signatures of interbedded mafic sills and dikes.

Metasedimentary rocks with similar characteristics can be recognized in western Precordillera (Cortaderas area, Davis et al., 2000). There, in the marine sequences, were emplaced microgabbros (576 ± 17 Ma), gabbros and ultramafic rocks (450 ± 20 Ma) and mafic flows and sills (418 ± 10Ma).

In the Cordillera Frontal (Fig. 1), the Guarguaraz Complex is composed of calcareous metasiltstones, metasandstones, schists, phyllites and marbles, interbedded with metadiabases and ultramafic bodies. Dessanti and Caminos (1967), Caminos (1993) and López and Gregori (2004) considered the Bonilla Complex as being equivalent to the Guarguaraz Complex.

The correlation of the Bonilla Complex with the Guarguaraz Complex and rocks in the Cortaderas area suggests that these units were accumulated in an Ediacaran to Middle Cambrian passive margin (Fig. 11c). The maximum depositional age of the Bonilla Complex (592 Ma), the Guarguaraz Complex (556 Ma) and the Cortaderas Formation (early to 576 ± 17 Ma, see above) are coherent with the existence of such an open marine environment in the western (actual coordinates) margin of Gondwana. The presence of *Bavlinella* and *Leiosphaeridia* in the Guarguaraz Complex (López, 2005), comparable with palynomorphs of the Corumbá Group (Misi et al., 2006), supports an Ediacaran age.

Therefore, an open marine basin was developed in the western border of the Gondwana margin considerably earlier (~ 50 Ma) than the supposed detachment (~524-~510 Ma, Thomas et al., 2001) of the Cuyania Terrane from the Ouachita embayment in the Laurentia margin. Indeed, these ages are consistent with the younger pulse of volcanic (570-560 Ma) and intrusive activity (680 ± 4 Ma-562 ± 5 Ma), that led to continental separation and the opening of the Iapetus Ocean (Aleinikoff et al., 1995; Tollo et al., 2004).

GONDWANAN SOURCE OF ~500-600 MA ZIRCONS. In the Bonilla Complex, zircons population formed in between 0.7 and 0.5 Ga is coincident with the Brazilian or Pampean tectonic event. Prominent peaks are at 510, 592, 611, 656, 713 and 720 Ma. Secondary can be distinguished at 1012-1220 Ma, 1135 Ma, and 1242 Ma.

According to Schwartz and Gromet (2004), the detrital zircons from the metasedimentary assemblages of the Sierras de Córdoba display age distributions which point to typical Gondwana contributions (Brazilian: 500–700 Ma; Late Mesoproterozoic ~1000 Ma) and Transamazonian 1900–2200 Ma) provenances.

The Neoproterozoic Brazilian–Pan-African orogeny was a major amalgamation event in the development of Western Gondwana, and Neoproterozoic plutonic bodies are widespread in the Atlantic Shield region of eastern South America. The Brazilian belts, dated 0.53 to 0.93 Ga, are prevalent over the Brazilian Shield and resulted from the convergence of the Amazonia, the São Francisco craton and other crustal blocks during the final assembly of Gondwana (e.g. Pimentel et al., 1999; Brito-Neves et al., 1999; Kröner and Cordani, 2003; Veevers, 2004; Vaughan and Pankhurst, 2008; Cordani et al., 2009).

Thus, both the magmatic activity and the exhumational/erosional history of these regions support the idea that the São Françisco, Borborema and Mantiqueira provinces provided detritus during the development of marginal basins to South America for the Late Neoproterozoic to Early Cambrian period.

Further west in central Brazil, the western Goiás massif in the Tocantins Province hosts another important collection of intrusive granitic plutons of Late Neoproterozoic–Early

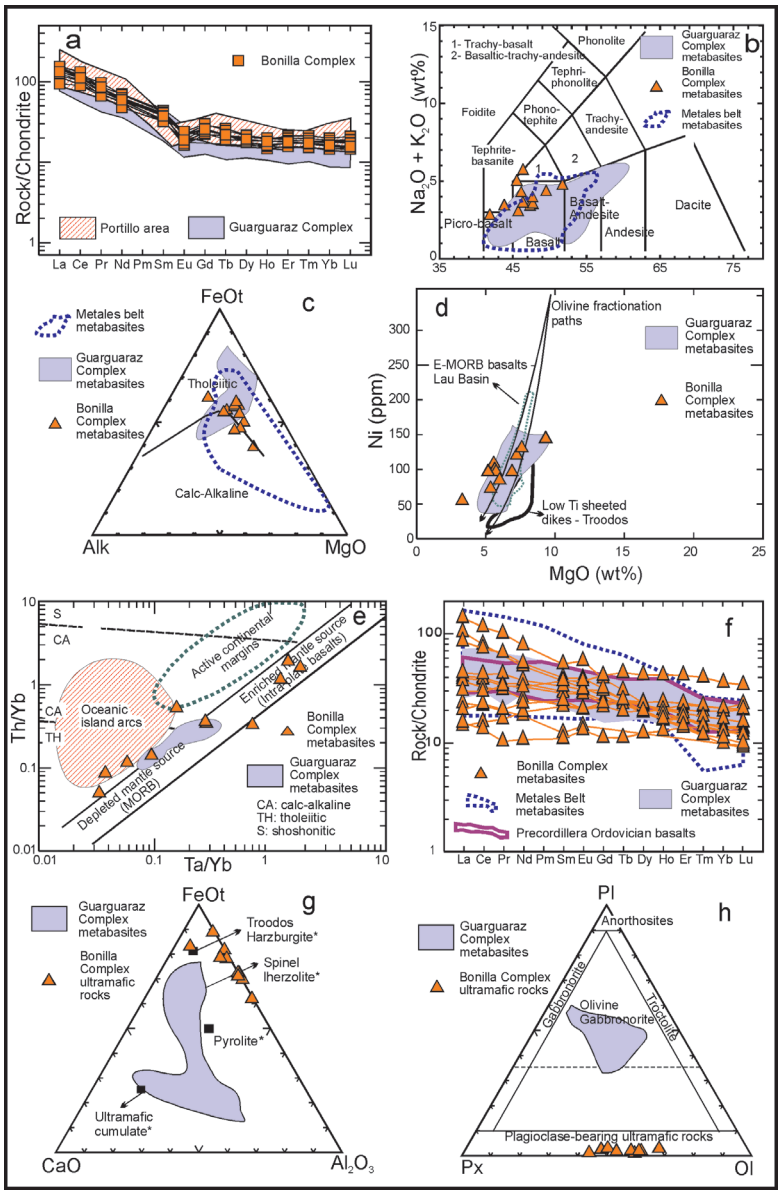

Figure 9. a) Rare Earth element plot (chondrite normalized) comparing the metasediments from the Bonilla Complex with the Guarguaraz Complex and the metasedimentary rocks of the Portillo area, b) Major element classification using TAS-SiO_2 diagram (LeMaitre et al., 1989), c) AFM plot of Bonilla Complex samples showing a tholeiitic trend, d) MgO-Ni discrimination plot indicating evolution trend by fractional crystallization of Ol. Comparison with Ol fractionation paths and Lau-basin EMORB field (Volpe et al., 1988), and Troodos low-Ti sheeted dikes (Bednarz and Schmincke, 1994). e) Th/Yb vs Ta/Yb diagram (Pearce, 1983), showing mixed component of depleted and enriched mantle source, discarding an arc-related setting, f) Rare earth elements chondrite-normalized plot (Sun and McDonough, 1989) of samples from the Bonilla Complex. Comparison with Precordillera Ordovician basalts (Kay et al., 1984) and metabasites from Metales Belt (Gregori and Bjerg, 1997), and Guarguaraz Complex(López and Gregori, 2004), g) CaO-FeOt-Al_2O_3 ternary plot showing the absence of the CaO component, and h) Px-Pl-Ol diagram (Yoder and Tilley, 1962), indicating scarce amount of plagioclase in the ultramafic rocks.

Figura 9. Gráficos de tierras raras normalizados a condrita, a) comparando los metasedimentos del Complejo Bonilla con los del Complejo Guarguaraz y las rocas de la zona del Cordón del Portillo, b) clasificación mediante elementos mayores utilizando el diagrama SiO_2- TAS (LeMaitre et al., 1989), c) diagrama AFM de muestras del Complejo Bonilla mostrando una tendencia tholeítica, d) diagrama de discriminación MgO-Ni mostrando diferentes evoluciones debido a la cristalización fraccionada de Ol. Campo EMORB de la cuenca Lau (Volpe et al., 1988) y diques con rocas de bao contenido de Ti en Troodos (Bednarz y Schmincke, 1994). e) diagrama Th/Yb vs. Ta/Yb (Pearce, 1983), mostrando componentes mixtos de manto enriquecido y empobrecido, descartando componentes de un ambiente de arco magmático, f) diagrama de elementos de tierras raras normalizados a condrita (Sun y McDonough, 1989) de muestras del Complejo Bonilla. Comparación con basaltos ordovícicos de Precordillera (Kay et al., 1984), metabasitas de la Faja Metales (Gregori y Bjerg, 1997) y el Complejo Guarguaraz (López y Gregori, 2004), g) diagrama ternario CaO-FeOt-Al_2O_3 mostrando la ausencia de CaO en las rocas, y h) diagrama Px-Pl-Ol (Yoder and Tilley, 1962), indicando escasa cantidad de plagioclasa en las rocas ultramáficas.

Cambrian age.

The presence of Late Neoproterozoic plutonic bodies undergoing uplift and denudation between 580 and 460 Ma fits remarkably well with detrital zircon data from sediments in the Puncoviscana Formation, the rocks of the Sierras Pampeanas, the Bonilla Complex and the low-degree metamorphic rocks of northern Patagonia.

Furthermore, Chew et al. (2008) proposed that a Neoproterozoic (Brazilian) active margin belt is buried under the present-day Andean Belt, according to the U–Pb ages of detrital and inherited zircons from sedimentary and granitoid rocks of the central to northern Andean area.

Late Neoproterozoic postorogenic Brazilian belts such as the Tucavaca belt south of the Sunsás belt and the Araguia–Paraguay belt (both 0.5- 0.6 Ga; Litherland and Bloomfield, 1981; Pimentel et al., 1999) as well as the Sierras Pampeanas basins in northern Argentina (0.52- 0.56 Ga; Rapela et al., 1998a) were probably formed during the rifting of eastern Laurentia from southwestern Gondwana and the opening of the Iapetus Ocean (Grunow et al., 1996; Trompette, 2000; Ramos, 2008; Cordani et al., 2009).

The Mesoproterozoic detrital zircons would have been from the southwestern margin of the Amazonian craton, which is marked by three belts: the Sunsás belt, the Aguapeí belt and the Nova Brasilândia belt of roughly 0.95 to 1.28 Ga (e.g. Litherland et al., 1989; Tohver et al., 2004; Boger et al., 2005; Santos et al., 2008; Vaughan and Pankhurst, 2008; Cordani et al., 2009).

In the Sierras Pampeanas of Santiago del Estero Province, located 400 km northeast of Bonilla Complex outcrops a Cambrian magmatism is also widely represented. The Ambargasta Batholith yielded ages of 627 ± 27 Ma, 628 ± 30 Ma and 523 ± 4 Ma (Rb-Sr, Castellote, 1985, Millone et al. 2003). In hornfels of La Clemira Formation, Kouhkarsky et al. (1999) reported an age of 567 ± 16 Ma (K/Ar, whole rock). Llambías et al. (2003) determined a U-Pb age in zircon of 684^{+22}_{-14} Ma for the ignimbritic rocks of La Lidia Formation cropping out east of the Ambargasta Batholith. The rhyolitic rocks of the Cerro de los Burros yielded a Rb-Sr age of 607 ± 7 Ma (Millone et al. 2003).

Conventional U-Pb dating in zircons of the Güiraldes Thondhemite, from the Sierras Pampeanas of Córdoba Province yielded an age of 645 ± 9 Ma , whereas El Pilón Granodiorite give 707 ± 14 Ma (Rapela et al*.,* 1998b)., Rapela et al. (2005) also dated cores of detrital igneous zircons from a para-amphibolite from the Difunta Correa metasedimentary sequence crop out in the Sierra Pampeanas de Pie de Palo. They obtained ages between 580 Ma and 620 Ma, considered as derived from Gondwanan areas. See also van Staal et al. (2011) and Mulcahy et al. (2007).

Further south, in the Sierras Pampeanas of San Luis Province, the Paso del Rey Granite was dated in 608^{+26}_{-25} Ma by von Gosen et al. (2002). The Nogolí Complex, located in

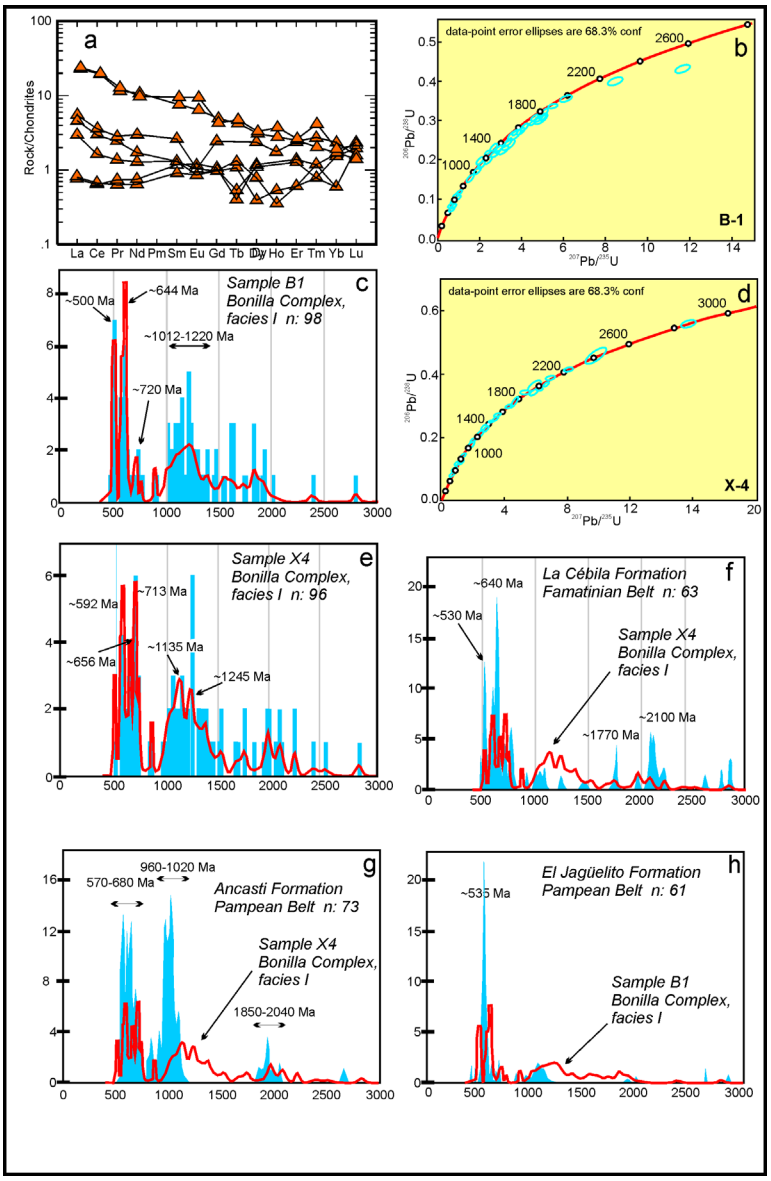

Figure 10. a) REE chondrite-normalized spidergrams (Sun and McDonough, 1989) that shown samples with enrichment characteristic of a plagioclase rich gabbro, and others with absence of such a behavior, b) $^{206}Pb/^{238}U$ vs. $^{207}Pb/^{235}U$ concordia diagram for sample B-1, c) U–Pb zircon provenance age patterns for metasedimentary sample B-1 from Bonilla Complex. The curves in the diagram are relative probability trends based on the preferred age derived from individual measurements, which are also shown. $^{206}Pb/^{238}U$ ages for values less than 1000 Ma were used. For ages 1 Ga or more $^{206}Pb/^{207}Pb$ ages were used, d) $^{206}Pb/^{238}U$ vs. $^{207}Pb/^{235}U$ concordia diagram for sample X-1, e) U–Pb zircon provenance age patterns for metasedimentary sample X-1 from Bonilla Complex. The curves in the diagram are relative probability trends based on the preferred age derived from individual measurements, which are also shown. $^{206}Pb/^{238}U$ ages for values less than 1000 Ma were used. For ages 1 Ga or more $^{206}Pb/^{207}Pb$ ages were used, f) Comparison between La Cébila Formation (Sierras Pampeanas) and sample X4 of Bonilla Complex, g) Idem for the Ancasti Formation (Sierras Pampeanas), and sample X4 of Bonilla Complex, h) Diagram for the El Jagüelito Formation (Northern Patagonia), and sample B1 of Bonilla Complex.

Figura 10. a) diagramas de tierras raras normalizadas a condrita (Sun y McDonough, 1989) que muestran ejemplos con enriquecimiento característico de un gabro rico en plagioclasa y otros con la ausencia de tal comportamiento, b) diagrama concordia $^{206}Pb/^{238}U$ b) vs $^{207}Pb/^{235}U$ de la muestra B-1, c) diseño de edades U–Pb de circones para la muestra B-1 del Complejo Bonilla. Las curvas en el diagrama son tendencias de probabilidad relativa basada en la edad preferida derivada de mediciones individuales, que también se muestran. Se utilizaron las edades $^{206}Pb/^{238}U$ para valores de menos de 1000 Ma. Para las edades 1 Ga o más fueron usadas edades $^{206}Pb/^{207}Pb$, d) diagrama concordia $^{206}Pb/^{238}U$ vs $^{207}Pb/^{235}U$ de la muestra X-1, e) diseño de edades U–Pb de circones de la muestra X 1 del Complejo Bonilla. Las curvas en el diagrama son tendencias de probabilidad relativa basada en la edad preferida derivada de mediciones individuales, que también se muestran. Se utilizaron las edades $^{206}Pb/^{238}U$ para valores de menos de 1000 Ma. Para las edades 1 Ga o más se usaron edades $^{206}Pb/^{207}Pb$. f) comparación entre la Formación La Cébila (Sierras Pampeanas) y la muestra X 4 del Complejo Bonilla, g) ídem para la Formación Ancasti (Sierras Pampeanas) y la muestra X 4, h) ídem para la Formación El Jagüelito (Patagonia Norte) y la muestra B1 del Complejo Bonilla.

western part of these sierras yielded an U-Pb age of 554 ± 4.8 Ma in gneisses (Vujovich and Ostera, 2003).

Consequently, the most proximal source of the Pampean zircons of the Bonilla Complex are the Sierras Pampeanas, located immediately east (actual coordinates). Both analyzed samples and therefore the sequences of this unit were formed by a major input of detritus from a Brazilian-Pampean-age source.

LAURENTIAN SOURCES OF ~500-600 MA ZIRCONS. In order to explain the Neoproterozoic igneous zircons found in the El Quemado Formation (ca. 630–550 Ma) outcropping in the Sierra de Pie de Palo, Naipauer et al. (2010) have cited the magmatic activity due to rifting of eastern Laurentia from western Gondwana during Cambrian times (Cawood and Nemchin, 2001; Cawood et al., 2001). In the area analyzed by Cawood and Nemchin (2001), the Newfoundland Appalachians, the rifting event is documented by several rift sequences including the South Brook, Summerside and Blow-Me-Down Brook formations. The first one showed only one zircon with an age of 572 ±14 Ma, whereas the second yielded ages of 586 ± 11 Ma (two zircons), 628 ± 12 Ma (two zircons) and 760 ± 40 Ma (one zircon). The Neoproterozoic detrital zircons are possibly associated with rift-related igneous activity which occurred from 760 Ma to 550 Ma (Cawood et al., 2001). As expected, the three above mentioned formations have ~ 1Ga age zircon populations appropriated for the Grenvillian basement they cover. The South Brook and Blow-Me-Down Brook formations have an important population of zircons with ages between 2.8 and 2.6 Ga. These were assigned to the large scale magmatic activity in the Superior craton and were also recognized in the Trans-Hudson, Penokean, Yavapai and Mazatzal orogens amongst others.

The known phases of silicic rift-related igneous activity within the orogeny are only from the U.S. Appalachians, located more the 2,000 km south. The Catoctin Formation outcrops from southern Pennsylvania to central Virginia (Aleinikoff et al., 1995), and consists mainly of tholeiitic flood metabasalt. At South Mountain, Pennsylvania, it is represented by 520 m of metarhyolites with interbedded metapelitic rocks (170 m). In the Blue Ridge anticlinorium, Virginia, the formation shows a lower part, 500 m thick, composed of metabasalt breccias, whereas the upper part, 2 km thick, is dominated by metabasalts, some of them referred to as subaqueous pillowed flows (Kline et al., 1987). Samples from the metarhyolites yielded ages from 564.3 ± 9.3 Ma to 801 Ma indicating inherited zircons, including ages of 648 Ma to 601 Ma. The ages from felsic dikes, that possible feed the metarhyolites yield a zircon age of 571.5 ± 4.7 Ma (Aleinikoff et al., 1995).

The Mount Roger Formation outcrops in southwestern Virginia, North Carolina and Tennessee. It is composed of 300 m thick, low-silica rhyolite lava flows of the Buzzard Rock Member, followed by a 750 m thick Whitetop Rhyolite Member that consists of high-silica, phenocryst-poor rhyolitic lava flows. The upper part, the Wilburn Rhyolite Member, is

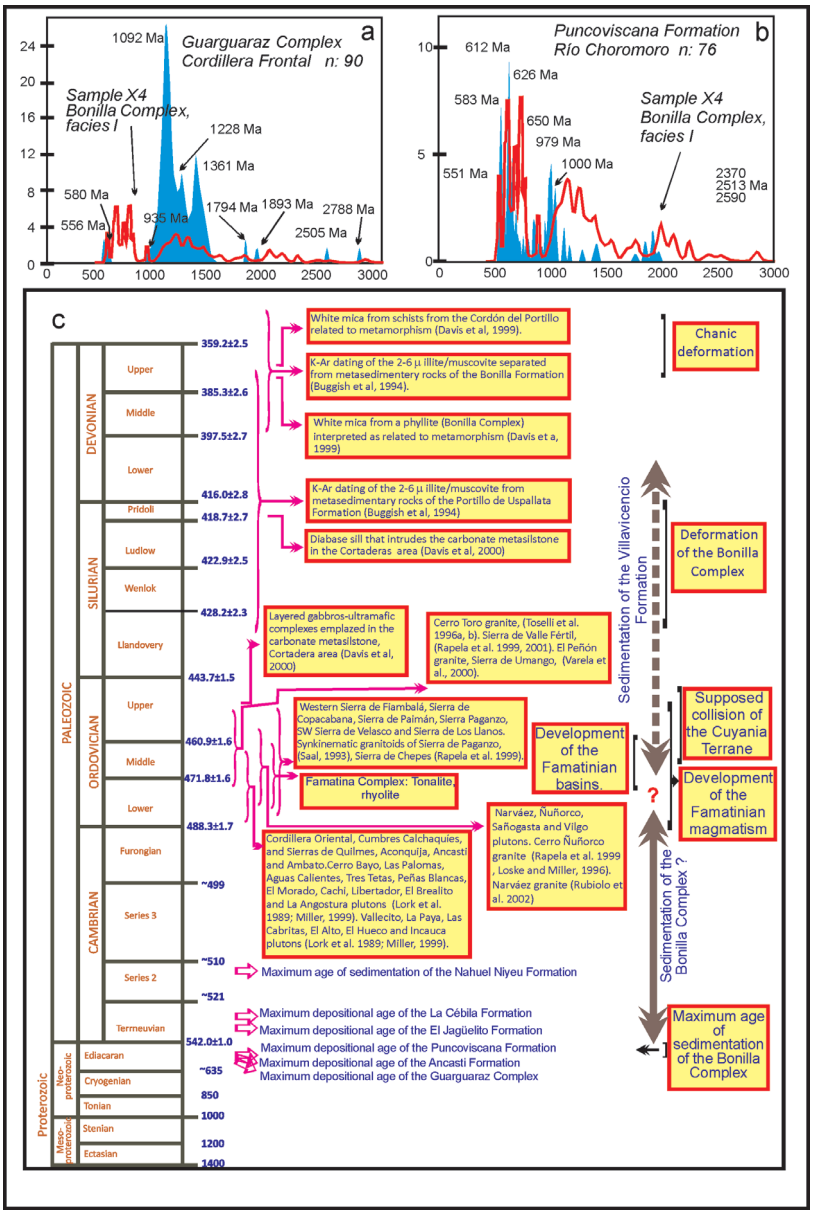

Figure 11. a) Diagram showing age results for the Guarguaraz Complex (Cordillera Frontal), and sample X4 of the Bonilla Complex, b) Idem with the Puncoviscana Formation, c) Chronological chart showing significant geological events during Neoproterozoic-Early Paleozoic development of the Gondwana western margin. Maximum ages of deposition for the metasedimentary rocks of Sierras Pampeanas, Precordillera and northern Patagonia are Ediacaran. The Famatinian magmatism and sedimentation is mainly restricted to the Lower and Middle Ordovician.
Figura 11. a) diagrama mostrando los resultados de edades para el Complejo Guarguaraz (Cordillera Frontal) y para la muestra X 4 del Complejo Bonilla, b) Ídem para la Formación Puncoviscana, c) gráfico cronológico que muestra los eventos geológicos importantes en el desarrollo del margen occidental de Gondwana durante el Neoproterozoico temprano y el Paleozoico inferior-medio. La edad máxima de depositation de las rocas metasedimentarias de las Sierras Pampeanas, Precordillera y Patagonia norte es Ediacara. El magmatismo y la sedimentación Famatiniana están principalmente restringidos al Ordovícico inferior y medio.

formed of 760 m of porphyritic high-silica welded ash-flow tuffs. According to Aleinikoff et al. (1995) two samples of the Whitetop Rhyolite Member yielded ages of 758 ± 12 Ma and 772 ± 24 Ma. Ages of 371, 703, 751, and 760 Ma were also obtained, but were considered as having been affected by the Carboniferous Alleghenian orogeny. All evidence points to a terrestrial origin for the Mount Rogers Formation. Therefore, the age of 760 Ma was considered by Aleinikoff et al. (1995) as the time of extrusion of the acidic magmatic event during an early episode of continental rifting (760-700 Ma) developed in the central and southern Appalachians, but without continental separation. A younger pulse of igneous activity (570-560 Ma) led to continental separation and the opening of the Iapetus Ocean. This event is associated with the emplacement of intrusive bodies (Tollo et al. 2004), mostly of A-type, including the Yonkers Gneiss (563 ± 2 Ma), the Pound Ridge Granite (562 ± 5 Ma), and the Suck Mountain Pluton at 680 ± 4 Ma.

Consequently, the Neoproterozoic-Cambrian sequences of the central and northern Appalachians show significant extensive bimodal volcanism, up to 2,000 m thick, associated with A-type magmatism recognized along 2,600 km from Newfoundland to North Carolina. If Cuyania or Precordillera terranes come from this area we should be able to find evidence of such a vast magmatic event in the western border of Cuyania.

However, there are notable differences when comparing the stratigraphy and tectonic of the Appalachians between Newfoundland and North Carolina with coeval sequences of the Cuyania Terrane. Here, the Neoproterozoic-Cambrian time is represented by passive-margin sequences, and acidic volcanic and intrusive events have never been recognized. Moreover, tholeiitic flood basalts like those of the Appalachian area were never recognized, not in Cuyania, Precordillera, nor Cordillera Frontal. If Cuyania was attached to the Laurentia margin at that time, they must share similar magmatic events. Thus, the Laurentia margin from Newfoundland to North Carolina is not a likely source region for the protolith of the Bonilla Complex, neither its zircons.

Latest Proterozoic-Early Cambrian sedimentary rocks outcrop between Alabama and Vermont and they have been assigned to the Chilhowee Group. Between Alabama and northwestern Virginia (Walker and Driese, 1991), the lower Unicoi and Cochran formations of this group are up to 500 m thick and represent coastal braid plain deposits. Basalt flows in the Unicoi occur at ~570-555 Ma (Southworth et al., 2007). The Nichols-Hampton formations are 275 m thick and represent a silt and mud dominated marine shelf. The Nebo and Murray formations are 120 and 220 m thick respectively. The first was coeval to the Nichols-Hampton formations and was deposited in storm-dominated inner shelf, shoreface and foreshore environments.

The second unit represents a low-energy mud shelf. The Hesse (100 m thick), Helenmode (60 m thick) and Shady formations form the upper part of the Chilhowee Group. They were deposited in shoreface and foreshore environments of a clastic-dominated shelf transitional to a carbonate ramp. A Rb-Sr recalculated age of 539 ± 30 Ma was obtained in glauconitic samples of the Murray Formation, which reinforces the Vendian to Early Cambrian age estimations based on determinations of trilobites, ostracodes, acritarchs, etc.

The Chilhowee Group then represents a fluvial-to-marine, late synrift to early drift succession that unconformably covers the Grandfather Mountain Formation considered Neoproterozoic (800-900 Ma). This unit is up to 9 km thick and represents alluvian-fan and braided river deposits (Schwab, 1977).

Such association of sedimentary environments has also never been recognized in the western border of the supposed Cuyania Terrane. Therefore, no evidence supports the idea

that the Precordillera or Cuyania Terranes were located adjacent to the North American craton between Alabama and Virginia at that time.

Further south, the Ouachita embayment was considered by Thomas et al. (2000) as the location of the rifting of the Precordillera Terrane. The time of the rifting event was constrained by the synrift rhyolites of the Arbuckle uplift in southern Oklahoma, with U-Pb zircon ages of 536 ± 5 Ma and 539 ± 5 Ma, also consistent with the age of the igneous rocks in the Wichita Mountains.

Gilbert (1983), McConnell and Gilbert (1990), and Puckett (2011) analyzed the igneous stratigraphy of the Southern Oklahoma Aulacogen, where the Arbuckle uplift is located. The Oklahoma Aulacogen is part of a series of rifts developed at high angles to the southern margin of the North American craton and extending from Oklahoma to Utah.

In the Southern Oklahoma Aulacogen the first pulse of magmatism, which appears on the ~1.2- 1.4 Ga basement, is represented by the ~600-577 Ma (Lambert et al., 1988) rocks of the Glen Mountains Layered Complex (anorthositic-gabbroid rocks) of the Raggedy Mountain Gabbro Group.

Basaltic volcanic rocks (320 m thick) of the Navajoe Mountain Basalt-Spilite Group (~550 Ma) seem to be associated with the intrusive event. These rocks are compositionally tholeiitic and the basalts were considered to be shallow submarine flows. Small later plutons (Roosevelt Gabbros) are intruding (552 Ma, U-Pb zircon, Bowring and Hoppe, 1982) the igneous sequence. The intrusion of this unit seems to be associated with uplift and erosion of older units, which were later covered by the Carlton Rhyolite Group (~525 Ma), associated with the intrusion of A-type acidic magmatism of the Wichita Granite Group. The rhyolites are up to 1,400 m thick and it is believed that they erupted along linear fissures (McConnell and Gilbert, 1990). McCleery and Hanson (2010) indicated more than 2 km thick and A-type magmatism characteristics typical of emplacement in rift settings. According to Gilbert (1983), the volume of these rocks can easily reach 40,000 km^3. Sedimentation continued in marine carbonate platforms, where the Cambro-Ordovician Timbered Hill and Arbuckle groups were deposited. A deep borehole (5,640 m, Puckett, 2011) cut 3,657 m of basaltic rocks and 650 m of rhyolites. The lower part of the borehole (470 m) showed interbedding of basalts, rhyolites, dolomites and lithic dolomitic conglomerates. The basaltic rocks were correlated with the Navajoe Mountain Basalt-Spilite Group.

Hanson et al. (2009) interpreted these rifting-related rocks as occurred during the opening of the Iapetus Ocean, either as part of an r-r-r triple junction or within a leaky transform at an offset in the Laurentian margin.

The orientation of the Southern Oklahoma Aulacogen suggests a transform fault that propagated into the Laurentian continental crust (Thomas, 1991). The fault system is nearly parallel to the Alabama-Oklahoma Transform, which was hailed as the northern border of the supposedly migrated Precordillera terrane (Thomas, 2011).

If this terrane was adjacent to the Ouachita border of the North American craton we could expect a similar transform fault system in the northern border of Precordillera, or at least evidence of such a noteworthy Cambrian magmatic event.

Further south, in the Llano and Devils River uplift, Texas, the metasedimentary-metavolcanic succession is 850 m thick, including basaltic rocks (529 ± 31 Ma, Rb-Sr, Nicholas and Rozendal, 1975). The last is located near the Texas Transform, which was referred to as the southern border of the Precordillera Terrane.

The Thomas (2011) palinspastic reconstruction of the Iapetan rifted margin of southern Laurentia, shows the location of the Precordillera Terrane between the Alabama-Oklahoma

and Texas transforms, extending more than 850 km in a north-south direction and 830 km in an east-west direction, with important basic and acidic magmatism near these transforms.

The supposed Cuyania Terrane is indeed more than 1,100 km long in a NNW-SSE direction if the Ordovician limestones of La Pampa Province are included, and 200 km wide in an east-west direction. Even if the E-W pre-Andean and Andean deformation is restored by a 55% (average using the values of Giambiagi et al., 2009), we are far away from the 800 km required by the Thomas (2011) model. Another possibility is to consider that part of the Cuyania Terrane extends below the Andes Cordillera until the Chilean coast of the actual Pacific Ocean. However, again there are considerable differences with the form and size of the model proposed by Thomas (2011). The northern and southern borders of the supposed Cuyania Terrane, the Alabama-Oklahoma and Texas transforms are not represented in the northern and southern tips of the area considered as the Cuyania Terrane, neither a trace nor relict of such structures were found. Another discrepancy of the Thomas (2011) model is the presence of the Southern Oklahoma Aulacogen, which propagates for more than 1,000 km into the North American craton. This structure and its conspicuous magmatism must be represented in the Cuyania Terrane because it was supposedly part of the North American craton during Neoproterozoic-Early Cambrian times. However, such elements were never found in Precordillera or Cuyania Terrane.

According the evidence discussed above, it is difficult to reconcile the idea that the zircons and the protolith of the Bonilla Complex were derived from the Ouachita area in Texas. Most evidence indicates a Gondwana origin for the zircons and the material that form the Bonilla Complex. It is not necessary to consider the presence of an exotic terrane between the Bonilla Complex and the Gondwana margin in order to explain the ~ 1Ga zircon recorded in the first. Such a population of zircons was also found widespread in many Pampean units of the Sierras Pampeanas, the Puncoviscana Formation and in northern Patagonia, but exotic terranes, located east or northeast of such outcrops, was not proposed to explain such a population.

POST-PASSIVE MARGIN EVOLUTION OF THE BONILLA COMPLEX. The development of the Bonilla Complex as a passive margin probably continued until the Dapingian (471 Ma, Middle Ordovician), see Figure 11c. As previously indicated, Ordovician to Devonian rocks with graptolites and flora fossil remains (Cuerda et al., 1988; Cortés, 1992) were found in the Villavicencio Formation and Cienaga del Medio Group, which outcrop immediately west, east and north of the area studied.

The age of the deformation of the Bonilla Complex and equivalent units were established by Buggisch et al. (1994), who dated illite/muscovite possibly related to this event in the metasedimentary rocks of the Bonilla area, determining an age of 437 Ma (K/Ar). The slices of the oceanic crust tectonically interbedded into the metasedimentary rocks of the Bonilla Complex rocks were emplaced and deformed coevally with their host rocks at 418 ± 10 Ma (Davis et al. 2000), see Figure 11c. The facies association documented in the Bonilla Complex can be assigned to an accretionary complex, similar to that recognized by Gregori and Bjerg (1997) in the Metales Belt of the Cordillera Frontal.

Buggisch et al. (1994) also determined an age of 353 Ma in the Bonilla Complex, whereas Davis et al. (1999), using Ar/Ar, reported ages of 384 and 385 and 372 and 377 Ma in the metamorphic rocks of the Portillo area. These ages are grouped between the Lower Mississippian and the Frasnian (Upper Devonian) and seem to represent the Chanic deformation, widely recognized in western Argentina (Fig. 11c).

THE CUYANIA TERRANE COLLISION. As suggested by several authors (Ramos et al., 1998;

Ramos, 2004; and references therein), the Cuyania Terrane collided with the Gondwana margin in the Middle Ordovician (465 to 454 Ma) or Middle–Late Ordovician (Thomas and Astini, 2003). The first ages are represented by the assumed syncollisional and postcollisional Famatinian magmatism in the Sierras Pampeanas.

The Famatinian magmatic event (Lower Ordovician-Late Devonian), supposedly due to the approach and collision of the Cuyania Terrane with the Pampean (Fig. 11c) margin of the Gondwana continent, extends from north to south between the Sierra de Quilmes, Aconquija, Belén, Ancasti, Ambato, Velasco, Chepes, Valle Fértil, La Huerta, San Luis, La Pampa and northern Patagonia (Toselli et al., 2003; Dahlquist and Baldo, 1996; Hauzenberger et al., 2001; Büttner et al., 2005; Otamendi et al., 2008, Delpino et al., 2007, Dahlquist et al., 2008). Some authors prolong this orogeny into Bolivia and Perú by more than 3,500 km (Collo et al., 2009).

The extensive Rb-Sr, K-Ar and U-Pb dating of magmatic rocks in the Sierras Pampeanas and Sierras de Famatina show that the development of this magmatism extends between ~488 and ~450 Ma (Fig. 11c). Specifically in the last region, the ages are partially overlapped by the development of the Famatinian basins (477-463 Ma) as indicated by Dahlquist et al., (2008). The magmatic arc is coeval with the sedimentary basin, being indicative of extensional conditions between ~488 and ~450 Ma. According to Alonso et al (2008) extensional deformation prevailed during Middle to Upper Ordovician times (~466-443 Ma) in the Don Polo, Alcaparrosa and other formations of western Precordillera.

These evidences, as well as the continental extension of the Famatinian magmatic event, is in conflict with the hypothesis that the Cuyania Terrane collided against the Gondwana margin between 465 and 454 Ma, and precludes consideration of its collision being responsible of the magmatic event.

THE LIMESTONES OF THE BONILLA COMPLEX, PRECORDILLERA AND SIERRAS PAMPEANAS. One of the most noted differences between the Cuyania Terrane and the rest of the Gondwana margin (Sierras Pampeanas, Famatina, Cordillera Oriental) is the abundance of Cambrian-Ordovician limestones in the former and their near absence in the others. Accordingly, the abundance of limestones in the Cuyania Terrane and in the southern and eastern margin of Laurentia was considered evidence of a similar origin.

As indicated above, the limestones represented by lithofacies III, up to 1 km thick, are interbedded into the metasedimentary sequence of the Bonilla Complex. These rocks can be successfully correlated with the carbonate metasilstone sequence of the Cortaderas Formation (Cucchi, 1972) and with the Alojamiento Formation, outcropping 40 km north of our studied area. The latter was assigned to the Middle-Upper Cambrian (Bordonaro, 2003). Equivalent units in the eastern Precordillera include the La Flecha, Zonda and La Laja formations.

Linares et al. (1982), Thomas et al. (2001), Buggisch et al. (2003), Galindo et al. (2004), Naipauer et al. (2005), Sial et al. (2008) and Murra et al. (2011) carried out carbon, oxygen, $^{87}Sr/^{86}Sr$, and other trace element isotope analyses in carbonate rocks of the Precordillera and the Sierras Pampeanas.

Thomas et al. (2001), reported $^{87}Sr/^{86}Sr$ values for gypsum of the Early Cambrian Cerro Totora Formation in the Precordillera and the Rome Formation of the Birmingham Graben in the Ouachita embayment. The values are between 0.70877 and 0.70867, indicative of an Early Cambrian (~524-~510 Ma) marine restricted environment.

Galindo et al. (2004) analyzed samples from Los Hornos and San Juan formations of the Precordillera, the Caucete Group, the Filo del Grafito marbles, the Difunta Correa Sequence,

and the Ophiolitic unit of the Sierra de Pie de Palo, and marbles of the Pan de Azucar, located in the Sierras Pampeanas of the San Juan Province. They also analyzed samples from the Sierra del Gigante in the San Luis Province, part of the Sierras Pampeanas. An important result of their study is that the Difunta Correa Sequence cannot be correlated with carbonate rocks of the Precordillera and the Caucete Group, but the $^{87}Sr/^{86}Sr$ and the $d^{13}C$ results are coincident with the values of marbles of the Sierra de Umango (Varela et al., 2001). The $^{87}Sr/^{86}Sr$ results for the Caucete Group (0.709017 to 0.711032) indicate strong similarities with the Filo del Grafito marbles and Los Hornos Formation (0.708813, Early to Middle Cambrian, 542-500 Ma)_Furthermore, isotopic values of rocks of the Sierra del Gigante show remarkable similarities with those of the Caucete Group and Filo del Grafito marbles (Galindo et al., 2004). After a detailed discussion about the absence of Neoproterozoic rock equivalents to the Difunta Correa Sequence in the southern Laurentian margin, it was concluded that the Difunta Correa Sequence and its Mesoproterozoic basement can be autochthonous or para-autochtonous to Gondwana.

Naipauer et al. (2005) reported results on carbon and oxygen isotopes, $^{87}Sr/^{86}Sr$, $^{206}Pb/^{207}Pb$ and Sm/Nd ratios from rocks of the Angacos Limestone and the limestones of Cerro Salinas in the Sierra de Pie de Palo. They also studied the carbonates of Loma de Las Chacras, and the Pan de Azucar Marble near de Sierra de Valle Fértil. From the Precordillera they analyzed the Cambrian La Laja Formation. For the Angacos Limestone the values of $d^{13}C$ are equivalent to those of Linares et al. (1982) and Buggisch et al. (2003), and equivalent with values of the La Laja Formation. The $^{87}Sr/^{86}Sr$ values (0.70884 and 0.70896) of the La Laja Formation are consistent with a Middle Cambrian age, whereas the limestones of Cerro Salinas are possibly upper Middle to Upper Cambrian (0.70915-0.70993).

Murra et al. (2011) analyzed the $^{87}Sr/^{86}Sr$ ratios in metacarbonates of the Sierra Brava Complex (Aceñolaza et al., 1983) in the Sierra de Ancasti (Sierras Pampeanas de Catamarca). According to Murra et al. (2011), two populations can be differentiated; one possibly deposited in the Ediacaran, (0.70745 to 0.70787) between 635 and 560 Ma and the other in_the Lower Cambrian, the first being comparable with those of the Sierras Bayas and the Arroyo del Soldado, from the Río de la Plata Craton. Because they can also be correlated with the Difunta Correa Sequence of Sierra de Pie de Palo and the marbles of the Sierra de Umango, it seem that all have a common origin.

Although the Lower Cambrian population (0.70831 to 0.70867) is smaller, and according to Murra et al. (2011) they probably underwent post-sedimentation alteration, they cannot be disregarded because the extensive outcrops of carbonates interbedded in Ediacaran to Cambrian sequences (Puncoviscana and equivalent formations) of the Sierras Pampeanas. Indeed, these results are curiously similar to those obtained for the Las Tienditas Formation, which is interbedded into the Puncoviscana Formation, as well as being similar to the Los Hornos Formation and the Caucete Group of the supposed Cuyania Terrane.

Misi et al. (2007) presented isotopic results for the Neoproterozoic-Cambrian carbonate rocks of the South American platform, including the Bambuí Group (740± 22Ma, Babinski and Kaufman, 2003), the Vazante Group (Latter Neoproterozoic, Azmy et al., 2001), the Una Group (600-750 Ma, Misi and Veizer, 1998), the Corumbá Group (550- 504 Ma, Misi et al., 2007), the Arroyo Soldado Group (633-532 Ma, Hartmann et al., 2002; Kawashita et al., 1999), as well as the Sierras Bayas Group of Tandil in the Rio de la Plata Craton (Gómez Peral et al., 2007). From these, the $^{87}Sr/^{86}Sr$ results for the Corumbá Group (0.70852, Boggiani et al., 2003) and the Serra do Garrote Formation Vazante_Group (0.70869-0.70886) are equivalent to those of the Los Hornos, Cerro Totora and La Laja formation of the

Precordillera, indicative of a Gondwana affinity.

The limestones and marbles intercalate into the Puncoviscana or equivalent formations can be recognized all along the Sierras Pampeanas. In the Loma Corral Formation (Sierra de Fiambalá, 27° 20´ S-67° 15´ W, Catamarca Province) there are outcrops of limestones and marbles, up to 1000 m thick, interbedded into low-degree metamorphic rocks that were correlated with the Puncoviscana Formation (Ruiz Huidobro, 1975). In the Sierra de Altohuasi, located 50 km northeastern (26° 57´ S-66° 53´ W) of the above mentioned outcrops, the Totoralilla Formation, constituted of marbles 400 m thick, 1 km long is interbedded into the Loma Corral Formation (García, 1974).

In the Sierra del Aconquija (Sierras Pampeanas, Tucuman Province, 26° 36´ S-65° 40´ W) there are outcrops of the Peñas Azules Limestones (up 300 m thick) interbedded with the Puncoviscana Formation (Gonzalez et al., 2000). Further north, in the eastern border of Puna, there are outcrops of limestones of the Cambrian Pachamama Formation (Hong et al., 2001).

Near Pomán, in the Sierra de Ambato (28° 26´ S-66° 13´ W, Catamarca Province) interbedded in schists and phyllites correlated with the Puncoviscana Formation, appear limestones up to 10 m thick. Other outcrops of limestones and marbles interbedded in equivalent units of the Puncoviscana Formation in the Catamarca Province appear in Muschaca (27° 30´ S-66° 20´ W), and Esquiú (29° 18´ S-65° 22´ W).

In the La Rioja Province, the outcrops are located in the Sierra de Umango (29° 05´ S-68° 42´ W) near Villa Unión (29° 17´ S-68° 17´ W) and in the Sierra Brava (29° 54´ S-65° 48´ W). The distribution of the outcrops of limestones and marbles interbedded in Neoproterozoic-Cambrian low-degree or metasedimentary rocks in the Sierras Pampeanas of Catamarca and La Rioja alone indicate an area of deposition more than 400 km long in a north-south direction and 350 km wide in a west-east direction.

In the Sierras Pampeanas of Córdoba and San Luis Provinces, the outcrops of limestones and marbles interbedded in Neoproterozoic-Cambrian low-degree or metasedimentary extend more than 325 km in a north-south direction and 170 km in a west-east direction. The main outcrops are located at Quilpo (30° 49´ S-64° 41´ W), Cunuputu (30° 52´ S-64° 40´ W), Ischilín (30° 39´ S-64° 20´ W), Sierra Chica (30° 56´ S-64° 24´ W), Candonga (31° 04´ S-64° 19´ W), Yulto (33° 15´ S-65° 32´ W), Achiras (33° 08´ S-64° 59´ W), and Alta Gracia (31° 46´ S-64° 27´ W).

There are also outcrops in the La Pampa Province (400 km south of the above mentioned site) including the Cerro Rogaziano marbles, the San Jorge Formation limestones (37° 27´ S-66° 21´ W), and scattered outcrops near Sierra de Lihuel Calel. However, these rocks were assigned to the Lower Paleozoic (Melchor et al., 2000) placing doubt on the correlation with the rocks of the Sierras Pampeanas.

Further south, in northern Patagonia, marbles up to 1 km thick are interbedded in the Mina Gonzalito Complex (535–540 Ma, Pankhurst et al., 2006) and in the El Jagüelito Formation (~535 Ma, Pankhurst et al., 2006). Indeed, in the El Jagüelito Formation the trace fossil content is comparable with those of the Puncoviscana Formation (González et al., 2002), suggestive of an Ediacaran-Cambrian depositional age and for the continuity of the marine basin where the Puncoviscana and equivalent units were deposited from the Sierras Pampeanas to northern Patagonia.

Therefore, as indicated above, Neoproterozoic to Cambrian limestones and marbles are common all along of the 2,000 km of the Pampean margin of the Gondwana-South America continent during the Neoproterozoic-Cambrian time, not only in the supposed Cuyania Terrane.

Conclusions

The provenance analyses of the Bonilla Complex indicate that its protolith was derived from an older exhumed felsic basement belonging to an upper continental crust.

No evidence of basic or acidic volcanism of continental rift type was found in the Bonilla Complex or equivalent units in western Precordillera, nor in the areas where the northern and southern borders of the Cuyania Terrane must be located. This is in conflict with the presence of thick sequences of such rocks in the Ouachita area of the Laurentia margin.

The detrital zircons from the Bonilla Complex place the maximum age of sedimentation at ca. 592 Ma. The distribution of the zircon populations are equivalent to those of the Puncoviscana, Ancasti, La Cébila, and Tuclame formations of the Cordillera Oriental and the Sierras Pampeanas. Equivalent units in the Sierras de Córdoba and San Luis yield similar results. They are also comparable with those of the El Jagüelito and Nahuel Niyeu formations of northern Patagonia. It is not necessary to suggest the presence of an allochthonous terrane between the Bonilla Complex and the Gondwana margin to explain the 1 Ga zircon population.

The limestones of the Bonilla Complex, deposited in a passive margin, can be correlated with Cambrian limestones of Precordillera, Sierras Pampeanas and northern Patagonia.

Therefore, the source of the Bonilla Complex protolith was located east (actual coordinates) and the rocks were deposited in a passive margin along the western coast of Gondwana during Neoproterozoic-Cambrian time, covering a basement that was already part of the Gondwana continent at that time.

Acknowledgments

We thank Nathalia Migueles (Ministerio de Producción, Río Negro Province) and Leonardo Strazzere (Minera Andacollo, Neuquén Province) for their assistance during the field work. Field and laboratory work were partially financed by CONICET-PIP 6087/05 to D. Gregori: "Geología del basamento metamórfico de la Precordillera Mendocina". We are also deeply grateful for the comments and suggestions made by the reviewers, Dr. A. Toselli (INSUGEO) and Dr. C. Cingolani (CIG) and Editor-in-Chief, Dr. F. Aceñolaza (INSUGEO), who provided a detailed critique of the manuscript which considerably improved its quality.

References

Abre, P., Cingolani, C. A., Cairncross, B., F. Chemale, F., 2012. Siliciclastic Ordovician to Silurian units of the Argentine Precordillera: Constraints on Provenance and tectonic setting in the Proto-Andean margin of Gondwana. Journal of South American Earth Sciences. Accepted Manuscript.

Abbruzzi, J.M.L., Kay, S.M., Bickford, E., 1993. Implications for the nature of the Precordilleran basement from the geochemistry and age of Precambrian xenoliths in Miocene volcanic rocks, San Juan Province. 12 Congreso Geológico Argentino, San Juan, 1, 331 –339.

Aceñolaza, F.G., Toselli, A.J., 1981. Geología del Noroeste Argentino. Facultad de Ciencias Naturales e Instituto Miguel Lillo, Universidad Nacional de Tucumán, Publicación Especial 1287: 1-212.

Aceñolaza, F., Miller, H., Toselli, A., 1983. Geología de la Sierra de Ancasti. Münstersche Forschungen zur Geologie und Paläontologie, 59, 1–372.

Adams, C.J., Miller, H., Acenolaza, F.G., Toselli, A.J., Griffin, W. L., 2011. The Pacific Gondwana margin in the Late Neoproterozoic-Early Paleozoic: Detrital zircon U-Pb ages from metasediments in northwest Argentina reveal their maximum age, provenance and tectonic setting. Gondwana Research, 19(1), 71–83.

Aleinikoff, J.N., Zartman, R.E., Walter, M., Rankin, D.W., Lyttle, P.T., Burton, W. C., 1995. U-Pb ages of metarhyolites of the Catoctin and mount Rogers formations, central and southern Appalachians: Evidence for two pulses of Iapetan rifting. American Journal of Science, 295, 428–544.

Alonso, J.L., Gallastegui, J., García-Sansegundo, J., Farias, P.,. Rodríguez Fernández, L.R., Ramos, V.A., 2008. Extensional tectonics and gravitational collapse in an Ordovician passive margin: The Western Argentine Precordillera. Gondwana Research 13, 204–215.

Amos, A.J., Quartino, B.J., Zardini, R.A., 1971. Geología de la región de Barreal-Calingasta, estratigrafía y estructura. In: Quartino, B.J., Zardini, R.A., Amos, A.J. (Eds.), Estudio y Exploración de la Región de Barreal-Calingasta. Provincia de San Juan, Argentina, (Monografía de la Asociación Geológica Argentina), 1, 15–67, pp.

Aparicio, V., Cuerda, A.J., 1976. Nuevos hallazgos de graptolites en la vertiente occidental de la Precordillera de San Juan, Calingasta. Ameghiniana 13, 159–168.

Astini, R., Benedetto, J., Vaccari, N., 1995. The Early Palaeozoic evolution of the Argentine Precordillera as a Laurentian rifted, drifted and collided terrane, a geodynamic model. Geological Society of America Bulletin, 107, 253–273.

Astini, R., Ramos, V., Benedetto, J., Vaccari, N., Cañas, F., 1996. La Precordillera: Un terreno exótico a Gondwana. 13 Congreso Geológico Argentino y 3 Congreso Exploración de Hidrocarburos, Buenos Aires, 5, 331–339.

Azmy, K., Veizer, J., Misi, A., Oliveira, T.F., Sanches, A.L., Dardenne, M.A., 2001. Dolomitization and isotope stratigraphy of the Vazante Formation, São Francisco Basin, Brazil. Precambrian Research, 112, 303–329.

Babinski, M., Kaufman, A.J., 2003. First direct dating of a Neoproterozoic post-glaciogenic cap carbonate. IV South American Symposium on Isotope Geology. Short Papers, 1, 321–323.

Baldo, E., Dahlquist, J., Rapela, C.W., Casquet, C., Pankhurst, R.J., Galindo, C., Fanning, C.M., 2005. Early Ordovician peraluminous magmatism in the Sierra de Pie de Palo, (Western Sierras Pampeanas): Geotectonic implications. In: Pankhurst, R.J., Veiga, G.D. (eds.), Gondwana 12: Geological and Biological Heritage of Gondwana. Academia Nacional de Ciencias, Abstracts, Córdoba, Argentina, 57.

Basei, M., Ramos, V.A., Vujovich, G.I., Poma, S., 1998. El basamento metamórfico de la Cordillera Frontal de Mendoza: Nuevos datos geocronológicos e isotópicos. 10 Congreso Latinoamericano de Geología y 6 Congreso Nacional de Geología Económica, Buenos Aires, 2, 412–417.

Bednarz, U., Schmincke, H.U., 1994.Petrological and chemical evolution of the northeastern Troodos Extrusive Series, Cyprus. Journal of Petrology,35, 489-523.

Blatt, H., Middleton, G., Murray, R., 1980. Origin of sedimentary rocks, 2nd edition. Prentice-Hall, New Jersey, 782 pp.

Boger, S.D., Raetz, M., Giles, D., Etchart, E., Fanning, C.M., 2005. U–Pb age data from the Sunsás region of Eastern Bolivia, evidence for the allochthonous origin of the Paraguay Block. Precambrian Research, 139, 121–146.

Boggiani, P. C., Sial, A. N., Babinski, M., Ferreira, V. P., 2003. New carbon isotopic data from the Corumbá Group as a contribution to a composite section for the Neoproterozoic III in South America. In: Frimmel, H.E. (Ed.), III International Colloquium Vendian-Cambrian of W-Gondwana, Programme and Extended Abstracts, Cape Town, 13–16.

Bordonaro, O., 1992. El Cámbrico de Sudamérica. In: Gutiérrez Marco J.C., Saavedra y Rábano, I. (Eds.), Paleozoico Inferior de Iberoamérica, Publicación Universidad de Extremadura, 69–84.

Bordonaro, O., 2003. Review of the Cambrian Stratigraphy of the Argentine Precordillera. Geologica Acta, 1(1), 11–21.

Borrello, A.V., 1969a. Los geosinclinales de la Argentina. Dirección Nacional de Geología y Minería. Anales XIV. 188 pp.

Borrello, A.V., 1969b. El flysh paleoídico de Mendoza. 4 Jornadas Geológicas Argentinas, Buenos Aires, 1, 75–89.

Bowring, S.A., Hoppe, W.J., 1982, U/Pb zircon ages from Mount Sheridan gabbro, Wichita Mountains, Oklahoma Geological Survey Guidebook, 21, 54–59.

Brito-Neves, B.D., Neto, M.D.C., Fuck, R.A., 1999. From Rodinia to Western Gondwana: An approach to the Brasiliano–Pan African Cycle and orogenic collage. Episodes: Journal of International Geoscience, 22, 155–166.

Brussa, E.D.,Mitchell,C.E.,Astini,R.A., 1999.Ashgillian (Hirnantian) graptolites from the western boundary of the Argentine Precordillera. In: Craft, P., Fatka, O. (Eds.), Quo Vadis Ordovician? Acta Universitatis Carolinae. Geologica,

vol. 43, pp. 199–202.

Buggisch, W., von Gosen, W., Henjes-Kunst, F., Krumm, S., 1994. The age of the early Paleozoic deformation and metamorphism in the Argentina Precordillera- evidence from K-Ar data. Zentralblat Geologie und Paläontologie, 1, 275–286.

Buggisch, W., Keller, M., Lehnert, O., 2003. Carbon isotope record of Late Cambrian to Early Ordovician carbonates of the Argentine Precordillera. Palaeogeography, Palaeoclimatology, Palaeoecology, 195, 357–373.

Büttner, S.H., Glodny, J., Lucassen, F., Wemmer, K., Erdmann, S., Handler, R., Franz, G., 2005. Ordovician metamorphism and plutonism in the Sierra de Quilmes metamorphic complex: Implications for the tectonic setting of the northern Sierras Pampeanas (NW Argentina). Lithos, 83(1-2), 143–181.

Caminos, R., 1993. El basamento metamórfico Proterozoico-Paleozoico inferior. 12 Congreso Geológico

Argentino y 2 Congreso de Exploración de Hidrocarburos. In: Ramos, V. (ed.), Geología y Recursos Naturales de Mendoza, 1(2), 11–19.

Castellote, P. R., 1985. Algunas observaciones geológicas en las sierras de Ambargasta y Sumampa (Provincia de Santiago del Estero). Acta Geológica Lilloana, 16(2), 259–269.

Cawood, P.A., Nemchin, A.A., 2001. Paleogeographic development of the east Laurentian margin constrained by U/Pb dating of detrital zircon in the Newfoundland Appalachians. Geological Society of America Bulletin, 113(9), 1234–1246.

Cawood, P.A., McCausland, P.J.A., Dunning, G.R., 2001. Opening Iapetus: Constraints from the Laurentian margin of Newfoundland. Geological Society of America Bulletin 113, 443–453.

Chew, D.M., Magna, T., Kirkland, C.L., Mišković, A., Cardona, A., Spikings, R., Schaltegger, U., 2008. Detrital zircon fingerprint of the proto-Andes: Evidence for a Neoproterozoic active margin? Precambrian Research, 167, 186–200.

Cingolani, C.A., Varela, R., 1999. Rb–Sr isotopic age of basement rocks of the San Rafael Block, Mendoza, Argentina. 2 South American Symposium on Isotope Geology, Villa Carlos Paz, Argentina, 23–26.

Collo, G., Astini, R.A., Cawood, P., Buchan, C., Pimentel, M., 2009. U-Pb detrital zircon ages and Sm-Nd isotopic features in low-grade metasedimentary rocks of the Famatina belt: Implications for late Neoproterozoic-Early Paleozoic evolution of the proto-Andean margin of Gondwana. Journal of the Geological Society of London, 166, 1–17.

Cordani, U.G., Teixeira, W., D'Agrella-Filho, M.S., Trindade, R.I., 2009. The position of the Amazonian Craton in supercontinents. Gondwana Research, 15, 396–407.

Cortés, J.M., 1992. Lavas almohadilladas en el Grupo Ciénaga del Medio, extremo noroccidental de la Precordillera mendocina. Revista de la Asociación Geológica Argentina, Buenos Aires, 47(1), 115–117.

Cortés, J.M., González Bonorino, G., Koukharsky, M.M.L., Pereyra, F. Brodtkorb, M., 1997. Hoja geológica 3369-09, Uspallata, provincia de Mendoza, Argentina. Subsecretaría de Minería de la Nación. SEGEMAR, Buenos Aires, 116 pp.

Cucchi, R.J., 1972. Geología y estructura de la sierra de Cortaderas, San Juan - Mendoza, Argentina. Revista Asociación Geológica Argentina, 27(2), 229–248.

Cuerda, A., Lavandaio, E., Arrondo, O., Morel, E., 1988. Investigaciones estratigráficas en el "Grupo Villavicencio", Canota, Provincia de Mendoza. Revista de la Asociación Geológica Argentina. 43(3), 356–365.

Dahlquist, J.A., Baldo, E.G., 1996. Metamorfismo y deformacion famatinianos en la Sierra de Chepes. 13 Congreso Geologico Argentino y 3 Congreso Geologico de Hidrocarburos. Simposio sobre el margen proto-Andino de Gondwana (IGCP 345 y 376), 5, 393–409.

Dahlquist, J.A., Pankhurst, R.J., Rapela, C.W., Galindo, C., Alasino, P., Fanning, C.M., Saavedra, J., Baldo, E., 2008. New SHRIMP U-Pb data from the Famatina Complex: Constraining Early–Mid Ordovician Famatinian magmatism in the Sierras Pampeanas, Argentina. Geologica Acta, 6(4), 319–333.

Davis, S., Roeske, S., McClelland, W., Snee, L., 1999. Closing the ocean between the Precordillera terrane and Chilenia: Early Devonian ophiolite emplacement and deformation in the southwest Precordillera. In: Ramos, V., Keppie, J. (Eds.), Laurentia and Gondwana connections before Pangea. Geological Society of America, Boulder, Colorado, Special Paper 336, 115–138.

Davis, J.S., Roeske, S.M., McClelland, W.C., Kay, S.M., 2000. Mafic and ultramafic crustal fragments of the southwestern Precordillera terrane and their bearing on tectonic models of the early Paleozoic in western Argentina. Geology, 28(2), 171–174.

Delpino, S.H., Bjerg, E.A., Ferracutti, G.R., Mogessie, A. 2007. Counterclockwise tectonometamorphic evolution of the Pringles Metamorphic Complex, Sierras Pampeanas of San Luis (Argentina). Journal of South American Sciences, 23, 147–175.

Dessanti, R. Caminos, R., 1967. Edades potasio-argón y posición estratigráfica de algunas rocas ígneas y metamórficas de la Precordillera, Cordillera Frontal y Sierras de San Rafael, provincia de Mendoza. Revista de la Asociación Geológica Argentina, 22(2), 135–162.

Escayola, M.P., Pimentel, M.M., Armstrong, R., 2007. Neoproterozoic backarc basin: Sensitive high-resolution ion microprobe U-Pb and Sm-Nd isotopic evidence from the Eastern Pampean Ranges, Argentina. Geology 35, 495–498.

Fanning, C.M., Pankhurst, R.J., Rapela, C.W., Baldo, E.G.,. Casque,t C. Galindo, C., 2004. K-bentonites in the Argentine Precordillera contemporaneous with rhyolite volcanism in the Famatinian Arc. Journal of the Geological Society, London, 161, 747–756.

Finney, S.C., 2007. The parautochthonous Gondwanan origin of the Cuyania (greater Precordillera) terrane of Argentina: A re-evaluation of evidence used to support an allochthonous Laurentian origin. Geologica Acta, 5(2), 127–158.

Floyd, P., Shail, R., Leveridge, B., Franke, W., 1991. Geochemistry and provenance of Rhenohercynian synorogenic sandstones: Implications for tectonic environment discrimination. Developments in Sedimentary Provenance.

In: Morton, A., Todd, S., Haughton, P. (Eds.), Geological Society of America, Special Paper 57, 173–188.
Folguera, A., Etcheverría, M., Pazos, P.J., Cortés, J.M., Fauqué, L., Rodriguez, M.F., Irigoyen, M.V., Fusari, C., 2004. Hoja geológica 3369-15, Potrerillos, provincia de Mendoza, Argentina. Subsecretaría de Minería de la Nación. SEGEMAR, Buenos Aires, 142 pp.
Galindo, C., Casquet, C., Rapela, C, Pankhurst, R.J., Baldo, E., Saavedra, J., 2004. Sr, C and O isotope geochemistry and stratigraphy of Precambrian and lower Paleozoic carbonate sequences from the Western Sierras Pampeanas of Argentina: Tectonic implications. Precambrian Research, 131, 55–71.
García, H. H., 1974. Las calizas cristalinas de Totorillas. Revista de la Asociación Geológica Argentina, 29(3), 295–303.
Gehrels, G.E., Valencia, V., Ruiz, J., 2008. Enhanced precision, accuracy, efficiency and spatial resolution of U-Pb ages by laser ablation-multicollector-inductively coupled plasma-mass spectrometry. Geochemistry, Geophysics, Geosystems, 9, Q03017, doi: 10.1029/2007GC001805.
Giambiagi, L., Ghiglione, M., Cristallini, E. Bottesi, G., 2009. Kinematic models of basement /cover interactions: Insights from the Malargüe fold and thrust belt, Mendoza, Argentina. Journal of Structural Geology, 31, 1443–1457.
Gilbert, M.C., 1983. Timing and chemistry of igneous events associated with the Southern Oklahoma Aulacogen. Tectonophysics, 94, 439–455.
Gómez Peral, L., Poire, D.G., Strauss, H., Zimmermann, U. 2007. Chemostratigraphy and diagenetic constraints on Neoproterozoic carbonate successions from the Sierras Bayas Group, Tandilia System, Argentina. Chemical Geology, 237, 109-128.
González, P.D., Poiré, D., Varela, R., 2002. Hallazgo de trazas fósiles en la Formación El Jagüelito y su relación con la edad de las metasedimentitas, Macizo Nordpatagónico Oriental, Provincia de Río Negro. Revista de la Asociación Geológica Argentina, 57, 35–44.
Gonzalez, O., Viruel, M., Mon, R., Tchilinguirian, P. Barber, E., 2000. Hoja Geológica 2766-II San Miguel de Tucumán, provincias de Tucumán, Catamarca, Salta y Santiago del Estero. Boletin No 245. SEGEMAR, Buenos Aires, 124 pp.
Gregori, D.A., Bjerg, E.A., 1997. New evidence on the nature of the Frontal Cordillera ophiolitic belt – Argentina. Journal South American Earth Science, 10(2), 147-155.
Grunow, A., Hanson, R., Wilson, T., 1996. Were aspects of Pan-African deformation linked to lapetus opening? Geology, 24, 1063–1066.
Haller, M., Ramos, V., 1993. Las Ofiolitas y otras rocas afines. 12 Congreso Geológico Argentino y 2 Congreso de Exploración de Hidrocarburos. In: Ramos, V. (Ed.), Geología y Recursos Naturales de Mendoza, 1(4), 31–39.
Hanson, R.E., McCleery, D.A., Crowley, J.L., Bowring, S.A., Burkholder, B.K., Finegan, S.A., Philips, C.M., Pollard, J.B., 2009. Large-scale Cambrian rhyolitic volcanism in southern Oklahoma related to opening of Iapetus. Paper No. 10-2. Geological Society of America, South-Central Section - 43rd Annual Meeting, 16-17 March 2009.
Hartmann, L.A., Santos, J.O., Bossi, J., Campal, N., Schipilov, A., MacNaughton, N.J., 2002. Zircon and titanite U–Pb SHRIMP geochronology of Neoproterozoic felsic magmatism on the eastern border of the Rio de la Plata Craton, Uruguay. Journal of South American Earth Science, 15, 229–236.
Haskin, M., Haskin, L., 1966. Rare earths in European shales: A redetermination. Science, 154, 507–509.
Hauzenberger, C.A., Mogessie, A., Hoinkes, G., Felfernig, A., Bjerg, E., Kostadinoff, J., Delpino, S., Dimieri, L., 2001. Metamorphic evolution of the Sierras de San Luis, Argentina: Granulite facies metamorphism related to mafic intrusions. Mineralogy and Petrology, 71, 95–126.
Hong, F.D., Seggiaro, R.E., Monardi, C.R., Alonso, R.N., González, R.E., Igarzábal, A.P., Ramallo, E., Godeas, M., Fuertes, A., García, R, Moya, F., 2001. Hoja Geológica 2566-III. Cachi. Provincias de Salta y Catamarca. Programa Nacional de Cartas Geológicas de la República Argentina. 1:250.000. Servicio Geológico Minero Argentino. Instituto de Geología y Recursos Minerales. Boletín Nro. 548. Buenos Aires, 88 pp.
Huff, W.D., Davis, D.W., Bergstrom, S.M., Krekeler, M.P.S., Kolata, D.R. Cingolani, C.A. 1997. A biostratigraphically well-constrained K-bentonite U–Pb zircon age of the lowermost Darriwilian stage (Middle Ordovician) from the Argentine Precordillera. Episodes, 20, 29–33.
International Commission on Stratigraphy, 2009. International Stratigraphic Chart.
Irvine, T.N., Baragar, W.R.A., 1971. A guide to the chemical classification of the common volcanic rocks. Canadian Journal of Earth Sciences, 8, 523–548.
Kawashita, K., Gaucher, C., Sprechmann, P., Teixeira, W., Victória, R., 1999. Preliminary chemostratigraphic insights on carbonate rocks from Nico Pérez Terrane (Uruguay). Actas 2 South American Symposiumon Isotope Geology, Córdoba, Argentina, 399–402.
Kay, S.M., Ramos, V.A., Kay, R.W., 1984. Elementos mayoritarios y trazas de las vulcanitas ordovícicas de la Precordillera occidental: Basaltos de rift oceánico temprano (?) próximos al margen continental. 9 Congreso Geológico Argentino, 2, 48–65. Buenos Aires.
Kay, S.M., Orrell, S., Abbruzzi, J.M., 1996. Zircon and whole rock Nd–Pb isotopic evidence for a Grenville age

and a Laurentian origin for the basement of the Precordillera in Argentina. Journal of Geology, 104, 637–648.
Keidel, J., 1939. Las estructuras de corrimientos paleozoicos de la Sierra de Uspallata (provincia de Mendoza). 2 Reunión de Ciencias Naturales, Physis, 14(46), 3–96.
Keller, M., 1999. Argentine Precordillera: Sedimentary and plate tectonic history of a Laurentian crustal fragment in South America. Geological Society of America, Special Paper 341, 131 pp.
Kline, S.W., Conley, J.F., Evans, N., 1987. The Catoctin Formation in the eastern Blue Ridge of Virginia: Evidence for submarine volcanism. Geological Society of America, Abstract with Program, 12(2), 93.
Koukharsky, M., Munizaga, F., Leal, O., Correa, M.J., de Brodtkorb, M.K., 1999. New K/Ar ages in the Ambargasta and Norte de Córdoba ranges, Argentina. 2 South American Symposium on Isotope Geology, Córdoba, 76–77.
Kröner, A., Cordani, U., 2003. African, southern Indian and South American cratons were not part of the Rodinia supercontinent: Evidence from field relationships and geochronology. Tectonophysics, 375, 325–352.
Lambert, D.D., Unruh, D.M., Gilbert, M.C., 1988. Rb-Sr and Sm-Nd isotopic study of the Glen Mountains layered complex: Initiation of rifting within the southern Oklahoma aulacogen. Geology, 16, 13–17.
Le Maitre. R.W., Bateman, P., Dudek, A., Keller, J., Lameyre, J.. Le Bas, M.J., Sabine, P.A., Schmid, R., Sorensen, H., Streckeisen, A., Woolley, A.R., Zanettin, B., 1989. A classification of igneous rocks and glossary of terms: Recommendations of the International Union of Geological Sciences Subcommission on the systematics of igneous rocks. Blackwell Scientific Publications, Oxford, U.K. 193 pp.
Leveratto, M.A. 1968. Geología de la zona al oeste de Ullún-Zonda, borde oriental de la Precordillera de San Juan, eruptividad subvolcánica y estructura. Revista de la Asociación Geológica Argentina, 23(2), 129–157.
Linares, E., Panarello, H.O., Valencio, S.A., García, C.M., 1982. Isótopos de carbono y oxígeno y el origen de las calizas de la sierras Chica e Zonda y de Pie de Palo, provincia de San Juan. Revista de la Asociación Geológica Argentina, 37, 80–90.
Litherland, M., Bloomfield, K., 1981. The proterozoic history of eastern Bolivia. Precambrian Research, 15, 157–179.
Litherland, M., Annells, R.N., Darbyshire, D.P.F., Fletcher, C.J.N., Hawkins, M.P., Klinck, B.A., Mitchell, W.I., O'Connor, E.A., Pitfield, P.E.J., Power, G., Webb, B.C., 1989. The proterozoic of Eastern Bolivia and its relationship to the Andean mobile belt. Precambrian Research, 43, 157–174.
Llambías, E.J., Gregori, D.A., Basei, M.A., Varela, R., Prozzi, C., 2003. Ignimbritas riolíticas neoproterozoicas en la Sierra Norte de Córdoba:¿evidencia de un arco magmático temprano en el ciclo Pampeano? Revista de la Asociación Geológica Argentina, 58(4), 572–582.
López, V., 2005. Geología y petrología de la Cuchilla de Guarguaraz, Cordillera frontal de Mendoza. Unpublished PhD, Universidad Nacional del Sur, Argentina, 237 pp.
López, V., Gregori, D., 2004. Provenance and evolution of the Guarguaraz Complex, Cordillera Frontal, Argentina. Gondwana Research, 7(4), 1197–1208.
López de Azarevich, V.L., Escayola, M., Azarevich, M.B., Pimentel, M.M. Tassinari, C., 2009. The Guarguaraz Complex and the Neoproterozoic–Cambrian evolution of southwestern Gondwana: Geochemical signatures and geochronological constraints. Journal of South American Earth Sciences, 28, 333–344
Loske, W., 1992, The west-Argentinian Precordillera: A lower Paleozoic back-arc basin?. In: Guttierrez, Marco J., and others. (Eds.), Paleozoico Inferior de Ibero America, Universidad de Extremadura, Mérida, p. 96-97.
McCleery, D.A., Hanson, R.E., 2010. Geochemistry of Cambrian rhyolites in the Wichita Mountains, southern Oklahoma: A-type felsic volcanism within the Southern Oklahoma Aulacogen. Geological Society of America, Abstracts with Programs, 42(2), 105.
McConnell, D.A., Gilbert, M.C., 1990. Cambrian extensional tectonics and magmatism within the Southern Oklahoma Aulacogen. Tectonophysics, 174, 147–157.
McLennan, S., 1989. Rare earths elements in sedimentary rocks: influence of provenance and sedimentary processes. In: Lipin, B., McKay, G. (Eds.), Geochemistry and mineralogy of rare earth elements. Reviews in Mineralogy, 21, 169–200.
McLennan, S., Taylor, S., McCulloch, M., Maynard, J., 1990. Geochemical and Nd-Sr isotopic composition of deep-sea turbidites: Crustal evolution and plate tectonic associations. Geochemical and Cosmochemical Acta, 54, 2015–2050.
Massonne, H.J., Calderón, M., 2008. P–T evolution of metapelites from the Guarguaráz Complex, Argentina - Evidence for Devonian crustal thickening close to the western Gondwana margin. Revista Geológica de Chile, 35, 1–17.
Melchor, R., Casadío, S., Tickyj, H., Quenardelle, S., 2000. Hoja Geológica 3766-III La Reforma, provincia de La Pampa. Programa Nacional de Cartas Geológicas 1:250.000. Servicio Geológico Minero Argentino, Boletín, No. 295., Buenos Aires, 71 p.
Millone, H.A., Tassinari, C.C.G., Lira, R., Poklepovic, M.F., 2003. Age and strontium-neodymium isotope geochemistry of granitoids of the Sierra Norte-Ambargasta Batholith, central Argentina. IV South American Symposium on Isotope Geology, Bahía, 617–620.

Misi, A., Veizer, J., 1998. Neoproterozoic carbonate sequences of the Una Group, Irece Basin, Brazil: Chemostratigraphy, age and correlations. Precambrian Research, 89, 87–100.

Misi, A., Kaufman, A.J., Veizer, J., Powis, K., Azmy, K., Boggiani, P.C., Gaucher, C., Teixeira, J.B.G., Sanches, A.L., Iyer, S.S.S., 2007. Chemostratigraphic correlation of Neoproterozoic sucessions in South America. Chemical Geology, 237, 143–167.

Mulcahy, S.R., Roeske, S.M., McClelland, W.C., Normade, S., Renne, P.R., 2007. Cambrian initiation of the Las Pirquitas thrust of the western Sierras Pampeanas, Argentina: implications for the tectonic evolution of the proto-Andean margin of South America. Geology 35, 443-446.

Murphy, J.B., Keppie, J.D., Nance, R.D., Dostal, J., 2010. Comparative evolution of the Iapetus and Rheic Oceans: A North America perspective. Gondwana Research, 17, 482–499.

Murra, J.A., Baldo, E.G., Galindo, C., Casquet, C., Pankhurst, R.J., Rapela, C.W., Dahlquist, J., 2011. Sr, C and O isotope composition of marbles from the Sierra de Ancasti, Eastern Sierras Pampeanas, Argentina: Age and constraints for the Neoproterozoic–Lower Paleozoic evolution of the proto-Gondwana margin. Geologica Acta, 9, 1, 72–92.

Naipauer, M., Cingolani, C.A., Valencio, S., Chemale Jr., F., Vujovich, G.I., 2005. Estudios isotopicos en carbonatos marinos del Terreno Precordillera-Cuyania: ¿Plataforma común en el Neoproterozoico-Paleozoico inferior? Latin American Journal of Sedimentology and Basin Analysis, 12(2), 89–108.

Nesbitt, H., Young, G., 1996. Petrogenesis of sediments in the absence of chemical weathering: effects of abrasion and sorting on bulk composition and mineralogy. Sedimentology, 43, 341–358.

Nicholas, R.L., Rozendal, R.A., 1975, Subsurface positive elements within Ouachita foldbelt in Texas and their relation to Paleozoic cratonic margin. The American Association of Petroleum Geologists Bulletin, 59, 193–216.

Ortega, G., Brussa, E.D., Astini, R.A., 1991. Nuevos hallazgos de graptolitos y su connotación estratigráfica en la Formación Yerba Loca, Precordillera de San Juan, Argentina. Ameghiniana, 28, 163–178.

Otamendi, J.E., Tibaldi, A.M., Vujovich, G.I., Viñao, G.A. 2008. Metamorphic evolution of migmatitas from the deep Famatinian arc crust exposed in Sierras Valle Fértil - La Huerta, San Juan, Argentina. Journal of South American Earth Sciences, 25, 313–335.

Pankhurst, R.J., Rapela, C.W., 1998. The Proto–Andean margin of Gondwana: An introduction. In: Pankhurst, R.J., Rapela, C.W. (Eds.), The Proto–Andean Margin of Gondwana. Geological Society London, Special Publication 142, 1–9.

Pankhurst, R.J., Rapela, C.W., Fanning, C.M., 2000. Age and origin of coeval TTG, I- and S-type granites in the Famatinian belt of NW Argentina. Transactions of the Royal Society of Edinburgh, Earth Sciences, 91, 151–168.

Pankhurst, R.J., Rapela, C.W., Fanning, C.M., Márquez, M., 2006. Gondwanide continental collision and the origin of Patagonia. Earth Science Reviews, 76, 235–257.

Pearce, J.A., 1983, Role of the sub-continental lithosphere in magma genesis at active continental margins. In: Hawkesworth, C.J., Norry,M. J., (Eds.), Continental basalts and mantle xenoliths, Shiva, Nantwich, England, pp. 230–249.

Pettijohn, F., Potter, P., Siever, R., 1987. Sand and Sandstones. Springer-Verlag / Wiley, New York, 617 pp.

Pimentel, M.M., Fuck, R.A., Botelho, N.F., 1999. Granites and the geodynamic history of the neoproterozoic Brasília belt, Central Brazil: A review. Lithos, 46, 463–483.

Puckett, R.E., 2011. A thick sequence of rift-related basalts in the Arbuckle Mountains, Oklahoma, as revealed by deep drilling. Shale Shaker, The Journal of the Oklahoma City Geological Society, January/February 2011, 207–216.

Ramos, V.A., 1995. Sudamérica: Un mosaico de continentes y océanos. Ciencia Hoy (Buenos Aires), 6, 24–29.

Ramos, V. A., 2004. Cuyania, an exotic block to Gondwana: Review of a historical success and the present problems. Gondwana Research, 7(4), 1009–1026.

Ramos, V.A., 2008. The Basement of the Central Andes: The Arequipa and Related Terranes. Annual Review of Earth and Planetary Sciences, 36, 289–324.

Ramos, V.A., Basei, M., 1997. The basement of Chilenia: An exotic continental terrane to Gondwana during the Early Paleozoic. In: Bradshaw, J., Weaver, S. (Eds.), International Conference on Terrane Geology, Abstracts, 140–143.

Ramos, V.A., Dallmeyer, R. D., Vujovich, G., 1998. Time constrains on the Early Palaeozoic docking of the Precordillera, central Argentina. In: Pankhurst, R.J., Rapela, C.W. (Eds.), The Proto-Andean Margin of Gondwana. Special Publication 142. Geological Society of London, pp. 143–158.

Ramos, V.A., Vujovich, G., Dallmeyer, R., 1996. Los klippes y ventanas tectónicas preándicas de la Sierra de Pie de Palo (San Juan): Edad e implicaciones tectónicas. XIII Congreso Geológico Argentino y III Congreso de Exploración de Hidrocarburos, Buenos Aires, 377–391.

Rapela, C.W., Pankhurst, R.J., Casquet, C., Baldo, E., Saavedra, J., Galindo, C., 1998a. Early evolution of the Proto-

Andean margin of South America. Geology, 26, 707–710.
Rapela, C.W, Pankhurst, R.J., Casquet, C., Baldo, E., Saavedra, J., Galindo, C., Fanning, C.M., 1998b. The Pampean Orogeny of the southern proto-Andes: evidence for Cambrian continental collision in the Sierras de Córdoba. In: Pankhurst, R.J., Rapela, C.W. (Eds.), The Proto-Andean Margin of Gondwana. Special Publication 142. Geological Society of London, pp. 181–217.
Rapela, C., Pankhurst, R. J., Casquet, C., Fanning, C. M., C. Galindo, C., Baldo, E., 2005. U-Pb SHRIMP dating of detrital zircons of Neoproterozoic para-amphibolites from the Difunta Correa sequence (Western Sierras Pampeanas, Argentina). Geogaceta, 38, 227–230.
Rapela, C.W., Pankhurst, R.J., Casquet, C. Fanning, C. M., Baldo, E.G., González-Casado, M., Galindo, C., Dahlquist, J. 2007. The Río de la Plata craton and the assembly of SW Gondwana. Earth-Science Reviews, 83, 49–82.
Roser, B., Korsch, R., 1986. Determination of tectonic setting of sandstone-mudstone suites using SiO2 content and K2O/Na2O ratio. Journal of Geology, 94, 635–650.
Roser, B., Korsch, R., 1988. Provenance signatures of sandstones-mudstone suites determined using discriminant function analysis of mayor-element data. Chemical Geology, 67, 119–139.
Rubinstein, C.V., Steemans, P., 2007. New palynological data from the Devonian Villavicencio Formation, Precordillera of Mendoza, Argentina. Ameghiniana, 44(1), 3–9.
Ruíz Huidobro, O.J. 1975. Descripción geológica de la Hoja 12e, Laguna Helada, Prov. de Catamarca. Boletín del Servicio Geológico Nacional, Buenos Aires, 146, 1–55.
Santos, J.O.S., Rizzotto, G.J., Potter, P.E., McNaughton, N.J., Matos, R.S., Hartmann, L.A., Chemale Jr., F., Quadros, M.E.S., 2008. Age and autochthonous evolution of the Sunsás Orogen in West Amazon Craton based on mapping and U–Pb geochronology. Precambrian Research, 165, 120–152.
Sato, A.M., Tickyj, H., Llambías, E.J., 1998. Rb–Sr Grenvillian age from the Las Matras diorite, La Pampa Province, Argentina. 10 Congreso Latinoamericano de Geología and 6 Congreso Nacional de Geología Económica, Buenos Aires, 2, 418.
Sato, A.M., Tickyj, H., Llambías, E.J., Sato, K., 1999. Rb–Sr, Sm–Nd and K–Ar age constraints of the Grenvillian Las Matras pluton, central Argentina. 2 South American Symposium on Isotope Geology, Villa Carlos Paz, Argentina, 122–126.
Sato, A.M., Tickyj, H., Llambías, E.J., Sato, K. 2000. Las Matras tonalitic–trondhjemitic pluton, central Grenvillian-age constraints, geochemical characteristics, and regional implications. Journal of South American Earth Sciences, 13, 587–610.
Schauer, O., Varela, R., Cingolani, C., Cuerda, A.J., 1987. Presencia de una graptofauna llandeilliano-caradociana en la Formación Alcaparrosa, del flanco occidental de la Sierra del Tontal (Precordillera de San Juan). Ameghiniana, 24(3-4), 151–158.
Schwab, F.L., 1977. Grandfather Mountain Formation: Depositional environment, provenance, and tectonic setting of Late Precambrian alluvium in the Blue Ridge of North Carolina. Journal of Sedimentary Petrology, 47(2), 800–810
Schwartz, J.J., Gromet, L.P., 2004. Provenance of Late Proterozoic–Early Cambrian basin, Sierras de Córdoba, Argentina. Precambrian Research, 129, 1–21.
Sial, A.N., Peralta, S., Ferreira, V.P, Toselli, A.J., Aceñolaza, F.G., Parada, M.A., Gaucher, C., Alonso, R.N., Pimentel, M.M., 2008. Upper Cambrian carbonate sequences of the Argentine Precordillera and the Steptoean C-Isotope positive excursion (SPICE). Gondwana Research, 13, 437–452.
Sims, J.P., Ireland, T.R., Cmacho, A., Lyons, P., Pieters, P.E., Skirrow, R.G., Stuart-Smith, P.G., Miró, R., 1998. U–Pb, Th–Pb and Ar–Ar geochronology form the southern Sierras Pampeanas: implication for the Palaeozoic tectonic evolution of the western Gondwana margin. In: Pankhurst, R.J., Rapela, C.W. (Eds.), The Proto-Andean Margin of Gondwana. Special Publication 142. Geological Society of London, pp. 259–281.
Söllner, F., Leal, P.R., Miller, H., de Brodtkorb, M., 2000. Edades U/Pb en circones de la riodacita de la sierra de Ambargasta, Provincia de Córdoba. In: Schalamuk, I., Brodtkorb, M., Etcheverry, R. (Eds.), Mineralogía and Metalogenia 2000. La Plata. Publicación 6, 465–469.
Southworth, S., Aleinikoff, J.N., Bailey, C., Rankin, D.W., Tollo, R.P., 2007, Neoproterozoic to Cambrian rift architecture of eastern Laurentia: a prolonged record of extension before and after development of the Iapetus ocean. Paper No. 230-1 2007. Geological Society of America Annual Meeting, Denver.
Steenken, A., Siegesmund, S., López de Luchi, M.G., Frei, R., Wemmer, K., 2006. Neoproterozoic to Early Palaeozoic events in the Sierra de San Luis: Implications for the Famatinian geodynamics in the Eastern Sierras Pampeanas (Argentina). Journal of the Geological Society, London, 163, 965–982..
Sun, S.S., McDonough, W.F., 1989. Chemical and isotopic systematics of oceanic basalts: Implications for mantle composition and processes. In: Saunders, A.D., Norry, M.J. (Eds.), Magmatism in the Ocean Basins. Geological Society of London, Special Publication, 42, 313–345
Tarney, J., Wood, D., Varet, J., Saunders, A., Cann, J., 1979. Nature of mantle heterogeneity in the North Atlantic: evidence from leg 49 basalts. In: Talwani, M., Harrison, C., Hayes, D. (Eds.), Deep drilling results in the Atlantic

Ocean. Ocean Crust, Maurice Edwing Series 2, America Geophysical Union, Washington.
Taylor, S., McLennan, S., 1985. The Continental Crust: Its Composition and Evolution. Blackwell Scientific, Oxford, 312 pp.
Thomas, W.A., 1991. The Appalachian-Ouachita rifted margin of southeastern North America. Geological Society of America Bulletin, 103, 415–431
Thomas, W.A., 2011. The Iapetan rifted margin of southern Laurentia. Geosphere, 7, 97–120.
Thomas, W.A., Astini, R.A., 2003. Ordovician accretion of the Argentine Precordillera terrane to Gondwana: A review. Journal of South American Earth Sciences, 16, 67–79.
Thomas, W. A., Astini, R. A., Denison, R. E., 2001. Strontium isotopes, age, and tectonic setting of Cambrian Salinas?? along the rift and transform margins of the Argentine Precordillera and southern Laurentia. Journal of Geology, 109, 2, 231–246.
Thomas, W. A., Tucker, R. D., Astini, R. A., 2000. Rifting of the Argentine Precordillera from Southern Laurentia: Palinspastic restoration of basement provinces. Abstracts 3788, 2000 Geological Society of America Annual Meeting, Reno, Nevada.
Tohver, E., Bettencourt, J.S., Tosdal, R., Mezger, K., Leite, W.B., Payolla, B.L., 2004. Terrane transfer during the Grenville orogeny: tracing the Amazonian ancestry of southern Appalachian basement through Pb and Nd isotopes. Earth and Planetary Science Letters, 228(1/2), 161–176.
Tollo R.P., Aleinikoff, J.N., Bartholomew, M.J., Rankin, D.W., 2004. Neoproterozoic A-type granitoids of the central and southern Appalachians: Intraplate magmatism associated with episodic rifting of the Rodinian supercontinent. Precambrian Research, 128, 3–38.
Toselli, A.J., Basei, M.A., Rossi de Toselli, J.N., Dudas, R., 2003. Análisis geoquímico-geocronológico de rocas granulíticas y calcosilicáticas de las Sierras Pampeanas Noroccidentales. Revista de la Asociación Geológica Argentina, 58(4), 629–642.
Totten, M., Hanan, M., Weaver, B., 2000. Beyond whole-rock geochemistry of shales: The importance of assessing mineralogical controls for revealing tectonic discriminants of multiple sediment sources for the Ouachita Mountain flysch deposits. Geological Society America Bulletin, 112(7), 1012–1022.
Trompette, R., 2000. Gondwana evolution; its assembly at around 600 Ma. Évolution du Gondwana; son assemblage autour de 600 Ma. Comptes Rendus de bAcadémie des Sciences - Series IIA, Earth and Planetary Science, 330, 305–315.
Turco Greco, E., Zardini, R., 1984. Un equinodermo del Paleozoico inferior en la Precordillera de San Juan, Calingasta. Revista de la Asociación Geológica Argentina 39, 300–303
Unrug, R, 1992. The supercontinent cycle and Gondwanaland assembly: component cratons and the timing of suturing events. Journal of Geodynamics, 16, 215–240.
Unrug, R, 1994. The contact zone of East Gondwana and West Gondwana. Abstracts. 9th International Gondwana Symposium, Hyderabad, India, 137.
van Staal, C.R., Vujovich, G.I., Currie, K.L., Naipauer, M., 2011. An Alpine-style Ordovician collision complex in the Sierra de Pie de Palo, Argentina: Record of subduction of Cuyania beneath the Famatina arc. Journal of Structural Geology, 33, 3, 343-361.
Varela, R., 1973. Estudio geotectónico del extremo sudoeste de la Precordillera de Mendoza, República Argentina. Revista de la Asociación Geológica Argentina, 28(3), 241–267.
Varela, R., Dalla Salda, L.H., 1992. Geocronología Rb–Sr de metamorfitas y granitoides del tercio sur de la Sierra de Pie de Palo, San Juan, Argentina. Revista de la Asociación Geológica Argentina, 47, 271–275.
Varela, R., López de Luchi, M., Cingolani, C., Dalla Salda, L., 1996. Geocronología de gneises y granitoides de la Sierra de Umango, La Rioja: Implicancias tectónicas. 13 Congreso Geológico Argentino Argentino and 3 Congreso de Exploración de Hidrocarburos, 3, 519–527.
Varela, R., Valencio, S., Ramos, A., Sato, K., González, P., Panarello, H., Roverano, D., 2001. Isotopic strontium, carbon and oxygen study on Neoproterozoic marbles from Sierra de Umango, Andean Foreland, Argentina. 3 South American Symposium on Isotope Geology, Abstracts, 450 –453.
Varela, R., Basei, M.A.S., González, P.D., Sato, A.M., Naipauer, M., Campos Neto, M., Cingolani, C.A., Meira, V.T., 2011. Accretion of Grenvillian terranes to the southwestern border of the Rı´o de la Plata craton, western Argentina. International Journal Earth Science, 100: 243–272.
Vaughan, A.P.M., Pankhurst, R.J., 2008. Tectonic overview of the West Gondwana margin. Gondwana Research, 13, 150–162.
Veevers, J.J., 2004. Gondwanaland from 650–500 Ma assembly through 320 Ma merger in Pangea to 185–100 Ma breakup: supercontinental tectonics via stratigraphy and radiometric dating. Earth-Science Reviews, 68, 1–132.
Volpe, A.M., Macdougall, J.D., Hawkins, J.W., 1988. Lau Basin basalts (LBB): Trace element and Sr-Nd isotopic evidence for heterogeneity in back-arc basin mantle. Earth Planetary Science Letters, 90, 174-186.
von Gosen, W., Loske, W., Prozzi, C., 2002. New isotopic dating of intrusive rocks in the Sierra de San Luis (Argentina): Implications for the geodynamic history of the Eastern Sierras Pampeanas. Journal of South

American Earth Sciences, 15(2), 237–250.
Vujovich, G.I., Gregori, D., 2002. Cordón del Portillo, Cordillera Frontal, Mendoza: caracterización geoquímica de las metamorfitas. 15 Congreso Geológico Argentino, Calafate, 2, 217–222.
Vujovich, G.I., Ostera, H. A., 2003. Evidencias del ciclo Pampeano en el basamento del sector noroccidental de la sierra de San Luis. Revista de la Asociación Geológica Argentina, 58(4), 541–548
Walker, D., Driese, S.G., 1991. Constraints on the position of the Precambrian-Cambrian boundary in the southern Appalachians. American Journal of Science, 291, 258–283.
Wareham, C.D., Pankhurst, R.J., Thomas, R.J., Storey, B.C., Grantham, G.H., Jacobs, J., Eglington, B.M., 1998. Pb, Nd, and Sr isotope mapping of Grenville- age crustal provinces in Rodinia. The Journal of Geology, 106, 647–659.
Willner, A.P., Toselli, A.J., Bazán, C., Vides de Bazán, M.E., 1983. Rocas metamórficas. In: Aceñolaza, F.G., Miller, H., Toselli, A. (Eds.), Geología de la Sierra de Ancasti. Münstersche Forschungen zur Geologie und Paläontologie, 59, 31–78.
Willner, A.P., Gerdes, A., Massonne, H.J., 2008. History of crustal growth and recycling at the Pacific convergent margin of South America at latitudes 29°–36° S revealed by a U–Pb and Lu–Hf isotope study of detrital zircon from Late Paleozoic accretionary systems. Chemical Geology, 253, 114–129
Yoder, H., Tilley, C., 1962. Origin of basalt magmas: An experimental study of natural and synthetic rock systems. Journal of Petrology, 3, 342–532.

Recibido: 27 de marzo de 2012.
Aceptado: 4 de marzo de 2013.

sample	3140292	4110292A	4100292B	1140292T	2110292U	U29	B6	X4	E32	B2	B8	X17	8090292U	X12	U13	X16	B20
area	Rivadavia	Rivadavia	Matuasto	Toro	Bonilla	Guanaco	Burros	W Bonilla	Cueva	Burros	Burros	W Bonilla	Guanaco	W Bonilla	Guanaco	W Bonilla	Burro
SiO[2]	76.69	72.13	71.46	72.84	73.2	75.09	70.25	75.9	74.29	66.96	67.56	14.61	27.67	24.24	19.61	45.59	43.89
Al[2]O[3]	10.08	9.97	10.96	11.18	11.79	11.23	11.52	9.8	11.07	11.37	13.82	1.41	1.73	3.15	1.28	15.87	13.75
Fe[2]O[3]	4.92	5.13	5.92	6.19	5.31	4.09	6.22	5.37	3.51	7.71	6.86	0.33	0.99	3.68	1.96	12.39	13.58
MnO	0.08	0.06	0.07	0.09	0.05	0.047	0.075	0.075	0.026	0.213	0.055	0.022	0.08	0.834	0.086	0.139	0.161
MgO	1.65	1.14	2.28	1.75	1.27	1.1	2.41	1.6	0.34	4.06	2.1	1.16	0.77	12.6	10.85	5.39	6.05
CaO	0.28	1.54	0.5	0.33	0.7	0.36	0.74	1.04	0.96	0.34	0.88	46.12	37.98	20.5	28.28	5.27	8.74
Na[2]O	1.86	3	1.94	1.71	5.32	3.38	1.83	2.12	5.91	0.34	2.29	0.02	0.05	1.68	0.03	4.83	3.3
K[2]O	1.82	1.14	2.08	2.09	0.06	1.56	1.97	1.35	0.1	2.95	2.54	0.35	0.27	0.1	0.29	0.16	0.11
TiO[2]	0.92	0.72	1.01	1.07	0.96	0.794	1.091	0.959	0.839	0.511	0.919	0.044	0.08	0.128	0.057	3.385	3.235
P[2]O[5]	0.2	0.15	0.18	0.18	0.21	0.18	0.19	0.18	0.18	0.19	0.19	0.16	0.22	0.05	0.05	0.65	0.4
LOI	1.78	4.29	2.36	2	2.12	2.07	2.73	2.41	1.86	4.2	3.48	36.64	30.89	31.97	35.97	6.29	6.71
TOTAL	100.27	99.27	98.74	99.42	100.99	99.9	99.02	100.8	99.08	98.85	100.7	100.9	100.72	98.95	98.46	99.96	99.95
Sc	11	11	14	14	11	11	14	12	11	11	17	1	2	3	2	21	27
V	77.76	74.13	123	99	91.82	76	149	113	97	135	133	6	8	26	63	328	384
Cr	72.73	41.72	nd	nd	56.44	60	90	70	70	60	70	20	nd	30	30	100	120
Co	10.51	11.58	nd	nd	10.28	8	14	12	12	10	4	1	nd	1	1	38	41
Ni	56.01	nd	nd	nd	15.99	30	40	30	30	30	30	20	nd	20	50	60	70
Cu	13.92	nd	nd	nd	10.62	10	30	40	10	110	60	10	nd	40	30	40	50
Zn	59.91	nd	nd	nd	43.6	40	80	110	40	30	80	30	nd	70	70	140	120
Ga	13.46	12.26	nd	nd	15.53	12	16	13	14	16	17	1	nd	3	2	23	21
Ge	1.34	1.29	nd	nd	1.02	1	2	2	1	3	2	0.8	nd	0.9	1	2	2
As	0	7.63	nd	nd	9.9	7	4	6	32	14	5	3	nd	4	3.5	7	2
Rb	72.95	39.42	nd	nd	2.61	51	82	62	3	106	106	11	nd	3	18	2	5
Sr	31.93	71.66	37	44	67.34	51	45	78	54	40	44	1215	847	1557	786	131	765
Y	36.15	24.61	26	32	25.23	23	26	28	24	29	28	8	12	8	20	25	22

Table 1.I Chemical analyses of the metasedimentary rocks of the Bonilla Complex.

sample	3140292	4110292A	4100292B	1140292T	2110292U	U29	B6	X4	E32	B2	B8	X17	8090292U	X12	U13	X16	B20
area	Rivadavia	Rivadavia	Matuasto	Toro	Bonilla	Guanaco	Burros	W Bonilla	Cueva	Burros	Burros	W Bonilla	Guanaco	W Bonilla	Guanaco	W Bonilla	Burro
Zr	363.9	232.57	236	284	372.77	205	304	360	271	85	194	33	82	56	15	145	115
Nb	13.65	9.34	nd	nd	12.85	11	14	12	12	9	13	1	nd	3	2	42	25
Cs	2.35	1.44	nd	nd	0.58	2.4	3.8	3	0.5	3.9	5.1	0.5	nd	0.4	1.1	0.5	0.7
Ba	241.75	168.47	352	284	14.1	219	340	196	42	1805	424	321	98	22	243	50	65
La	33.35	29.2	26.5	34.1	32.74	27.6	21.8	35.3	35.8	30.7	9.8	8.2	9.3	9.3	7.6	32.7	19.8
Ce	71.67	63.07	55	69	68.12	61.6	53.7	71.5	79	66.8	24.5	16.5	23	18	14.6	69.6	44.1
Pr	7.96	6.99	nd	nd	7.08	6.3	6.17	8.98	7.8	7.98	2.85	1.55	0	1.7	1.96	9.4	6.22
Nd	32.23	28.21	25	27	26.57	26.2	21.7	31.4	28.6	27.2	13.6	6.4	8	5.8	7.3	36	24.4
Sm	6.58	5.88	4.84	6.09	5.02	5.8	4.8	6.3	6.1	5.6	3.9	1.3	1.79	1.2	1.8	7.9	5.9
Eu	1.23	1.25	1	1.3	0.92	1.24	1.05	1.36	0.97	1.07	0.94	0.28	0.5	0.36	0.67	3.19	2.2
Gd	5.78	5.25	nd	nd	4.44	5	4.6	6	4.9	5.2	4.1	1.3	nd	1.2	2.3	7.8	6.3
Tb	0.96	0.8	nd	nd	0.79	0.8	0.7	0.9	0.8	0.8	0.9	0.2	nd	0.2	0.4	1.1	0.9
Dy	5.37	4.33	nd	nd	4.44	4.4	4.6	5.3	4.6	4.8	4.9	1.2	nd	1.2	2.3	5.7	4.8
Ho	1.06	0.81	nd	nd	0.87	0.9	1	1.1	1	1	1	0.2	nd	0.3	0.5	1	0.9
Er	3.43	2.54	nd	nd	2.79	2.8	3	3.2	3	2.9	3.2	0.7	nd	0.9	1.6	2.7	2.3
Tm	0.53	0.38	nd	nd	0.44	0.42	0.46	0.49	0.46	0.43	0.5	0.11	nd	0.14	0.23	0.35	0.29
Yb	3.3	2.43	2.4	2.9	2.91	2.6	3	3.1	2.9	2.7	3.1	0.6	0.8	0.8	1.3	2.1	1.8
Lu	0.52	0.36	0.38	0.44	0.47	0.38	0.46	0.47	0.43	0.39	0.45	0.09	0.13	0.12	0.16	0.29	0.24
Hf	8.69	5.87	nd	nd	9.26	5.6	8.8	10.7	7.6	2.5	5.7	0.9	nd	1.6	0.4	4.2	3.6
Ta	1.2	0.83	nd	nd	1.07	0.9	1.3	1.2	0.9	0.9	1.2	0.2	nd	0.2	0.2	3.8	2.2
W	0.78	0.82	nd	nd	0.79	1	4	4	4	5	2	1	nd	2	3	6	3
Tl	0.41	0.19	nd	nd	0	0.4	0.4	0.5	0.2	0.1	0.8	0.2	nd	0.1	0.6	0.2	0.3
Pb	16.17	0	nd	nd	7.32	4	9	16	3	4	9	4	nd	21	5	3	5
Th	12.73	8.89	nd	nd	11.27	8.6	8.8	10.6	8.6	8.8	10.9	1.1	nd	2.1	1.2	3.4	2.1
U	2.16	2.08	nd	nd	3.12	2	2.5	2.4	2.7	3.3	3.2	2.2	nd	1.5	2	1.5	0.6

Table 1.II Chemical analyses of the metasedimentary rocks of the Bonilla Complex.

sample	7110292	12110292	5110292	6110292	21050296	U36	10100292A	U24B	B12	E49	U25	B21	B10
area	Rivadavia	Rivadavia	Guanaco	Guanaco	Mendocina	Guanaco	Bonilla	Guanaco	Burro	Cueva	Guanaco	Burros	Burros
SiO[2]	45.77	46.17	46.43	47.76	47.36	47.74	49.54	51.75	47.71	46.41	41.94	59.49	55.27
Al[2]O[3]	18.12	16.39	14.73	16.21	16.2	16.45	15.27	14.26	17	16.71	12.48	17.19	18.7
Fe[2]O[3]	11.87	11.63	14.02	11.92	12.47	10.81	10.77	10.17	8.55	12.66	9.28	8.02	8.32
MnO	0.16	0.15	0.18	0.15	0.17	0.158	0.17	0.175	0.151	0.179	0.147	0.221	0.107
MgO	5.86	5.16	3.34	5.63	5.69	7.28	7.64	6.94	9.37	5.79	5.21	0.23	1.56
CaO	11.7	9.49	6.35	10.26	10.97	8.44	7.55	7.13	7.59	8.99	12.12	1.65	1.99
Na[2]O	1.85	2.7	4	3.19	2.53	3.38	3.53	4.7	3.23	3.19	2.79	5.63	5.16
K[2]O	1.18	1.56	1.7	0.31	0.87	0.15	0.8	0.04	0.7	0.4	0.01	6.1	4.14
TiO[2]	0.84	2.8	3.18	2.02	2.02	1.083	1.34	1.618	0.757	2.164	1.337	0.422	1.172
P[2]O[5]	0.09	0.42	1.33	0.24	0.2	0.12	0.12	0.15	0.08	0.21	0.12	0.12	0.9
LOI	2.11	3.11	5.14	3.06	2.38	4.45	2.9	2.63	3.94	2.81	13.86	1.61	3.22
TOTAL	99.55	99.57	100.39	100.75	100.85	100.1	99.63	99.56	99.07	99.52	99.28	100.7	100.6
Sc	33	25	17	32	32	42	39	37	44	33	42	3	4
V	192	264	110.03	283.61	289.65	371	251.52	272	136	366	281	5	13
Cr	nd	nd	0	89.13	86.71	220	224.14	260	390	110	220	20	20
Co	nd	nd	26.14	38.76	40.19	47	38.11	31	38	45	27	1	6
Ni	nd	nd	45.39	90.14	82.69	100	108.81	80	120	80	80	19	20
Cu	nd	nd	20.56	163.1	158.67	90	58.82	60	70	170	70	10	20
Zn	nd	nd	126.55	90.76	92.14	60	80.38	100	40	90	150	70	160
Ga	nd	nd	24.99	21.06	21.3	17	16.23	12	12	20	13	30	26
Ge	nd	nd	1.55	1.53	1.49	3	1.02	1	1	2	1	2	2
As	nd	nd	13.06	25.58	0	4	0	5	3	4	16	4	5
Rb	nd	nd	68.8	12.12	26.38	7	23.35	2	19	14	1	92	61
Sr	318	703	801	474	335	920	459	151	281	438	390	44	561
Y	15	23	44.61	27.32	26.72	25	33.79	31	17	26	58	41	29

Table 2.I Chemical analyses of the mafic rocks of the Bonilla Complex.

sample	7110292	12110292	5110292	6110292	21050296	U36	10100292A	U24B	B12	E49	U25	B21	B10
area	Rivadavia	Rivadavia	Guanaco	Guanaco	Mendocina	Guanaco	Bonilla	Guanaco	Burro	Cueva	Guanaco	Burros	Burros
Zr	49	178	319.75	131.85	128.78	86	86.66	91	63	111	68	568	654
Nb	nd	nd	63.21	8.8	8.47	6	1.09	3	3	12	3	137	91
Cs	nd	nd	37.38	4.21	0.99	1.2	0.53	0.5	0.9	0.7	0.3	21.6	5.8
Ba	185	526	492.22	69.45	122.35	226	703.66	48	679	98	45	134	3995
La	5.3	24.2	56.9	9.41	8.93	8.5	3.27	4.6	3.5	10.1	6.9	92.7	83.2
Ce	13	48	120.03	23.54	22.77	19.2	9.16	13.5	7.9	25.5	17.5	188	179
Pr	nd	nd	14.01	3.22	3.07	2.83	1.51	1.85	0.94	3.98	3.07	23.3	17.2
Nd	8	23	61.54	15.9	14.8	11.5	8.68	10.4	4.8	17	14.7	76.5	59.7
Sm	1.82	5.53	13.28	4.39	4.24	3.3	3.18	3.6	1.6	4.9	5.5	13.7	12.5
Eu	0.8	1.8	4.42	1.63	1.57	1.16	1.14	1.15	0.73	1.74	2.08	3.07	3.94
Gd	nd	nd	12.29	4.9	4.59	4.3	4.23	4.6	2.2	6	8.3	11	9.2
Tb	nd	nd	1.92	0.87	0.82	0.7	0.89	0.9	0.4	0.9	1.6	1.5	1.4
Dy	nd	nd	9.62	4.85	4.67	4.8	5.3	5.8	3	5.5	10.4	8.5	6.6
Ho	nd	nd	1.67	0.91	0.88	1.1	1.11	1.3	0.7	1.1	2.3	1.6	1.1
Er	nd	nd	4.63	2.73	2.64	3.2	3.58	3.7	2.2	3	6.7	4.4	3.1
Tm	nd	nd	0.58	0.37	0.37	0.48	0.53	0.54	0.34	0.43	0.99	0.62	0.39
Yb	1.6	1.6	3.45	2.31	2.23	3.2	3.41	3.4	2.1	2.7	5.9	4	2.2
Lu	0.22	0.23	0.44	0.34	0.33	0.49	0.56	0.5	0.31	0.38	0.84	0.59	0.29
Hf	nd	nd	8.32	3.33	3.19	2.7	2.38	2.8	1.7	3.6	2.4	14.2	14.5
Ta	nd	nd	4.91	0.64	0.63	0.5	0.13	0.2	0.2	1.9	0.2	10.3	7
W	nd	nd	0.88	0	0	4	0	1	9	4	4	3	1
Tl	nd	nd	0.89	0.12	0.18	0.1	0.35	0.2	0.2	0.2	0.2	0.2	0.5
Pb	nd	nd	5.94	0	0	5	0	5	6	8	4	5	6
Th	nd	nd	6.61	0.84	0.77	1.7	0.3	0.4	0.3	0.9	0.3	11.7	9.4
U	nd	nd	1.7	0.26	0.26	0.5	0	0.2	0.1	0.4	0.3	2.8	3

Table 2.II Chemical analyses of the mafic rocks of the Bonilla Complex.

sample	5090292U	6090292U	7090292U	13090292U	26050296U	27050296U	11100292U	12100292U	U24A	U20
area	Mendocina	Mendocina	Mendocina	Mendocina	Rivadavia	Rivadavia	Bonilla	Bonilla	Guanaco	Guanaco
SiO[2]	38.77	39.95	39.62	40.42	39.65	40.01	41.52	39.51	40.96	39.81
Al[2]O[3]	3.27	3.97	3.32	3.58	1.79	2.1	1.74	4.33	1.06	0.59
Fe[2]O[3]	8.42	9.05	8.71	8.99	8.05	7.89	7.44	7.1	8.88	8.78
MnO	0.09	0.1	0.96	0.56	0.12	0.09	0.12	0.07	0.094	0.135
MgO	36.25	33.05	35.44	33.44	37.59	38	35.99	35.7	38.07	37.82
CaO	0.07	0.1	0.11	0.2	0.1	0.2	0.38	0.16	0.14	1.29
Na[2]O	0	0	0.06	0.08	0	0	0.02	0.01	0.04	0.05
K[2]O	0	0	0.04	0.05	0	0	0.02	0.03	0.02	0.02
TiO[2]	0.11	0.2	0.1	0.15	0.04	0.06	0.02	0.18	0.065	0.012
P[2]O[5]	0.04	0.04	0.01	0.05	0.01	0.01	0.03	0.02	0.01	0.01
LOI	12.13	13.13	11.83	10.83	12	11.84	11.92	12.55	11.39	12.46
TOTAL	99.15	99.59	100.2	98.35	99.35	100.2	99.2	99.66	100.7	101
Sc	13	15	13	15	11	12	7	18	5	6
V	66.78	68	69	70	53.15	55	26	93	13	9
Cr	2460	2000	117	120	2420	2357	2020	5735	3680	3070
Co	76.73	80	38.3	40	87.97	90	99.4	92.9	110	115
Ni	1350	1000	73	75	1480	1523	1470	1391	1580	2180
Cu	17.29	19	52	55	0	10	19	12	10	30
Zn	55.29	45	89	90	42.85	56	116	446	90	60
Ga	2.69	2.27	23	21	2.29	3	3	3	1	1
Ge	nd	nd	1.5	1.7	nd	1.09	2.1	1.7	1.9	2
As	nd	nd	nd	nd	nd	nd	96	40	4	8
Rb	nd	nd	40.9	42	nd	nd	0.9	1.1	1	1.5
Sr	3.92	4.1	19	20	3.12	5	7.2	4.9	6	7
Y	1.7	1.83	24	25	0	1.5	0	6	1	0.5

Table 3.I Chemical analyses of the ultramafic rocks of the Bonilla Complex.

sample	5090292U	6090292U	7090292U	13090292U	26050296U	27050296U	11100292U	12100292U	U24A	U20
area	Mendocina	Mendocina	Mendocina	Mendocina	Rivadavia	Rivadavia	Bonilla	Bonilla	Guanaco	Guanaco
Zr	0	0	13	13	0	20	151	9	4	12
Nb	0	0	44.9	46	0	23	6.4	0.3	0.8	5
Cs	0	0	1.1	2	0	0	0.8	0.1	0.4	34.8
Ba	3.54	2.95	114	120	5.57	7	10.5	4	41	2
La	0.19	0.18	28.8	30	0.14	0.2	0.2	1.3	0.7	1.1
Ce	0.41	0.39	63.4	65	0.28	0.5	0.3	2.2	1	1.8
Pr	0.06	0.07	5.97	6.6	nd	2	nd	0.27	0.13	0.23
Nd	0.3	0.35	27.5	25	0.18	5	0.1	1.4	0.6	0.8
Sm	0.14	0.18	6.4	8	0	5	nd	0.4	0.2	0.2
Eu	0	1	2.08	3	0	1.8	nd	0.06	0.06	0.05
Gd	0.21	0.22	5.7	5	0.1	3.5	nd	0.5	0.2	0.2
Tb	0.75	0.8	0.9	1	nd	1.8	nd	nd	0.1	0.2
Dy	0.28	0.3	4.5	4.77	0.15	3.4	nd	0.6	0.2	0.1
Ho	0	0	0.9	1.2	0	1.3	nd	0.1	0.1	0.2
Er	0.21	0.23	2.4	2.5	0.11	1.6	nd	0.4	0.1	0.1
Tm	0	0.35	0.3	0.6	0	0.8	nd	0.07	0.06	0.06
Yb	0.26	0.28	1.7	1.9	0.11	0.2	nd	0.4	0.1	0.1
Lu	0.05	0.06	0.21	0.32	nd	0.4	nd	0.04	0.05	0.05
Hf	nd	3.8	4.7	4.89	nd	3.5	5.8	0	0.2	0.3
Ta	nd	1.9	2.73	2.8	nd	1.9	0	0	0.2	6.2
W	nd	13	21.5	15	nd	2	9.5	5.8	3	7
Tl	0.1	0.1	0.2	0.6	nd	0	0.3	nd	0.2	0.3
Pb	nd	nd	nd	nd	nd	nd	17	nd	4	5
Th	0.17	0.18	2.87	3	0	2.1	0.06	nd	0.1	0.4
U	0	0	0.91	1	nd	nd	0.2	0.29	0.4	0.3

Table 3.II Chemical analyses of the ultramafic rocks of the Bonilla Complex.
Analyst: Actlabs. Major elements in wt %. trace and REE in ppm. nd: not determined.

SAMPLE B1				Isotope ratios									Apparent ages (Ma)						
#	U	206Pb	U/Th	206Pb*	±	207Pb*	±	206Pb*	±	error	206Pb*	±	207Pb*	±	206Pb*	±	Best age	±	Conc
	(ppm)	204Pb		207Pb*	(%)	235U*	(%)	238U	(%)	corr.	238U*	(Ma)	235U	(Ma)	207Pb*	(Ma)	(Ma)	(Ma)	(%)
B1-1	80	1815	0.8	16.0365	3.9	0.6355	7.0	0.0739	5.8	0.83	459.7	25.9	499.5	27.7	686.4	82.9	459.7	25.9	67.0
B1-2	369	28796	8.3	15.1675	1.7	1.1420	2.3	0.1256	1.6	0.68	762.8	11.4	773.4	12.6	804.1	35.7	762.8	11.4	94.9
B1-3	140	32937	0.6	8.8963	1.5	5.1103	1.7	0.3297	0.8	0.48	1837.0	12.8	1837.8	14.3	1838.7	26.8	1838.7	26.8	99.9
B1-4	187	25209	1.3	15.9751	2.2	1.0206	2.4	0.1183	0.9	0.39	720.5	6.3	714.2	12.2	694.6	46.7	720.5	6.3	103.7
B1-5	215	28536	2.9	10.4351	1.2	3.3181	1.8	0.2511	1.3	0.74	1444.2	17.3	1485.3	14.1	1544.4	22.9	1544.4	22.9	93.5
B1-6	601	6776	4.9	12.1277	1.7	2.2519	2.2	0.1981	1.4	0.62	1164.9	14.5	1197.4	15.5	1256.4	33.9	1256.4	33.9	92.7
B1-7	135	11907	3.0	13.8486	1.9	1.4965	4.5	0.1503	4.1	0.91	902.7	34.2	928.9	27.3	991.8	38.6	902.7	34.2	91.0
B1-8	39	16727	2.0	12.1532	3.7	2.4550	4.0	0.2164	1.4	0.34	1262.8	15.7	1258.9	28.7	1252.2	73.0	1252.2	73.0	100.8
B1-9	228	21009	3.7	12.2845	2.7	2.2548	5.1	0.2009	4.3	0.85	1180.1	46.7	1198.3	35.9	1231.2	53.1	1231.2	53.1	95.8
B1-10	415	43061	3.8	11.4774	2.2	2.7521	2.3	0.2291	0.7	0.29	1329.7	8.2	1342.6	17.2	1363.3	42.6	1363.3	42.6	97.5
B1-11	134	17540	2.9	12.0434	2.3	2.4308	2.9	0.2123	1.7	0.59	1241.2	19.2	1251.8	20.8	1270.0	45.5	1270.0	45.5	97.7
B1-12	42	4820	2.2	12.5738	2.5	2.2302	2.8	0.2034	1.2	0.41	1193.5	12.5	1190.6	19.5	1185.4	49.9	1185.4	49.9	100.7
B1-14	247	79056	1.8	9.9836	3.5	3.6195	4.4	0.2621	2.5	0.58	1500.5	33.9	1553.8	34.6	1627.1	65.9	1627.1	65.9	92.2
B1-15	174	9473	2.8	13.3067	2.5	1.6820	2.6	0.1623	0.6	0.23	969.7	5.5	1001.7	16.7	1072.5	51.1	1072.5	51.1	90.4
B1-16	131	8484	1.8	17.2152	3.3	0.6615	3.4	0.0826	0.8	0.23	511.5	3.9	515.5	13.9	533.1	73.0	511.5	3.9	96.0
B1-17	271	21156	1.0	16.4030	2.4	0.7989	3.0	0.0950	1.9	0.62	585.3	10.6	596.2	13.6	638.0	50.8	585.3	10.6	91.7
B1-18	67	5961	0.5	6.5410	1.9	8.4290	2.5	0.3999	1.6	0.65	2168.4	30.2	2278.3	22.8	2378.4	32.4	2378.4	32.4	91.2

Table 4.I U-Pb geochronological analyses.

SAMPLE B1				Isotope ratios									Apparent ages (Ma)						
#	U	206Pb	U/Th	206Pb*	±	207Pb*	±	206Pb*	±	error	206Pb*	±	207Pb*	±	206Pb*	±	Best age	±	Conc
	(ppm)	204Pb		207Pb*	(%)	235U*	(%)	238U	(%)	corr.	238U*	(Ma)	235U	(Ma)	207Pb*	(Ma)	(Ma)	(Ma)	(%)
B1-20	250	12068	1.6	12.7182	1.8	1.8915	2.9	0.1745	2.2	0.77	1036.7	21.3	1078.1	19.1	1162.7	36.0	1162.7	36.0	89.2
B1-21	152	24288	2.7	12.4553	2.8	2.1042	2.8	0.1901	0.6	0.19	1121.8	5.7	1150.2	19.5	1204.0	54.8	1204.0	54.8	93.2
B1-22	78	11148	0.8	10.0326	2.6	3.3725	3.1	0.2454	1.7	0.55	1414.7	21.8	1498.0	24.4	1618.0	48.3	1618.0	48.3	87.4
B1-23	116	12044	2.6	16.7557	2.5	0.8138	2.6	0.0989	0.7	0.26	607.9	3.9	604.6	11.9	592.0	54.7	607.9	3.9	102.7
B1-24	245	13955	2.4	15.5264	2.3	1.0289	2.7	0.1159	1.3	0.49	706.7	8.6	718.4	13.7	755.0	48.9	706.7	8.6	93.6
B1-25	291	48657	2.3	11.3504	1.3	2.6879	1.7	0.2213	1.1	0.65	1288.6	12.7	1325.1	12.3	1384.7	24.2	1384.7	24.2	93.1
B1-26	97	10008	1.5	11.3418	1.5	2.4293	3.3	0.1998	3.0	0.89	1174.4	31.9	1251.3	24.0	1386.2	28.9	1386.2	28.9	84.7
B1-29	477	8414	2.8	16.5488	1.2	0.6798	1.9	0.0816	1.5	0.78	505.6	7.2	526.6	7.8	618.9	25.8	505.6	7.2	81.7
B1-30	150	53484	2.5	10.0735	1.9	3.7828	2.1	0.2764	0.7	0.33	1573.1	9.5	1589.1	16.5	1610.4	36.2	1610.4	36.2	97.7
B1-31	105	14022	1.9	12.9782	3.3	1.8003	3.4	0.1695	0.9	0.27	1009.1	8.5	1045.6	22.1	1122.6	65.1	1122.6	65.1	89.9
B1-32	253	21267	1.3	16.2731	2.1	0.8489	2.2	0.1002	0.8	0.36	615.5	4.6	624.0	10.2	655.0	44.0	615.5	4.6	94.0
B1-33	178	12500	1.0	17.6816	2.9	0.6239	3.6	0.0800	2.2	0.60	496.2	10.3	492.3	14.1	474.3	64.0	496.2	10.3	104.6
B1-34	66	3380	1.3	17.4974	3.7	0.7398	4.1	0.0939	1.8	0.43	578.5	9.7	562.3	17.6	497.4	81.3	578.5	9.7	116.3
B1-35	106	12038	2.5	12.8730	2.2	1.9612	2.3	0.1831	0.9	0.37	1083.9	8.6	1102.3	15.7	1138.8	43.0	1138.8	43.0	95.2
B1-36	43	19388	1.2	8.7310	1.9	5.0937	2.3	0.3225	1.3	0.55	1802.2	20.0	1835.1	19.7	1872.6	35.0	1872.6	35.0	96.2
B1-37	434	19310	12.3	13.7860	1.5	1.6520	2.7	0.1652	2.3	0.84	985.5	20.8	990.3	17.2	1001.0	29.9	1001.0	29.9	98.4

Table 4.II U-Pb geochronological analyses.

SAMPLE B1				Isotope ratios									Apparent ages (Ma)						
#	U	206Pb	U/Th	206Pb*	±	207Pb*	±	206Pb*	±	error	206Pb*	±	207Pb*	±	206Pb*	±	Best age	±	Conc
	(ppm)	204Pb		207Pb*	(%)	235U*	(%)	238U	(%)	corr.	238U*	(Ma)	235U	(Ma)	207Pb*	(Ma)	(Ma)	(Ma)	(%)
B1-38	308	92124	4.0	9.3679	1.7	4.1371	3.0	0.2811	2.4	0.82	1596.8	34.5	1661.7	24.4	1744.6	31.5	1744.6	31.5	91.5
B1-39	215	31973	2.5	16.1413	2.9	0.8546	3.6	0.1000	2.2	0.61	614.7	12.8	627.2	16.9	672.5	61.3	614.7	12.8	91.4
B1-40	271	6252	1.4	12.4377	1.8	1.9045	3.5	0.1718	3.1	0.86	1022.0	28.8	1082.7	23.6	1206.9	35.7	1206.9	35.7	84.7
B1-41	256	14246	2.0	16.3847	1.6	0.8599	2.3	0.1022	1.7	0.73	627.2	10.2	630.1	10.9	640.4	33.8	627.2	10.2	97.9
B1-42	299	35055	1.7	12.3295	2.3	2.3589	2.4	0.2109	0.7	0.29	1233.8	7.7	1230.3	17.1	1224.0	45.0	1224.0	45.0	100.8
B1-43	104	25692	2.1	11.6714	2.2	2.7752	2.5	0.2349	1.1	0.45	1360.2	13.9	1348.9	18.6	1330.9	42.9	1330.9	42.9	102.2
B1-44	104	19808	2.8	11.9781	2.6	2.3319	4.0	0.2026	3.0	0.75	1189.1	32.7	1222.0	28.3	1280.6	50.9	1280.6	50.9	92.9
B1-45	253	8205	5.0	15.6910	2.9	0.9893	3.3	0.1126	1.5	0.47	687.7	10.0	698.3	16.7	732.7	61.9	687.7	10.0	93.9
B1-46	105	6584	1.5	17.6315	3.3	0.6560	3.5	0.0839	1.1	0.31	519.3	5.3	512.2	14.0	480.5	73.1	519.3	5.3	108.1
B1-47	260	52667	1.7	8.9914	1.6	4.9947	1.7	0.3257	0.6	0.36	1817.6	9.8	1818.4	14.8	1819.4	29.6	1819.4	29.6	99.9
B1-48	142	38187	1.1	12.4578	2.3	2.1700	3.5	0.1961	2.6	0.75	1154.1	27.7	1171.5	24.3	1203.6	45.4	1203.6	45.4	95.9
B1-49	124	3923	0.8	16.5013	3.7	0.6828	4.2	0.0817	1.9	0.46	506.3	9.3	528.4	17.3	625.1	80.3	506.3	9.3	81.0
B1-50	208	13676	1.4	10.9178	4.9	2.7101	5.1	0.2146	1.2	0.23	1253.3	13.1	1331.2	37.6	1459.0	93.9	1459.0	93.9	85.9
B1-52	474	13146	4.1	13.3299	3.6	1.6255	3.7	0.1571	0.8	0.21	940.9	6.7	980.1	23.0	1069.0	71.8	1069.0	71.8	88.0
B1-53	232	9275	0.8	10.9126	3.1	2.7058	3.7	0.2142	2.0	0.53	1250.9	22.4	1330.0	27.5	1459.9	59.9	1459.9	59.9	85.7
B1-54	45	8363	2.5	12.5123	2.7	2.0374	3.1	0.1849	1.6	0.50	1093.6	15.7	1128.1	21.2	1195.1	53.3	1195.1	53.3	91.5

Table 4.III U-Pb geochronological analyses.

SAMPLE B1				Isotope ratios									Apparent ages (Ma)						
#	U	206Pb	U/Th	206Pb*	±	207Pb*	±	206Pb*	±	error	206Pb*	±	207Pb*	±	206Pb*	±	Best age	±	Conc
	(ppm)	204Pb		207Pb*	(%)	235U*	(%)	238U	(%)	corr.	238U*	(Ma)	235U	(Ma)	207Pb*	(Ma)	(Ma)	(Ma)	(%)
B1-57	671	8126	5.8	16.1036	2.2	0.9097	3.0	0.1062	2.0	0.67	650.9	12.6	656.9	14.6	677.5	47.4	650.9	12.6	96.1
B1-58	316	44492	7.2	13.1693	1.5	1.9348	1.5	0.1848	0.5	0.32	1093.1	5.0	1093.2	10.3	1093.3	29.2	1093.3	29.2	100.0
B1-59	608	66755	8.0	12.9724	2.1	2.0405	2.2	0.1920	0.5	0.23	1132.1	5.2	1129.1	14.9	1123.4	42.5	1123.4	42.5	100.8
B1-60	26	5501	1.3	13.6726	1.9	1.7314	2.3	0.1717	1.2	0.53	1021.4	11.3	1020.3	14.7	1017.8	39.4	1017.8	39.4	100.4
B1-61	159	50681	0.8	8.9465	2.9	4.7180	3.5	0.3061	1.8	0.53	1721.6	27.8	1770.4	29.0	1828.5	53.1	1828.5	53.1	94.2
B1-62	79	36215	1.1	8.4860	2.6	5.4773	2.8	0.3371	1.0	0.36	1872.8	16.4	1897.1	23.9	1923.7	46.5	1923.7	46.5	97.4
B1-63	89	13638	2.4	13.5767	2.2	1.6456	4.1	0.1620	3.4	0.84	968.1	30.7	987.9	25.6	1032.0	44.3	1032.0	44.3	93.8
B1-64	102	12021	2.0	13.7873	1.1	1.6526	3.5	0.1653	3.3	0.95	985.9	30.0	990.6	21.9	1000.9	22.7	1000.9	22.7	98.5
B1-65	50	12515	1.0	12.7794	3.8	1.9605	4.3	0.1817	2.0	0.46	1076.3	19.4	1102.1	28.8	1153.2	75.5	1153.2	75.5	93.3
B1-66	394	31974	2.0	16.3625	2.8	0.8508	4.2	0.1010	3.2	0.75	620.1	18.7	625.1	19.8	643.3	60.5	620.1	18.7	96.4
B1-67	155	39701	1.3	8.9701	1.1	4.5679	2.3	0.2972	2.0	0.87	1677.3	29.1	1743.4	19.0	1823.7	20.7	1823.7	20.7	92.0
B1-69	145	31863	4.3	10.9264	2.1	3.1471	2.6	0.2494	1.5	0.56	1435.3	18.7	1444.3	19.9	1457.5	40.7	1457.5	40.7	98.5
B1-68	265	11055	2.5	16.6506	2.9	0.7984	3.2	0.0964	1.5	0.45	593.4	8.3	595.9	14.5	605.6	61.9	593.4	8.3	98.0
B1-70	172	9624	6.4	16.8317	3.5	0.7483	3.6	0.0913	1.0	0.28	563.5	5.4	567.2	15.8	582.2	76.0	563.5	5.4	96.8
B1-71	98	4613	0.9	8.0791	2.4	6.0896	2.9	0.3568	1.6	0.55	1967.1	26.8	1988.8	25.0	2011.4	42.5	2011.4	42.5	97.8
B1-72	101	44616	3.3	11.9419	1.8	2.3724	1.9	0.2055	0.7	0.38	1204.6	7.9	1234.3	13.7	1286.5	34.5	1286.5	34.5	93.6

Table 4.IV U-Pb geochronological analyses.

SAMPLE B1				Isotope ratios									Apparent ages (Ma)						
#	U	206Pb	U/Th	206Pb*	±	207Pb*	±	206Pb*	±	error	206Pb*	±	207Pb*	±	206Pb*	±	Best age	±	Conc
	(ppm)	204Pb		207Pb*	(%)	235U*	(%)	238U	(%)	corr.	238U*	(Ma)	235U	(Ma)	207Pb*	(Ma)	(Ma)	(Ma)	(%)
B1-73	335	20829	1.9	12.8868	3.4	1.7635	3.7	0.1648	1.4	0.38	983.5	12.9	1032.1	24.0	1136.6	68.1	1136.6	68.1	86.5
B1-74	261	21975	5.7	15.1247	2.8	1.0891	5.0	0.1195	4.2	0.83	727.5	28.6	748.1	26.5	810.1	58.2	727.5	28.6	89.8
B1-75	67	11702	2.0	5.0993	1.4	11.6724	2.1	0.4317	1.6	0.73	2313.3	30.1	2578.5	19.7	2794.0	23.4	2794.0	23.4	82.8
B1-75A	306	19701	1.6	17.8164	3.4	0.6192	3.8	0.0800	1.7	0.44	496.2	8.1	489.3	14.8	457.5	76.0	496.2	8.1	108.5
B1-76	176	10083	1.4	16.5516	1.7	0.7893	1.8	0.0948	0.5	0.28	583.6	2.8	590.8	8.0	618.5	36.9	583.6	2.8	94.4
B1-77	365	15428	1.8	15.9727	3.2	0.8647	4.2	0.1002	2.7	0.65	615.4	16.1	632.7	19.8	694.9	68.2	615.4	16.1	88.6
B1-78	160	28439	2.1	8.8677	3.9	4.7420	4.3	0.3050	1.7	0.40	1716.0	25.9	1774.7	36.0	1844.5	71.2	1844.5	71.2	93.0
B1-79	182	38481	1.8	10.0956	4.7	3.0685	5.9	0.2247	3.6	0.61	1306.6	42.3	1424.9	45.0	1606.3	86.9	1606.3	86.9	81.3
B1-80	145	19376	1.8	8.5844	2.3	4.8484	3.8	0.3019	3.0	0.79	1700.5	44.5	1793.3	31.6	1903.0	40.9	1903.0	40.9	89.4
B1-81	158	7464	1.4	16.4763	2.8	0.8081	3.0	0.0966	1.1	0.36	594.2	6.1	601.4	13.5	628.4	59.7	594.2	6.1	94.6
B1-82	387	35504	9.3	13.7325	2.5	1.6785	3.2	0.1672	1.9	0.60	996.5	17.5	1000.4	20.2	1008.9	51.6	1008.9	51.6	98.8
B1-83	42	20241	1.0	12.2244	4.6	2.2486	5.7	0.1994	3.3	0.58	1171.9	35.3	1196.4	39.9	1240.8	90.6	1240.8	90.6	94.4
B1-84	195	4760	1.1	17.1834	2.9	0.7529	5.2	0.0938	4.3	0.83	578.1	23.8	569.9	22.7	537.2	64.0	578.1	23.8	107.6
B1-85	323	15180	0.8	16.5860	1.0	0.8283	1.2	0.0996	0.6	0.49	612.3	3.3	612.7	5.4	614.0	22.0	612.3	3.3	99.7
B1-86	197	11771	7.0	17.3972	3.4	0.6433	3.7	0.0812	1.4	0.37	503.1	6.6	504.4	14.6	510.0	75.0	503.1	6.6	98.7
B1-87	198	16584	2.2	9.9539	4.6	3.3415	6.4	0.2412	4.5	0.70	1393.1	56.0	1490.8	49.9	1632.6	84.8	1632.6	84.8	85.3

Table 4.V U-Pb geochronological analyses.

SAMPLE B1				Isotope ratios									Apparent ages (Ma)						
#	U	206Pb	U/Th	206Pb*	±	207Pb*	±	206Pb*	±	error	206Pb*	±	207Pb*	±	206Pb*	±	Best age	±	Conc
	(ppm)	204Pb		207Pb*	(%)	235U*	(%)	238U	(%)	corr.	238U*	(Ma)	235U	(Ma)	207Pb*	(Ma)	(Ma)	(Ma)	(%)
B1-88	144	32631	2.1	9.4909	1.4	3.9555	2.9	0.2723	2.6	0.88	1552.3	35.3	1625.1	23.6	1720.7	25.4	1720.7	25.4	90.2
B1-90	305	14889	21.8	12.7765	1.5	1.9488	2.3	0.1806	1.8	0.77	1070.2	17.7	1098.0	15.6	1153.7	29.5	1153.7	29.5	92.8
B1-89	99	11411	1.2	13.1956	1.6	1.8532	1.8	0.1774	0.9	0.48	1052.5	8.4	1064.6	11.9	1089.3	31.7	1089.3	31.7	96.6
B1-91	311	31530	4.7	10.0358	2.6	3.7342	3.6	0.2718	2.5	0.69	1549.9	33.9	1578.7	28.4	1617.4	47.7	1617.4	47.7	95.8
B1-92	412	52421	9.9	12.8227	3.4	1.8573	3.9	0.1727	2.1	0.53	1027.1	19.7	1066.0	26.0	1146.6	66.6	1146.6	66.6	89.6
B1-93	785	113201	5.2	13.2789	1.7	1.7341	1.8	0.1670	0.5	0.30	995.6	4.9	1021.3	11.5	1076.7	34.3	1076.7	34.3	92.5
B1-94	95	23439	3.0	12.2859	1.4	2.1993	1.7	0.1960	1.1	0.63	1153.6	11.7	1180.8	12.2	1231.0	26.6	1231.0	26.6	93.7
B1-95	136	13391	1.6	16.5677	1.1	0.8278	1.3	0.0995	0.7	0.53	611.3	3.9	612.4	5.8	616.4	22.9	611.3	3.9	99.2
B1-96	554	9231	2.7	8.4982	1.6	5.0282	2.2	0.3099	1.5	0.67	1740.3	22.4	1824.1	18.6	1921.2	29.2	1921.2	29.2	90.6
B1-97	193	2423	2.3	16.8564	3.1	0.7585	4.3	0.0927	2.9	0.69	571.6	16.0	573.1	18.6	579.0	67.1	571.6	16.0	98.7
B1-98	321	37634	2.8	10.4730	1.9	3.1607	5.8	0.2401	5.5	0.95	1387.1	69.0	1447.6	45.1	1537.6	35.3	1537.6	35.3	90.2
B1-99	356	22085	2.2	16.8737	3.6	0.6633	3.9	0.0812	1.5	0.37	503.1	7.0	516.6	15.8	576.8	78.5	503.1	7.0	87.2
B1-100	359	9465	2.2	15.9589	11.0	0.7212	11.1	0.0835	1.4	0.12	516.8	6.8	551.4	47.3	696.8	235.6	516.8	6.8	74.2
B1-100	359	12620	2.2	15.8830	11.0	0.7249	11.1	0.0835	1.4	0.12	517.0	6.8	553.6	47.4	706.9	234.9	517.0	6.8	73.1

Table 4.VI U-Pb geochronological analyses.

SAMPLE X4				Isotope ratios									Apparent ages (Ma)						
#	U	206Pb	U/Th	206Pb*	±	207Pb*	±	206Pb*	±	error	206Pb*	±	207Pb*	±	206Pb*	±	Best age	±	Conc
	(ppm)	204Pb		207Pb*	(%)	235U*	(%)	238U	(%)	corr.	238U*	(Ma)	235U	(Ma)	207Pb*	(Ma)	(Ma)	(Ma)	(%)
X4-1	93	37560	1.5	15.8934	1.1	0.9786	1.2	0.1128	0.6	0.45	689.0	3.7	692.9	6.2	705.5	23.6	689.0	3.7	97.7
X4-2	92	59748	1.1	11.4626	1.7	2.8198	2.1	0.2344	1.2	0.58	1357.6	14.8	1360.8	15.6	1365.8	32.6	1365.8	32.6	99.4
X4-3	276	92972	1.0	16.2630	2.1	0.9361	2.2	0.1104	0.5	0.23	675.2	3.2	670.9	10.8	656.4	45.8	675.2	3.2	102.9
X4-4	207	148768	0.7	7.7137	1.2	6.8195	1.8	0.3815	1.4	0.75	2083.4	24.2	2088.3	16.1	2093.1	21.3	2093.1	21.3	99.5
X4-5	122	19936	2.3	17.0023	4.4	0.7663	4.4	0.0945	0.7	0.17	582.1	4.1	577.7	19.6	560.3	95.6	582.1	4.1	103.9
X4-6	437	550968	3.7	13.2773	2.5	1.9078	2.6	0.1837	0.7	0.26	1087.2	6.8	1083.8	17.5	1077.0	50.8	1077.0	50.8	101.0
X4-7	78	41940	0.7	12.8568	1.5	2.0461	1.7	0.1908	0.8	0.47	1125.7	8.3	1131.0	11.5	1141.2	29.5	1141.2	29.5	98.6
X4-8	20	8024	0.4	13.5660	1.3	1.6641	2.1	0.1637	1.7	0.80	977.5	15.5	994.9	13.5	1033.6	25.7	1033.6	25.7	94.6
X4-9	535	20468	8.9	13.9156	3.8	1.2147	6.3	0.1226	5.1	0.80	745.5	35.6	807.4	35.0	982.0	76.4	745.5	35.6	75.9
X4-10	199	47896	1.5	17.0573	3.2	0.7732	3.3	0.0957	0.8	0.23	588.9	4.3	581.6	14.7	553.2	70.3	588.9	4.3	106.5
X4-11	63	40172	0.7	9.7637	2.2	4.2062	2.4	0.2979	1.0	0.40	1680.6	14.5	1675.2	19.9	1668.4	41.1	1668.4	41.1	100.7
X4-12	90	134516	1.5	6.4363	2.0	9.7819	4.0	0.4566	3.5	0.87	2424.6	70.7	2414.4	37.3	2405.9	34.5	2405.9	34.5	100.8
X4-13	124	86132	2.1	10.6499	2.6	3.5133	3.0	0.2714	1.5	0.49	1547.7	20.0	1530.2	23.3	1506.0	48.6	1506.0	48.6	102.8
X4-14	93	70728	1.4	16.3811	1.1	0.8983	1.6	0.1067	1.1	0.69	653.7	6.8	650.8	7.6	640.9	24.5	653.7	6.8	102.0
X4-15	143	299868	1.1	7.1068	1.4	8.0419	1.6	0.4145	0.6	0.40	2235.5	11.9	2235.7	14.1	2236.0	24.7	2236.0	24.7	100.0
X4-16	320	12936	1.2	15.2415	2.7	0.8774	3.0	0.0970	1.3	0.43	596.7	7.4	639.6	14.2	793.9	56.8	596.7	7.4	75.2
X4-17	125	235688	1.7	11.8121	1.9	2.6347	2.2	0.2257	1.2	0.53	1312.0	14.2	1310.4	16.5	1307.7	36.9	1307.7	36.9	100.3
X4-18	384	221400	7.0	12.2002	1.2	2.3958	2.4	0.2120	2.0	0.85	1239.4	22.6	1241.4	16.9	1244.7	24.3	1244.7	24.3	99.6
X4-19	35	53360	1.2	9.6557	1.8	4.2750	2.3	0.2994	1.5	0.63	1688.2	21.5	1688.6	19.0	1689.0	33.2	1689.0	33.2	100.0
X4-20	106	121536	1.9	10.9958	2.2	3.1674	2.4	0.2526	0.9	0.37	1451.9	11.4	1449.2	18.6	1445.4	42.7	1445.4	42.7	100.4
X4-21	13	15272	1.1	8.8537	4.7	5.3462	4.8	0.3433	1.2	0.25	1902.5	19.8	1876.3	41.5	1847.4	85.0	1847.4	85.0	103.0

Table 4.VII U-Pb geochronological analyses.

SAMPLE X4				Isotope ratios									Apparent ages (Ma)						
#	U (ppm)	206Pb 204Pb	U/Th	206Pb* 207Pb*	± (%)	207Pb* 235U*	± (%)	206Pb* 238U	± (%)	error corr.	206Pb* 238U*	± (Ma)	207Pb* 235U	± (Ma)	206Pb* 207Pb*	± (Ma)	Best age (Ma)	± (Ma)	Conc (%)
X4-22	103	125208	1.1	8.2225	2.5	6.0657	3.6	0.3617	2.6	0.71	1990.4	43.7	1985.3	31.1	1980.1	44.5	1980.1	44.5	100.5
X4-23	252	263180	2.6	8.2050	2.2	6.0772	2.7	0.3616	1.6	0.59	1990.0	27.4	1987.0	23.8	1983.9	39.3	1983.9	39.3	100.3
X4-24	729	49200	11.8	15.8063	0.9	1.0137	1.3	0.1162	0.9	0.70	708.7	6.2	710.7	6.8	717.2	20.0	708.7	6.2	98.8
X4-25	222	18324	0.8	15.3386	1.8	1.0653	2.6	0.1185	1.8	0.69	722.0	12.1	736.4	13.4	780.6	38.7	722.0	12.1	92.5
X4-26	586	268352	3.9	12.9930	1.1	2.0418	1.5	0.1924	0.9	0.64	1134.4	9.8	1129.6	10.0	1120.3	22.6	1120.3	22.6	101.3
X4-27	63	77244	1.1	12.4439	2.9	2.3509	3.0	0.2122	1.0	0.33	1240.4	11.1	1227.8	21.5	1205.8	56.2	1205.8	56.2	102.9
X4-28	108	69404	1.3	13.1022	1.5	1.9841	1.7	0.1885	0.8	0.45	1113.4	8.0	1110.1	11.6	1103.6	30.6	1103.6	30.6	100.9
X4-29	181	86744	3.6	13.2655	2.0	1.9606	2.0	0.1886	0.6	0.27	1114.0	5.7	1102.1	13.7	1078.7	39.4	1078.7	39.4	103.3
X4-30	262	100156	1.1	16.3238	2.5	0.8739	2.7	0.1035	1.0	0.37	634.7	6.1	637.7	12.9	648.4	54.2	634.7	6.1	97.9
X4-31	244	255604	5.3	12.1372	2.4	2.5335	2.4	0.2230	0.5	0.21	1297.8	5.9	1281.7	17.6	1254.8	46.3	1254.8	46.3	103.4
X4-32	232	76092	0.6	13.9437	2.4	1.6701	2.4	0.1689	0.5	0.22	1006.0	4.9	997.2	15.4	977.9	48.1	977.9	48.1	102.9
X4-33	60	40724	0.9	8.2428	1.2	5.9156	3.1	0.3536	2.9	0.93	1952.0	48.8	1963.5	27.1	1975.7	20.5	1975.7	20.5	98.8
X4-34	369	179000	2.6	15.6373	0.9	1.0709	1.2	0.1215	0.8	0.65	738.9	5.5	739.2	6.4	739.9	19.5	738.9	5.5	99.9
X4-35	44	27592	1.2	13.1887	4.3	1.9931	4.6	0.1906	1.8	0.39	1124.9	18.7	1113.2	31.3	1090.4	85.5	1090.4	85.5	103.2
X4-36	199	90440	1.9	11.4400	1.5	2.8988	1.7	0.2405	0.8	0.49	1389.4	10.5	1381.6	12.9	1369.6	28.7	1369.6	28.7	101.4
X4-37	193	705648	1.6	11.6094	1.7	2.7512	1.9	0.2316	0.9	0.45	1343.1	10.5	1342.4	14.5	1341.2	33.6	1341.2	33.6	100.1
X4-38	254	53656	0.9	17.1340	3.3	0.7484	3.3	0.0930	0.5	0.15	573.3	2.7	567.3	14.4	543.4	71.8	573.3	2.7	105.5
X4-39	101	26848	1.1	9.2967	1.8	4.6829	4.3	0.3158	3.9	0.91	1768.9	60.2	1764.2	35.9	1758.6	33.2	1758.6	33.2	100.6
X4-40	69	15476	1.6	15.3935	1.9	1.0567	2.8	0.1180	2.0	0.73	718.9	13.7	732.2	14.5	773.1	39.9	718.9	13.7	93.0
X4-41	140	68188	1.8	11.7375	2.2	2.7543	3.3	0.2345	2.5	0.75	1357.9	30.7	1343.2	24.8	1320.0	42.3	1320.0	42.3	102.9
X4-42	429	44052	1.6	16.0403	2.8	0.9589	3.5	0.1116	2.1	0.59	681.8	13.4	682.7	17.4	685.9	60.4	681.8	13.4	99.4

Table 4.VIII U-Pb geochronological analyses.

SAMPLE X4				Isotope ratios									Apparent ages (Ma)						
#	U	206Pb	U/Th	206Pb*	±	207Pb*	±	206Pb*	±	error	206Pb*	±	207Pb*	±	206Pb*	±	Best age	±	Conc
	(ppm)	204Pb		207Pb*	(%)	235U*	(%)	238U	(%)	corr.	238U*	(Ma)	235U	(Ma)	207Pb*	(Ma)	(Ma)	(Ma)	(%)
X4-43	470	355864	4.4	4.9277	1.5	15.6434	1.7	0.5591	0.8	0.48	2862.8	19.0	2855.3	16.1	2849.9	24.1	2849.9	24.1	100.5
X4-45	149	43108	2.2	16.0821	2.2	0.9995	4.1	0.1166	3.5	0.84	710.8	23.4	703.5	21.0	680.3	47.4	710.8	23.4	104.5
X4-46	104	92732	3.1	14.7277	1.3	1.3434	1.5	0.1435	0.8	0.51	864.4	6.1	864.7	8.5	865.5	26.0	864.4	6.1	99.9
X4-47	395	25248	2.2	16.4904	2.9	0.7712	3.4	0.0922	1.8	0.52	568.8	9.6	580.5	14.9	626.5	62.1	568.8	9.6	90.8
X4-48	137	83628	2.0	12.8491	1.1	2.1125	1.4	0.1969	0.9	0.63	1158.5	9.1	1152.9	9.5	1142.4	21.3	1142.4	21.3	101.4
X4-49	73	36412	0.8	10.5655	1.6	3.4700	1.8	0.2659	0.7	0.37	1520.0	8.9	1520.4	14.0	1521.1	31.0	1521.1	31.0	99.9
X4-50	507	15636	2.2	12.5837	3.0	1.9288	3.3	0.1760	1.4	0.42	1045.3	13.5	1091.1	22.0	1183.8	58.9	1183.8	58.9	88.3
X4-51	148	52484	2.1	16.3436	2.6	0.9004	3.2	0.1067	1.9	0.59	653.7	11.6	651.9	15.2	645.8	54.8	653.7	11.6	101.2
X4-52	60	61540	1.0	7.7295	2.9	6.9035	3.1	0.3870	1.3	0.41	2108.9	23.0	2099.1	27.8	2089.5	50.3	2089.5	50.3	100.9
X4-53	228	191816	2.4	12.5494	1.5	2.2091	2.3	0.2011	1.7	0.75	1181.0	18.1	1183.9	15.7	1189.2	29.6	1189.2	29.6	99.3
X4-54	97	65880	2.1	15.3164	1.8	1.0909	3.1	0.1212	2.6	0.82	737.3	17.8	748.9	16.5	783.7	37.5	737.3	17.8	94.1
X4-55	64	22644	0.9	15.7073	1.8	1.0114	3.2	0.1152	2.7	0.82	703.0	17.7	709.6	16.4	730.5	38.7	703.0	17.7	96.2
X4-56	224	241704	1.2	8.2230	1.4	6.0853	2.1	0.3629	1.5	0.73	1996.0	26.4	1988.1	18.3	1980.0	25.5	1980.0	25.5	100.8
X4-57	105	196608	1.2	11.3369	1.9	2.9579	2.0	0.2432	0.5	0.25	1403.3	6.3	1396.9	15.0	1387.0	36.7	1387.0	36.7	101.2
X4-58	109	110704	2.1	12.1950	2.8	2.4831	3.0	0.2196	1.2	0.38	1279.9	13.5	1267.1	21.9	1245.5	54.6	1245.5	54.6	102.8
X4-60	125	25444	1.1	15.7926	2.4	1.0243	2.4	0.1173	0.5	0.20	715.1	3.4	716.1	12.6	719.0	50.9	715.1	3.4	99.5
X4-61	256	75892	0.9	16.7815	2.1	0.7955	2.2	0.0968	0.8	0.34	595.8	4.3	594.3	10.0	588.7	45.2	595.8	4.3	101.2
X4-62	307	365900	4.9	8.4290	3.9	5.9616	4.8	0.3644	2.7	0.56	2003.2	46.1	1970.3	41.5	1935.8	70.5	1935.8	70.5	103.5
X4-63	635	48128	2.8	16.2953	1.4	0.9139	4.2	0.1080	3.9	0.94	661.2	24.8	659.1	20.2	652.1	29.6	661.2	24.8	101.4
X4-64	57	23124	1.5	16.1421	2.9	0.9853	3.0	0.1154	0.9	0.31	703.8	6.3	696.3	15.3	672.4	61.6	703.8	6.3	104.7
X4-65	140	219604	1.6	11.8284	1.0	2.6426	2.0	0.2267	1.7	0.86	1317.2	20.4	1312.6	14.7	1305.0	19.8	1305.0	19.8	100.9

Table 4.IX U-Pb geochronological analyses.

SAMPLE X4				Isotope ratios									Apparent ages (Ma)						
#	U (ppm)	206Pb 204Pb	U/Th	206Pb* 207Pb*	± (%)	207Pb* 235U*	± (%)	206Pb* 238U	± (%)	error corr.	206Pb* 238U*	± (Ma)	207Pb* 235U	± (Ma)	206Pb* 207Pb*	± (Ma)	Best age (Ma)	± (Ma)	Conc (%)
X4-66	225	152144	3.6	6.0155	2.5	8.6712	2.9	0.3783	1.4	0.47	2068.4	23.9	2304.1	26.0	2520.1	42.3	2520.1	42.3	82.1
X4-67	125	54604	7.5	16.5555	1.8	0.8289	2.4	0.0995	1.6	0.66	611.6	9.2	613.0	10.9	618.0	38.3	611.6	9.2	99.0
X4-68	570	597136	6.4	13.8539	1.4	1.6746	1.9	0.1683	1.3	0.68	1002.5	11.9	998.9	11.9	991.1	27.8	991.1	27.8	101.2
X4-69	133	149032	2.3	13.4289	2.0	1.8113	3.3	0.1764	2.7	0.80	1047.3	25.8	1049.5	21.8	1054.2	40.1	1054.2	40.1	99.4
X4-70	80	155868	3.6	13.1015	1.0	1.8214	1.4	0.1731	1.0	0.70	1029.0	9.1	1053.2	9.0	1103.7	19.6	1103.7	19.6	93.2
X4-71	59	89204	1.6	7.1322	1.1	7.8502	1.5	0.4061	1.0	0.67	2196.9	19.2	2214.0	13.8	2229.8	19.7	2229.8	19.7	98.5
X4-72	44	8388	3.3	15.5423	2.0	0.8471	2.2	0.0955	0.9	0.42	587.9	5.1	623.0	10.0	752.8	41.3	587.9	5.1	78.1
X4-73	173	771480	2.7	12.2254	0.8	2.3530	1.0	0.2086	0.6	0.58	1221.5	6.5	1228.5	7.2	1240.7	16.1	1240.7	16.1	98.5
X4-74	229	109388	4.9	12.3304	1.3	2.3299	1.6	0.2084	1.0	0.63	1220.1	11.3	1221.5	11.5	1223.9	24.6	1223.9	24.6	99.7
X4-75	407	142460	1.5	16.7768	4.4	0.6917	5.5	0.0842	3.3	0.60	520.9	16.4	533.8	22.8	589.3	95.7	520.9	16.4	88.4
X4-76	287	326164	3.0	11.0588	1.7	2.8555	2.8	0.2290	2.2	0.79	1329.4	26.3	1370.3	20.9	1434.5	32.8	1434.5	32.8	92.7
X4-77	242	78444	3.7	16.1621	2.4	0.7738	2.8	0.0907	1.4	0.52	559.7	7.7	582.0	12.3	669.7	50.7	559.7	7.7	83.6
X4-78	269	284784	5.1	9.3407	1.1	4.5622	2.7	0.3091	2.4	0.91	1736.1	37.0	1742.4	22.3	1749.9	20.7	1749.9	20.7	99.2
X4-79	380	122908	5.6	12.7354	1.8	1.9145	2.9	0.1768	2.3	0.78	1049.7	22.3	1086.2	19.6	1160.1	36.3	1160.1	36.3	90.5
X4-80	208	137680	1.1	13.5530	1.8	1.7319	1.9	0.1702	0.5	0.26	1013.4	4.7	1020.4	12.3	1035.6	37.2	1035.6	37.2	97.9
X4-81	185	88876	1.8	13.2829	1.5	1.8465	1.9	0.1779	1.0	0.56	1055.4	10.1	1062.2	12.2	1076.1	30.9	1076.1	30.9	98.1
X4-82	183	126572	2.2	12.1860	1.7	2.3579	2.1	0.2084	1.2	0.59	1220.3	13.5	1230.0	14.7	1247.0	32.7	1247.0	32.7	97.9
X4-83	428	110508	3.9	13.7491	1.6	1.6475	1.9	0.1643	1.0	0.55	980.5	9.2	988.6	11.7	1006.5	31.4	1006.5	31.4	97.4
X4-84	292	68076	4.5	16.2498	2.2	0.8299	2.7	0.0978	1.6	0.59	601.5	9.1	613.5	12.4	658.1	46.3	601.5	9.1	91.4
X4-85	132	393784	4.3	7.6663	1.5	6.6483	2.1	0.3697	1.5	0.70	2027.8	26.3	2065.8	19.0	2103.9	26.9	2103.9	26.9	96.4
X4-86	206	174804	1.4	12.9094	1.1	1.9027	2.0	0.1781	1.6	0.83	1056.8	16.0	1082.0	13.2	1133.1	22.1	1133.1	22.1	93.3

Table 4.X U-Pb geochronological analyses.

SAMPLE X4				Isotope ratios									Apparent ages (Ma)						
#	U	206Pb	U/Th	206Pb*	±	207Pb*	±	206Pb*	±	error	206Pb*	±	207Pb*	±	206Pb*	±	Best age	±	Conc
	(ppm)	204Pb		207Pb*	(%)	235U*	(%)	238U	(%)	corr.	238U*	(Ma)	235U	(Ma)	207Pb*	(Ma)	(Ma)	(Ma)	(%)
X4-87	636	157644	3.1	17.0211	1.5	0.6680	1.6	0.0825	0.6	0.40	510.8	3.1	519.5	6.4	557.9	31.6	510.8	3.1	91.6
X4-88	767	421604	23.4	12.4488	1.2	2.1610	1.8	0.1951	1.3	0.76	1149.0	14.0	1168.6	12.2	1205.1	22.6	1205.1	22.6	95.3
X4-89	294	31396	3.2	7.9295	2.8	6.1207	2.9	0.3520	0.8	0.26	1944.2	12.6	1993.2	25.2	2044.4	49.3	2044.4	49.3	95.1
X4-90	29	181664	3.7	12.6222	3.7	2.1811	4.3	0.1997	2.3	0.54	1173.6	25.0	1175.0	30.3	1177.8	72.6	1177.8	72.6	99.6
X4-91	276	662520	18.0	12.8293	1.0	2.0409	2.5	0.1899	2.3	0.92	1120.8	23.8	1129.3	17.2	1145.5	19.9	1145.5	19.9	97.8
X4-92	112	156504	1.2	13.4835	1.7	1.7667	2.0	0.1728	0.9	0.48	1027.4	8.9	1033.3	12.7	1046.0	34.7	1046.0	34.7	98.2
X4-93	397	120204	3.4	12.1600	1.3	2.1807	1.5	0.1923	0.7	0.47	1134.0	7.3	1174.9	10.3	1251.2	25.6	1251.2	25.6	90.6
X4-94	536	313264	1.7	16.3237	1.1	0.9036	1.4	0.1070	0.8	0.55	655.2	4.7	653.6	6.6	648.4	24.5	655.2	4.7	101.0
X4-95	37	25632	0.9	11.7232	3.7	2.4673	4.5	0.2098	2.5	0.57	1227.7	28.4	1262.5	32.3	1322.4	71.2	1322.4	71.2	92.8
X4-96	330	543868	20.9	13.2470	1.6	1.8680	2.0	0.1795	1.1	0.57	1064.1	11.2	1069.8	13.2	1081.5	32.9	1081.5	32.9	98.4
X4-97	245	80312	2.6	11.3734	1.1	2.7353	1.7	0.2256	1.4	0.78	1311.5	16.0	1338.1	12.9	1380.8	20.8	1380.8	20.8	95.0
X4-98	97	102092	2.9	14.5414	2.4	1.3368	4.7	0.1410	4.0	0.85	850.3	31.8	861.9	27.1	891.8	50.2	850.3	31.8	95.3
X4-100	179	182432	3.9	10.4956	1.4	3.4068	2.1	0.2593	1.6	0.73	1486.4	20.7	1506.0	16.7	1533.6	27.1	1533.6	27.1	96.9

Table 4.XI U-Pb geochronological analyses.